March 13, 2012

MEMORANDUM TO: Patrick L. Hiland, Director
Division of Engineering
Office of Nuclear Reactor Regulation

FROM: Michael J. Case, Director */RA/*
Division of Engineering
Office of Nuclear Regulatory Research

SUBJECT: Review of Draft NUREG/CR – XXXX Entitled, "Ultrasonic Phased Array Assessment of the Interference Fit and Leak Path of the North Anna Unit 2 Control Rod Drive Mechanism Nozzle 63 with Destructive Validation"

REFERENCE: Office of Nuclear Reactor Regulation User Need 2006-006: "User Need Request for Information on PWSCC of Nickel-Base Alloy Primary Pressure Boundary Components"

In Task 8 of the referenced user need request, the Office of Nuclear Reactor Regulation asked the Office of Nuclear Regulatory Research (RES) to evaluate long-term industry solutions for primary water stress corrosion cracking (PWSCC) of nickel-base primary pressure boundary components. One aspect of the industry approach involves ultrasonic testing (UT) to identify potential primary water leakage paths between penetrations such as the control rod drive mechanism (CRDM) nozzle and the upper reactor pressure vessel (RPV) head. The attached draft NUREG/CR documents a RES-sponsored evaluation of the UT leak path assessment methodology conducted at Pacific Northwest National Laboratory (PNNL).

For this investigation, PNNL used a phased array UT system to acquire leak path data for an Alloy 600 CRDM nozzle, referred to as Nozzle 63, from the North Anna Unit 2 RPV head that was replaced in 2002. The UT data indicated a potential leakage path on the downhill side of Nozzle 63, with suspected boric acid deposits on either side of the flow path. The data also indicated other partial leakage paths and scattered boric acid deposits. Following acquisition of the UT data, PNNL cut Nozzle 63 to separate the nozzle from the RPV head and expose the annulus. Visual examination confirmed the presence of the leakage paths and boric acid deposits in the locations indicated by the UT data. Surface replication of the main leakage path on the RPV head showed that fabrication machining marks were still visible, indicating minimal loss of material from boric acid corrosion. This suggests that wastage of the RPV head material is not necessary for a leak path to be detected by the UT methodology. The results of this investigation are expected to help staff to interpret and evaluate licensees' leak path assessments for upper head penetrations.

CONTACT: Greg Oberson
301-251-7675

B134

The RES staff wishes to acknowledge Mr. Jay Collins and Dr. Stephen Cumblidge of your staff for their assistance with the development of this NUREG/CR. We look forward to working with your staff to finalize the report and would appreciate receiving your comments within 2 months from the date of this memo.

Enclosure:
As stated

DISTRIBUTION:

DE r/f	T. Lupold, NRR	H. Cruz, NRR	J. Collins, NRR
	M. Cheok, NRR	S. Cumblidge, NRR	T. Bergman, NRO
	M. Shuaibi, NRO		

ADAMS ACCESSION No: ML120660069

OFFICE	RES/DE/CMB	BC: RES/DE/CMB	D: RES/DE
NAME	G. Oberson	M. Gavrilas	M. Case
DATE	03/06/12	03/06/12	03/13/12

OFFICIAL RECORD COPY

U.S.NRC
United States Nuclear Regulatory Commission
Protecting People and the Environment

NUREG/CR-XXXX
PNNL-XXXXX

Ultrasonic Phased Array Assessment of the Interference Fit and Leak Path of the North Anna Unit 2 Control Rod Drive Mechanism Nozzle 63 with Destructive Validation

Office of Nuclear Regulatory Research

U.S.NRC
United States Nuclear Regulatory Commission
Protecting People and the Environment

NUREG/CR-XXXX
PNNL-XXXXX

Ultrasonic Phased Array Assessment of the Interference Fit and Leak Path of the North Anna Unit 2 Control Rod Drive Mechanism Nozzle 63 with Destructive Validation

Manuscript Completed: February 2012
Date Published:

Prepared by
S. L. Crawford, A. D. Cinson, P. J. MacFarlan, B. D. Hanson,
R. A. Mathews

Pacific Northwest National Laboratory
P.O. Box 999
Richland, WA 99352

G. Oberson, NRC Project Manager

NRC Job Code N6783

Office of Nuclear Regulatory Research

ABSTRACT

The objective of this investigation was to evaluate the efficacy of ultrasonic testing (UT) for primary water leak path assessments of reactor pressure vessel (RPV) upper head penetrations. Operating reactors have experienced leakage when stress corrosion cracking of nickel-based alloy penetrations allowed primary water into the annulus of the interference fit between the penetration and the low-alloy steel RPV head. In this investigation, UT leak path data were acquired for an Alloy 600 control rod drive mechanism nozzle penetration, referred to as Nozzle 63, which was removed from the North Anna Unit 2 reactor when the RPV head was replaced in 2002. In-service inspection prior to the head replacement indicated that Nozzle 63 had a probable leakage path through the interference fit region. Nozzle 63 was examined using a phased-array UT probe with a 5.0-MHz, eight-element annular array. Immersion data were acquired from the nozzle inner diameter surface. The UT data were interpreted by comparing to responses measured on a mockup penetration with known features. Following acquisition of the UT data, Nozzle 63 was destructively examined to determine if the features identified in the UT examination, including leakage paths and crystalline boric acid deposits, could be visually confirmed. Additional measurements of boric acid deposit thickness and low-alloy steel wastage were made to assess how these factors affect the UT response. The implications of these findings for interpreting UT leak path data are described.

FOREWORD

In the previous decade, a number of U.S. pressurized water reactors (PWRs) experienced primary water leakage through cracks in the control rod drive mechanism (CRDM) nozzle penetration in the upper reactor pressure vessel (RPV) head. At the Davis Besse plant in 2002, such leakage contributed to significant wastage of the low alloy steel RPV head, leaving only a thin layer of stainless steel cladding at the reactor pressure boundary. NRC and industry analyses attributed these events to primary water stress corrosion cracking (PWSCC), which can affect nickel-based alloys such as those used to fabricate the CRDM nozzle and its associated J-groove. The CRDM nozzle has a compression or interference fit with bored holes in the RPV head. PWSCC of the J-groove weld may allow primary water leakage into the annulus of the interference fit region, which could eventually reach the top of the RPV head at operating pressures. Following the incident at Davis Besse, NRC updated its inspection requirements to mandate that PWR licensees perform a demonstrated surface or volumetric leak path assessment of all J-groove welds in the RPV head. Licensees have proposed to use ultrasonic testing (UT) to satisfy this requirement. In principle, the UT methodology can detect evidence of primary water leakage, such as a gap in the interference fit between the nozzle and RPV head that could be a flow path or crystalline boric acid deposits in the annulus.

In 2006, the Office of Nuclear Reactor Regulation requested that the Office of Nuclear Regulatory Research (RES) evaluate long-term industry solutions for PWSCC of nickel-base primary pressure boundary components. This NUREG/CR documents an independent RES-sponsored evaluation of the UT leak path assessment methodology conducted at Pacific Northwest National Laboratory (PNNL). For this investigation, PNNL used a phased array UT system to acquire leak path data for an Alloy 600 CRDM nozzle, referred to as Nozzle 63, from the North Anna Unit 2 RPV head that was replaced in 2002. In-service inspection indicated that Nozzle 63 was leaking prior to the head replacement. Following the acquisition of UT data at PNNL, the nozzle was destructively examined to determine if the features identified in the UT examination could be visually confirmed.

The UT data from PNNL indicated a gap in the interference fit or potential leakage path on the downhill side of Nozzle 63, with suspected boric acid deposits on either side of the flow path. The data also indicated the presence of other partial leakage paths and scattered boric acid deposits. Destructive visual examination confirmed the presence of the leakage paths and boric acid deposits in the locations indicated by the UT data. Surface replication of the main leakage path on the RPV head revealed that fabrication machining marks were still visible, indicating minimal loss of material from boric acid corrosion. This suggests that wastage of the RPV head material is not necessary for a leak path be detected by the UT methodology. The results of this investigation are expected to help staff to interpret and evaluate licensees' ultrasonic leak path assessments for upper head penetrations.

Michael J. Case, Director
Division of Engineering
Office of Nuclear Regulatory Research
U.S. Nuclear Regulatory Commission

CONTENTS

ABSTRACT iii
FOREWORD v
FIGURES ix
TABLES xii
EXECUTIVE SUMMARY xiii
ACKNOWLEDGMENTS xv
ACRONYMS AND ABBREVIATIONS xvii
1 INTRODUCTION 1-1
2 NOZZLE PREPARATION 2-1
3 ULTRASONIC TESTING EQUIPMENT FOR NOZZLE 63 EXAMINATION 3-1
3.1 Phased-Array Electronics 3-1
3.2 Phased-Array Probe and Software Simulations 3-2
3.3 Scanner 3-6
4 CALIBRATION MOCKUP 4-1
4.1 Mockup Design and Fabrication 4-1
4.1.1 Simulated Boric Acid Deposits 4-2
4.1.2 Simulated Cracking, Cutting and Wastage 4-4
4.1.3 Mockup Assembly 4-7
4.2 Ultrasonic Evaluation of Mockup 4-10
4.2.1 Alloy 600 Tube Notches 4-10
4.2.2 Carbon Steel Notches 4-15
4.2.3 Simulated Boric Acid Deposits 4-18
4.2.4 Amplitude Response 4-20
5 NOZZLE 63 NONDESTRUCTIVE LEAK PATH ASSESSMENT 5-1
5.1 Scanner Setup 5-1
5.2 Data Acquisition 5-1
5.3 Amplitude Analysis 5-4
5.4 Industry Standard Nondestructive Evaluations 5-8
6 DESTRUCTIVE VALIDATION OF NOZZLE 63 6-1
7 CORRELATION OF ULTRASONIC AND DESTRUCTIVE RESULTS 7-1
8 ADDITIONAL PHYSICAL MEASUREMENTS ON THE REACTOR PRESSURE VESSEL HEAD 8-1
8.1 Boric Acid Measurements – Thickness Gage 8-1
8.2 Boric Acid Measurements – Microset Cross Sections 8-9

8.3 Replicated Surfaces – Stereomicroscope 8-10
9 SUMMARY AND CONCLUSIONS 9-1
10 REFERENCES 10-1
Appendix A – PRECISION EDM NOTCH INFORMATION A-1
Appendix B – THEORETICAL AND PRACTICAL INCONEL TUBE SHRINKAGE B-1
Appendix C – SUPPLEMENTAL INFORMATION ON DESTRUCTIVE CUTTING C-1

FIGURES

1.1 CRDM J-groove Weld Schematic 1-2

1.2 The Triple Point in the Assembly Where the Alloy 600 Nozzle, RPV Head, and Buttering Material Meet 1-3

2.1 As-Received Condition of Nozzle 63 2-1

2.2 Nozzle 63 with Painted Edges 2-2

2.3 Nozzle 63 Wrapped in Plastic for Contamination Control 2-2

2.4 Nozzle 63 on Modified Cart 2-3

2.5 Nozzle 63 with Hydraulic Rotary Pipe Cutting Tool 2-4

2.6 Cutting of Nozzle 63 Penetration Tube 2-4

2.7 CRDM Installed in Containment Glovebag 2-5

2.8 Final Configuration of CRDM Nozzle 63 for Examination 2-6

3.1 Data Acquisition System and Laboratory Workstation. Left: Tomoscan III phased-array data acquisition system. Right: Laboratory workstation/laptop computer for both data acquisition and data analysis, with the Tomoscan III system below. 3-1

3.2 5.0-MHz Phased-Array Probe 3-3

3.3 Annular Phased-Array Probe Attached to Scanner Arm 3-4

3.4 Side View—Left: Law Formation. Right: Sound Field Simulation for a Depth Focus of 15 mm (0.59 in.). Blue and red lines are measurement cursors from the origin defined as center of probe in X,Y and material face in Z. 3-4

3.5 C-Scan View at a Depth Focus of 15 mm (0.59 in.). Top: –6 dB spot size. Bottom: –3 dB spot size. Blue and red lines are measurement cursors from the origin defined as center of probe in X,Y. The cursors are positioned at the -6 and -3dB locations. 3-5

3.6 Scanner on Mockup Nozzle Specimen. Left: Scanner alone. Right: Scanner with PA probe attached sitting on the calibration mockup specimen. 3-7

3.7 Transducer Attachment 3-8

3.8 Scanning Setup/Orientation Schematic 3-9

3.9 Scanner System on Nozzle 63 in the Custom Glovebag 3-10

4.1 Assembled CRDM Interference Fit Mockup Specimen 4-2

4.2 Boric Acid Pattern Conceptual Design 4-3

4.3 Boric Acid Application. Left: Blue painter's tape was used to mask off boric acid regions on the nozzle. Right: The arrow indicates a region where boric acid was intentionally removed. 4-4

4.4 Interference Fit #2; Notch and Pattern Conceptual Design 4-5

4.5 EDM Notches in Alloy 600 Tube 4-6

4.6 EDM Notches on Carbon Steel Block 4-7

4.7 Filling Alloy 600 Tube with Liquid Nitrogen 4-8
4.8 PVC Spacer Shown at Bottom of Specimen 4-9
4.9 Assembled Calibration Specimen 4-10
4.10 Top View, Plan View, or C-scan Ultrasonic Image of the Upper Interference Fit Region Containing Calibration Notches in the Alloy 600 Tube. Calibration notches are circled. 4-11
4.11 D-scan End View of the Axial Resolution Notches in the Inconel Tube 4-12
4.12 B-scan Side View of the Circumferential Resolution Notches in the Inconel Tube 4-13
4.13 The Second Echo is Gated in the Side View Image in the Top of with the Horizontal Lines. The corresponding C-scan top view is displayed in the bottom image. This second echo captures a disturbance in the back-wall echo showing some depth information, noted by the red arrows at top. The yellow arrows note the depth-varying notches. 4-14
4.14 B-scan Side View on Top and C-scan Plan View on Bottom of the Width Varying Notches in the Inconel Tube 4-15
4.15 C-scan Plan View of the Notches in the Carbon Steel from the First Ultrasonic Echo. The calibration notches are circled. 4-16
4.16 C-scan Plan View of the Depth Notches in Carbon Steel, Circled on the Upper Right. This image was acquired from the first ultrasonic echo. 4-17
4.17 C-scan Plan View of the Depth Notches in Carbon Steel, Noted by Red Arrows on the Upper Right. This image was acquired from the second ultrasonic echo. 4-17
4.18 C-scan Plan View of the Width Notches in Carbon Steel, Noted by Red Arrows on the Bottom. This image was acquired from the second ultrasonic echo. 4-18
4.19 C-scan Plan View of the Boric Acid Deposits, Boxed in Red, in the Lower Interference Fit Region. The horizontal axis represents the circumferential range of 60–240 degrees. This image is from the first ultrasonic echo. 4-19
4.20 C-scan Plan View of the Boric Acid Deposits, Boxed in Red, in the Lower Interference Fit Region. The horizontal axis represents the circumferential range of 240–60 degrees. This image is from the first ultrasonic echo. 4-19
4.21 The Interference Fit Region Containing Boric Acid is Subdivided into Three Regions. The red box represents the presence of boric acid in the interference fit region, the black dashed boxes represent the tube region, and the black dotted boxes represent the interference fit region. 4-20
5.1 Alloy 600 Tube ID Response Before (left) and After (right) Centering the Scanner on the Nozzle. The horizontal axis represents approximately 180 degree and the vertical axis 20 mm (0.79 in.). 5-2
5.2 First PA Ultrasonic Data from Nozzle 63. The front surface or nozzle ID echo is on the top and the interference fit echo on the bottom. The horizontal axis represents the 86 to 274 degree area and the vertical axis represents 360 mm (14.17 in.). The color scale is represented on the far left. 5-3

5.3 PA Ultrasonic Data from the Interference Fit in Nozzle 63 Acquired After the Second Brushing of the Nozzle ID. The horizontal axis represents the full 360-degree area and the vertical axis represents 360 mm (14.17 in.). Black arrows indicate primary leak path. The left edge marks the –90 degree location and the right edge the 270 degree location. 5-4

5.4 Interference Fit Data Image After First Brushing. The horizontal axis represents approximately 90 to 270 degrees. The vertical axis represents 360 mm (14.17 in.). Boxed regions were used in an amplitude analysis. 5-5

5.5 Interference Fit Data Image After First Brushing. The horizontal axis represents approximately –90 to +90 degrees. The vertical axis represents 360 mm (14.17 in.). Boxed regions were used in an amplitude analysis. 5-6

5.6 Mean Amplitude Response from the Regions Indicated in Figures 5.4 and 5.5 5-6

5.7 A Tri-Color Representation of the Interference Fit Data. The dark blue represents a leak path or gap, the light blue represents the interference fit and counter bore regions and the white represents the weld and suspected boric acid presence in the interference fit. 5-8

5.8 Ultrasonic Data from Nozzle 63 as Obtained by WesDyne International. The image was acquired with a 5-MHz probe. The horizontal axis represents the nozzle circumference in units of degrees. The vertical axis represents the nozzle axis in units of millimeters. 5-9

5.9 Ultrasonic Data from Nozzle 63 as Obtained by WesDyne International. The image was acquired with a 2.25-MHz probe. The horizontal axis represents the nozzle circumference in units of degrees. The vertical axis represents the nozzle axis in units of millimeters. 5-9

6.1 Size Reduction Cutting Activity 6-1

6.2 Start of the Dissection Cut 6-2

6.3 Nozzle 63 Assembly Cut in Half by Dissection Cut. The red line indicates where the weld removal cut was made. 6-3

6.4 End of J-groove Weld Removal Cut 6-4

6.5 Exposed RPV Head and Nozzle from High Side Section 6-5

6.6 Exposed RPV Head and Nozzle from Low-Side Section 6-6

7.1 Nozzle Surface. The red line marks the interference fit region and the two black arrows identify the main leak path. 7-1

7.2 RPV Head Surface. The red line marks the interference fit region and the two yellow arrows identify the main leak path. 7-3

7.3 Ultrasonic Data Stretched to Best Match the RPV Head Photograph 7-3

8.1 Photograph of the RPV Head Material with Boric Acid Measurement Points. The interference fit region is marked by the red line. 8-2

8.2 Boric Acid Thickness Values in Microns 8-3

8.3 Ultrasonic Response Profile at Top, Acquired Along the Red Horizontal Line in the Image Below. The left image profile is in the interference fit and the right image profile is outside of the interference fit. 8-5

8.4 Ultrasonic and Boric Acid/Corrosion Layer Thickness Along a Line Across the Main Leak Path in the Interference (I) Fit. 8-6

8.5 Ultrasonic and Boric Acid/Corrosion Layer Thickness Along a Line Across the Main Leak Path Outside the Interference Fit. 8-7

8.6 Comparison of Ultrasonic Response and Boric Acid/Corrosion Layer Thickness at all 70 Acquired Data Points. 8-8

8.7 Comparison of Ultrasonic Response and Boric Acid/Corrosion Layer Thickness at the Leak Path and Bare Metal Data Points. 8-9

8.8 Comparison of Ultrasonic Response and Boric Acid/Corrosion Layer Thickness at Data Points Not in the Leak Paths Nor at Bare Metal Points. 8-9

8.9 Eight Areas Selected for Boric Acid Thickness Measurements on Cross-Sectional Slices of Microset Replica. 8-11

8.10 Leak Path Replica with Cuts and Pieces Identified. The interference fit region is noted with the black line and is contained in pieces 4 through 9. 8-12

8.11 Staining Streaks in the Leak Path Below the Interference Fit from Replica Pieces 2 and 3, Left and Right, Respectively. The red line represents 2.0 mm (0.80 in.) in length. 8-13

8.12 Transition from Below the Interference Fit to the Interference Fit Region. Machining marks are evident in this replica piece 4. The red line represents 2.0 mm (0.80 in.) in length. 8-13

8.13 Piece 5 from the Interference Fit Region Shows an Indication of a Scrape. In the left image the red line represents 2.0 mm (0.80 in.) in length. The image on the right at twice the magnification of the left shows more detail. 8-14

8.14 Corrosion Areas Observed Above the Interference Fit Region. The red line represents 2.0 mm (0.80 in.) in length. 8-14

TABLES

5.1 Mean Amplitude Responses (%). 5-7

EXECUTIVE SUMMARY

Research is being conducted for the U.S. Nuclear Regulatory Commission (NRC) at the Pacific Northwest National Laboratory (PNNL) to assess the effectiveness and reliability of advanced nondestructive examination (NDE) methods for the detection and characterization of flaws in nuclear power plant components. One area of concern is in primary water stress corrosion cracking (PWSCC) in the nickel-base alloys used in primary pressure boundary components in pressurized water reactors (PWRs). Nickel-based alloys exposed to reactor coolant in PWRs may experience a form of degradation known as PWSCC. One PWR component that has an operational history of PWSCC is the control rod drive mechanism (CRDM) nozzle. The CRDM nozzles are cylindrical penetrations in the upper reactor pressure vessel (RPV) head that allow for the insertion and removal of control rods. The penetration tube is held in place with an interference fit, and is seal-welded to the vessel head with a J-groove weld. Cracking in the nozzle or weld metal can allow borated water to leak to the top of the RPV head. Corrosion of the RPV head is a concern, as was discovered at Davis Besse, as is nozzle ejection in the presence of extensive circumferentially oriented cracking. In response to a number of occurrences of RPV head leakage, NRC regulations were updated to require PWR licensees to perform a demonstrated surface or volumetric leak path assessment of all J-groove welds in the RPV head.

The original construction materials for the CRDM nozzles at North Anna 2 were Alloy 600 base metal and Alloy 82/182 weld metal. During the Fall-2001 refueling outage, coolant leakage was noted near Nozzle 63. NDE showed crack-like indications near the J-groove weld and butter layer in the nozzles and shallow axial cracking on the inner diameter. The leaking welds were repaired with Alloy 52/152 material, thought to have higher PWSCC resistance than Alloy 82/182. Subsequent visual examination of the RPV head in the Fall-2002 outage again revealed leaking nozzles. The head was replaced and several nozzles including Nozzle 63 became available for study. The purpose of this investigation was to confirm features previously identified by industry in an ultrasonic evaluation with an equivalent or better examination and to validate the findings by opening the nozzle assembly to reveal the annulus surfaces.

This study resulted in a successful ultrasonic examination of the interference fit region of control rod drive mechanism Nozzle 63 from the North Anna Unit 2 power plant. A phased-array ultrasonic system was calibrated on a mockup specimen containing two interference fit regions. The probe spot size at the interference fit was modeled at 1.2 by 1.2 mm (0.04 by 0.04 in.) at the −6 dB level. Ultrasonic data from notches in the carbon steel material from one of the mockup interference fit regions showed system resolution at nominally 4 mm (0.16 in.) in both the axial and circumferential directions. Notches as shallow as 0.028 mm (0.0011 in.) were detected as well as notches as narrow as 0.80 mm (0.10 in.) in the circumferential direction. The second interference fit mockup contained regions with boric acid deposits. These regions were ultrasonically imaged and suggested that the ultrasonic responses could be segmented into three categories: 1) good interference fit, 2) interference fit with boric acid, and 3) leak path or gap based on the amplitude responses, mid-range, low and high, respectively.

Ultrasonic data were acquired on Nozzle 63 and clearly showed a variation of responses throughout the annulus region. The primary leak path at the downhill position of the nozzle was

imaged as a high-amplitude response that definitively spanned the annulus region, thus providing a path for borated water to reach the top of the head. Partial leak paths were also identified by their large-amplitude response and boric acid deposits by their low-amplitude response. A comparison of the PNNL ultrasonic images to data obtained by industry showed similar results.

After sectioning of the nozzle assembly to reveal the interference fit and photographing the exposed surfaces, the primary leak path was confirmed. Also confirmed was the excellent agreement of the ultrasonic images and revealed features on the annulus surfaces such as boric acid deposits.

Additional measurements were made to quantify the thickness of the boric acid deposits or corrosion layer on the RPV head. It was reasonable to assume that any gap in the annulus could fill with boric acid deposits. As the gap between Alloy 600 tube and low-alloy steel head varied so too did the boric acid thickness. The leak path or bare metal corrosion layer thickness throughout the annulus was 16 microns (0.63 mils) or less with ultrasonic responses greater than 65%. Boric acid apparently did not deposit in the leak path due to the flow of borated water through the area, and the large ultrasonic response indicates an air gap was present. On both sides of the primary leak path, the ultrasonic responses quickly drop off and the boric acid/corrosion layer increases. This inverse relationship with a sharp transition at the edge of the leak path defines one of the leak path characteristics. Another characteristic of a leak path is that it fully traverses the interference fit zone. The data additionally show that the boric acid/corrosion deposits outside of the primary leak path in the interference fit are below 75-microns (3.0-mils) thick and are assumed to be compacted due to the low ultrasonic response (less than 50%), indicating good energy transmission through the material. Conversely, the boric acid deposits outside of the primary leak path and above or below the interference fit are larger, in the 130–190 micron (5.12–7.48 mils) range. These deposits are likely not compacted as the ultrasonic responses are higher (greater than 50%) and indicate poor transmission or good reflectance as in the presence of an air gap or less dense material.

Lastly, the leak path region of the RPV head was replicated and limited confirmatory measurements made on the replica for boric acid thickness. The replica surfaces were imaged with a stereomicroscope and showed minor evidence of corrosion product streaking and little or no corrosion or wastage. Machining marks were clearly evident across the main leak path. Two small areas with minor corrosion were found above the main leak path with depths of 0.25 mm (0.01 in.). Attempts to remove the boric acid deposits on the RPV head to determine wastage underneath were unsuccessful, but dental pick probing indicated that all areas were sound. Therefore, in this leaking nozzle assembly, there was minimal corrosion or wastage occurring on the low-alloy steel RPV head, suggesting a low leakage rate.

ACKNOWLEDGMENTS

The work reported here was sponsored by the U.S. Nuclear Regulatory Commission (NRC) and conducted under NRC Job Code Number N6783. Greg Oberson is the NRC project manager. The Pacific Northwest National Laboratory (PNNL) would like to thank Dr. Oberson, Mr. Darrell Dunn and Mr. Jay Collins for their guidance throughout the course of this effort.

Dr. Stephen Cumblidge is acknowledged and thanked for initiating this project.

The authors acknowledge and thank J. W. Hyres, et al. at Babcock & Wilcox Technical Services Group in Lynchburg, Virginia, for cutting the nozzle assembly, for acquiring additional measurements on the head material, and for excellent photography and documentation of their work. A special thanks to Jim for his flexibility and willingness to try new approaches to obtain requested data is due.

The authors acknowledge and thank John P. (Jack) Lareau from WesDyne International for providing information on in-service inspections (ISI) and nozzle fabrication as well as data from an ISI on Nozzle 63.

The authors also thank Kay Hass, PNNL, for her diligence and patience in editing and preparing the manuscript.

PNNL is operated by Battelle for the U.S. Department of Energy under Contract DE-AC05-76RL01830.

ACRONYMS AND ABBREVIATIONS

ASME	American Society of Mechanical Engineers
BA	boric acid
BW	bandwidth
B&W	Babcock and Wilcox Technical Services Group
CFR	Code of Federal Regulations
CRDM	control rod drive mechanism
dB	decibels
EC	eddy current
EDM	electric discharge machining
EPRI	Electric Power Research Institute
FSH	full screen height
I Fit	interference fit
ID	inner diameter
IR	infrared
ISI	inservice inspection
LN	liquid nitrogen
LWR	light water reactor
NDE	nondestructive examination
NPP	nuclear power plant
NRC	U.S. Nuclear Regulatory Commission
OD	outer diameter
PA	phased array
PA-UT	phased-array ultrasonic testing
PE	pulse-echo
PNNL	Pacific Northwest National Laboratory
PT	liquid penetrant testing
PWR	pressurized water reactor
PWSCC	primary water stress corrosion cracking
PZR	pressurizer
RMSE	root mean squared error
RPL	radiochemical processing laboratory
RPV	reactor pressure vessel
RT	room temperature
RVH	reactor vessel head
SNR	signal-to-noise ratio
TLR	technical letter report

TOFD	time-of-flight diffraction
UT	ultrasonic testing

1 INTRODUCTION

Research is being conducted for the U.S. Nuclear Regulatory Commission (NRC) at the Pacific Northwest National Laboratory (PNNL) to assess the effectiveness and reliability of advanced nondestructive examination (NDE) methods for the detection and characterization of flaws in nuclear power plant components. One area of concern is in primary water stress corrosion cracking (PWSCC) in the nickel-base alloys used in primary pressure boundary components in pressurized water reactors (PWRs). Nickel-based alloys exposed to reactor coolant in PWRs may experience a form of degradation known as PWSCC. One PWR component that has an operational history of PWSCC is the control rod drive mechanism (CRDM) nozzle. As shown in Figure 1.1, the CRDM nozzles are cylindrical penetrations in the upper reactor pressure vessel (RPV) head that allow for the insertion and removal of control rods. The penetration tube is held in place with an interference fit, represented as the area labeled 'shrink fit zone' between the two horizontal dashed lines in the figure, and is seal-welded to the vessel head with a J-groove weld. Counter bore regions are not designed to be compression-fit zones between the nozzle and RPV head and are shown exaggerated in the drawing. Most CRDM nozzles originally placed into service in PWRs were fabricated from the nickel-based alloy referred to as Alloy 600, along with the Alloy 82 and 182 weld metals. PWSCC of a CRDM nozzle in a PWR was first identified in the Bugey Unit 3 plant in France during an over-pressurization test in 1991 (Economou et al. 1994). The crack initiated in the Alloy 600 base metal and propagated into the Alloy 182 weld metal. In late 2000 and early 2001, reactor coolant leakage to the RPV head from axial through-wall cracks in CRDM nozzles was identified at Arkansas Nuclear One Unit 1 and Oconee Unit 1 (Grimmel 2005). Follow-up inspections at Oconee Units 2 and 3 in 2001 identified axial and circumferentially oriented cracks. The circumferentially oriented cracks were of particular concern because of the possibility of nozzle ejection.

Leakage of borated water to the RPV head may occur as cracks initiate on the J-groove weld surface, propagate through the weld to the triple point, and allow water into the annulus region between the nozzle outer diameter (OD) and the RPV head. The triple point is diagrammed in Figure 1.2 and is the point at which the RPV head, buttering, and Alloy 600 CRDM tube meet. Once the boundary formed by an intact J-groove weld is compromised, there is the potential for a leakage path through the interference fit allowing reactor coolant to reach the outer surface of the RPV. The coolant can flash to steam, leaving boric acid deposits on the head and in the interference fit region around the leakage path. Additionally, a steam-cut leakage path through the interference fit and annulus may also be produced at operating temperature and pressure in a plant when a gap in the carbon steel RPV head at the uphill and downhill positions opens due to material expansions.

In response to the discovery of the CRDM cracks at Oconee Unit 3, in August 2001, the NRC issued Bulletin 2001-01, "Circumferential Cracking of Reactor Pressure Vessel Head Penetration Nozzles." PWR licensees were directed to evaluate the susceptibility of head penetration nozzles to PWSCC and to provide inspection plans to detect potential cracking. Thereafter, CRDM cracking was identified at additional PWRs including Davis Besse (Bennetch et al. 2002) and North Anna Unit 2 (NRC 2002). At Davis Besse, reactor coolant leakage led to significant wastage of carbon steel in a portion of the RPV head, leaving only a thin layer of stainless steel cladding at the pressure boundary. In response to the repeated occurrence of

RPV head leakage, in 2004 NRC issued EA-03-009 for PWR licensees requiring additional periodic inspections and evaluation of boric acid deposits as they pertain to the reasonable assurance of plant operational safety. The requirements of EA-03-009 were superseded by the adoption of American Society of Mechanical Engineering (ASME) Section XI Code Case N-729-1 by rulemaking in Title 10 of the Code of Federal Regulations (10 CFR) Part 50.55(a)(g)(6)(ii)(D)(1). As a condition in 10 CFR 50.55(a)(g)(6)(ii)(D)(3), licensees are directed to perform a "demonstrated" surface or volumetric leak path assessment of all J-groove welds in the RPV head.

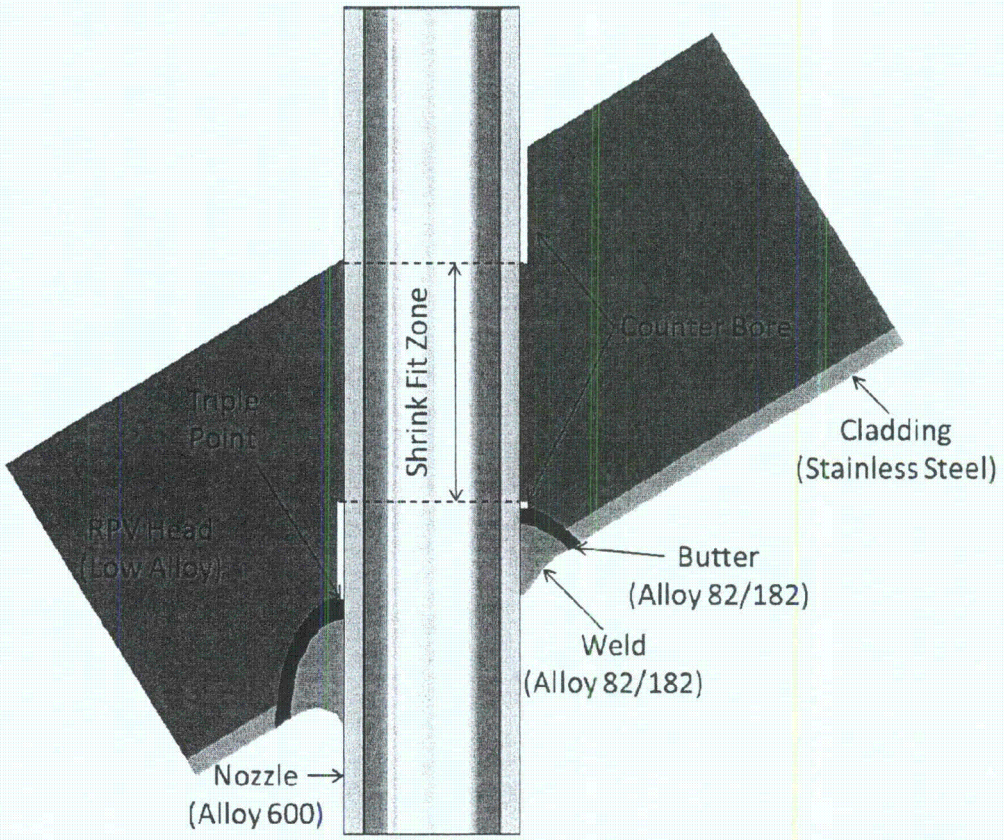

Figure 1.1 CRDM J-groove Weld Schematic

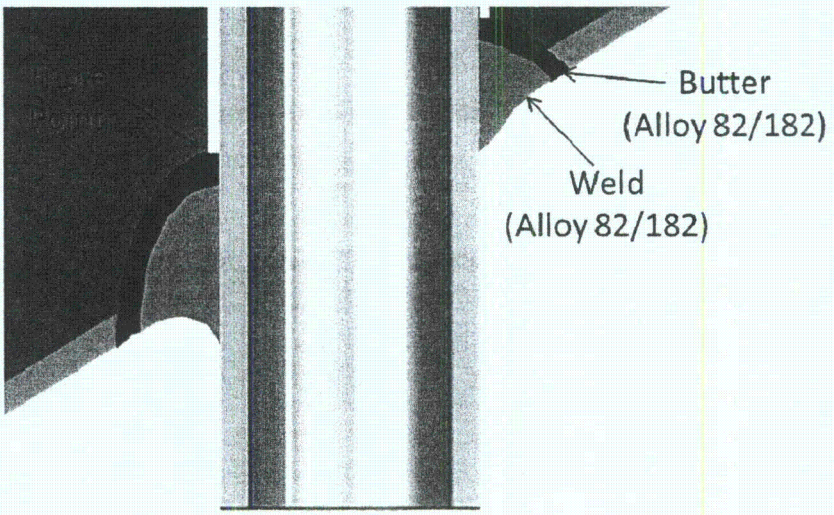

Figure 1.2 The Triple Point in the Assembly Where the Alloy 600 Nozzle, RPV Head, and Buttering Material Meet

A leak path assessment involves the use of an NDE technique, such as ultrasonic testing (UT), to determine whether a flow path exists through the interference fit that would allow reactor coolant to access the outside of the RPV head. The ultrasonic response from the interference fit examination will likely detect a leak path and may additionally detect corrosion or loss of material as well as the presence of boric acid in the annulus region. Industry groups, such as the Electric Power Research Institute (EPRI), are participating in programs to generically demonstrate the volumetric leak path assessment. As part of this initiative, EPRI obtained CRDM nozzles removed from operational service at the North Anna Unit 2 plant for further analysis and testing. North Anna Unit 2 is a three-loop Westinghouse PWR that was placed into service in 1980. The materials of construction for the original CRDM nozzles were Alloy 600 base metal and Alloy 82/182 weld metal.

Visual inspection of the outer surface of the North Anna Unit 2 RPV head during the Fall-2001 refueling outage indicated reactor coolant leakage in the proximity of penetrations 51, 62, and 63 as evinced by the presence of boric acid crystals (EPRI 2005). NDE of the nozzles showed crack-like indications near the J-groove weld/butter layer in the nozzles and shallow axial cracking on the inner diameter. The leaking welds in these nozzles were repaired using a temper bead repair technique with nickel-based Alloys 52 and 152, which are thought to have higher PWSCC resistance than Alloy 182. Subsequent visual examination of the RPV head during the Fall-2002 outage revealed 6 CRDM nozzles that were suspected of leaking and 21 that were masked to the extent that their status could not be determined. Eddy current and ultrasonic examinations showed numerous axial and circumferential indications in the nozzles, including those repaired during the previous outage. Given the extensive degradation of the RPV head, the utility made the decision to replace the head during the 2002 outage and make it available for further examination and study. EPRI took possession of six CRDM nozzles from the removed head including nozzles 10, 31, 51, 54, 59, and 63, which were transferred to

PNNL. Several of these nozzles were subsequently studied by EPRI and the NRC including nozzles 10, 31, 54, and 59 (EPRI 2006; Cumblidge et al. 2009).

The subject of this report is a leak path assessment of Nozzle 63 from North Anna Unit 2. This nozzle is of additional interest because of the Alloy 52/152 weld repair during the Fall-2001 outage. The purpose of this investigation is to determine whether features identified by a UT examination of the nozzle, including leak paths, voids, and the presence of boric acid in the interference fit, are confirmed by destructive analysis. The UT process is assumed to be equivalent to or better than that used in industry examinations. The radiological and mechanical steps taken to configure the nozzle for the ultrasonic evaluation are discussed in Section 2. Section 3 presents technical information on the ultrasonic transducer, the system electronics, and mechanical scanner. The calibration mockup specimen is described in Section 4 and consists of a notched specimen and a specimen with boric acid in the interference fit. Ultrasonic data on the mockup specimens are presented and system resolution and flaw detection capabilities are discussed. The ultrasonic evaluation of Nozzle 63 and corresponding results are presented in Section 5. Section 6 documents the cutting activities on the nozzle assembly to reveal the interference fit. Initial views of the annulus region are shown. Section 7 compares the ultrasonic findings to the visual evaluation of the interference fit. Section 8 contains additional measurements on the RPV head including boric acid thickness measurements in the annulus and Microset replication of the primary leak path region. Lastly, a summary of the findings are presented in Section 9 and conclusions that can be drawn at this time. Section 10 gives references cited in this report.

2 NOZZLE PREPARATION

When received at the Pacific Northwest National Laboratory (PNNL), the control rod drive mechanism (CRDM) Nozzle 63 from the North Anna Unit 2 reactor consisted of a flame-cut section of the upper reactor pressure vessel (RPV) head and a full-length Alloy 600 penetration tube, as shown in Figure 2.1. The CRDM was removed from its storage box and a radiologic survey performed. The flame-cut edges of the RPV head around the penetration were then painted with two coats (the first yellow, the second red) of a flexible, air-dried plastic coating from Plasti Dip to reduce the risk of workers being cut while handling the CRDM (Figure 2.2). An expandable 7.62-cm (3-in.) plug was inserted in the wetted side of the penetration tube so the tube could be filled with water. In retrospect, it would have been better to cut the nozzle prior to inserting the plug. This may have reduced some of the debris that first coated the ultrasonic scanner (see Section 5.2). With the plug inserted, the nozzle was wrapped in plastic (Figure 2.3) and bagged to contain contamination during the nozzle cutting. The nozzle was then secured on a wheeled cart that was modified to allow the penetration tube to be kept vertical during the testing, as seen in Figure 2.4.

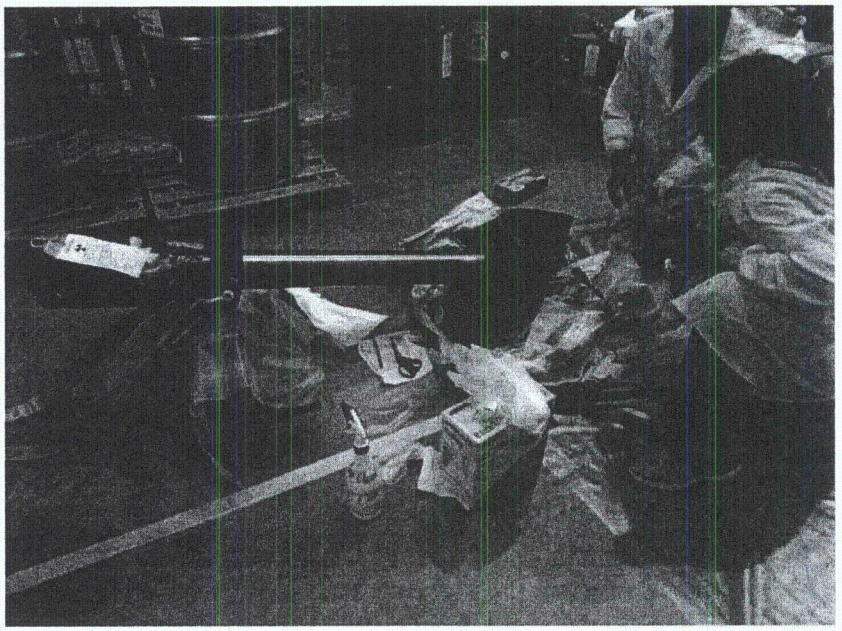

Figure 2.1 As-Received Condition of Nozzle 63

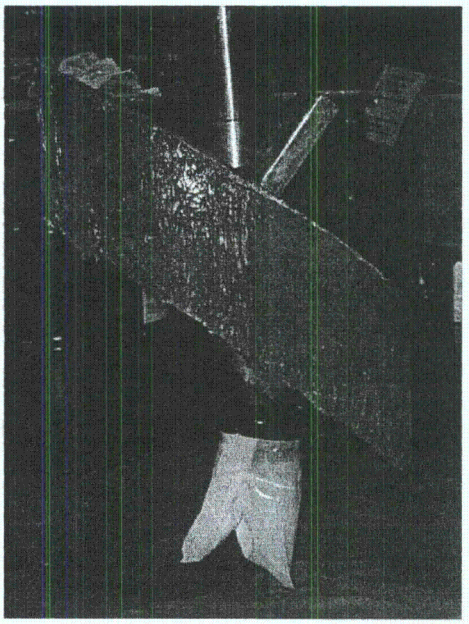

Figure 2.2 Nozzle 63 with Painted Edges

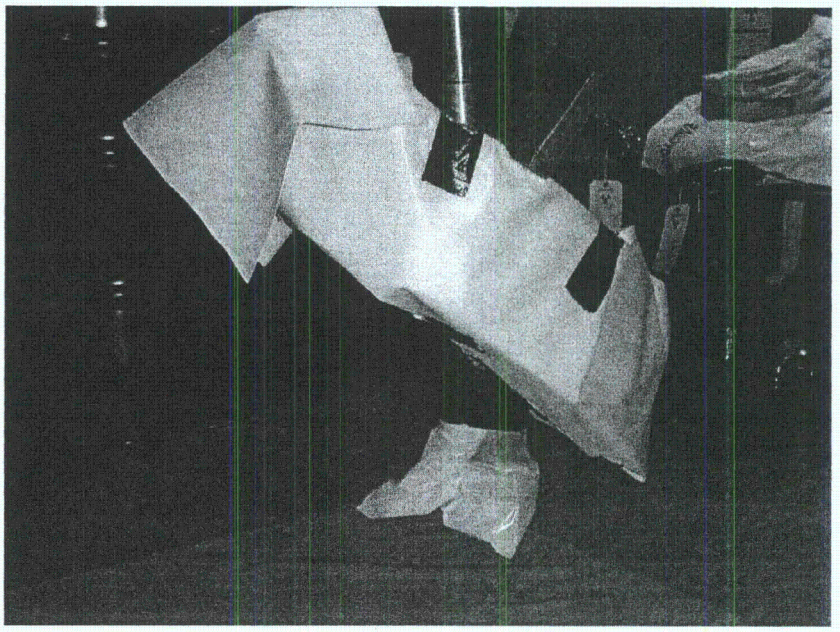

Figure 2.3 Nozzle 63 Wrapped in Plastic for Contamination Control

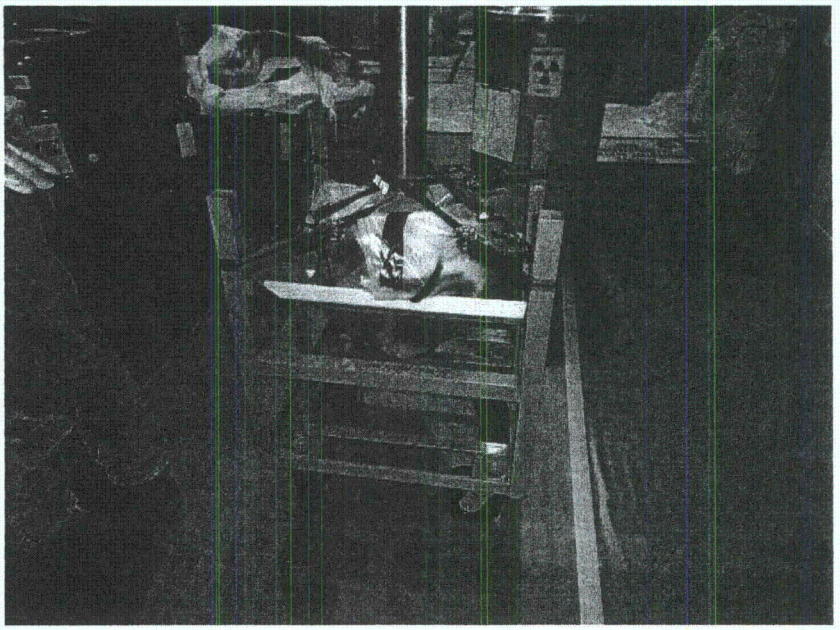

Figure 2.4 Nozzle 63 on Modified Cart

In order to better fit in a glovebag for contamination-control purposes and to facilitate connection of the scanner, approximately 61 cm (2 ft) of the penetration tube had to be removed. A catch pan was first fitted around the penetration tube below where the cut was to be made, approximately 30 cm (12 in.) above the RPV steel. A hydraulic rotary pipe-cutting tool was then fitted around the penetration tube as shown in Figure 2.5. The penetration tube and catch tray were wrapped in plastic to provide contamination control. The hydraulic cutting tool was connected and the first attempt at cutting the tube was made (Figure 2.6). A "hard spot" was encountered within the nozzle and two cutting heads broke before the decision was made to attempt a new cut approximately 2.54 cm (1 in.) above the previous cut attempt. Cutting proceeded without any other issues in this new location. The removed section of the penetration tube was placed into a 55-gallon drum for storage.

After cutting, the CRDM was completely wrapped in plastic to prevent the spread of contamination. The CRDM was then transported to the Radiochemical Processing Laboratory (RPL/33) where a containment glovebag had been assembled to house the nozzle. The cart with the nozzle was wheeled into the glovebag as shown in Figure 2.7. Once the nozzle was properly positioned, the two-axis scanner with attached ultrasonic phased-array probe was lowered through an upper access port and centered onto the penetration tube. The scanner was secured to the penetration tube using three set screws. The main door and the upper access port were sealed and the control cables secured to the upper frame. Approximately 1.5 liters of distilled water was added to the penetration tube. The final configuration of the scanner in the glovebag is shown in Figure 2.8.

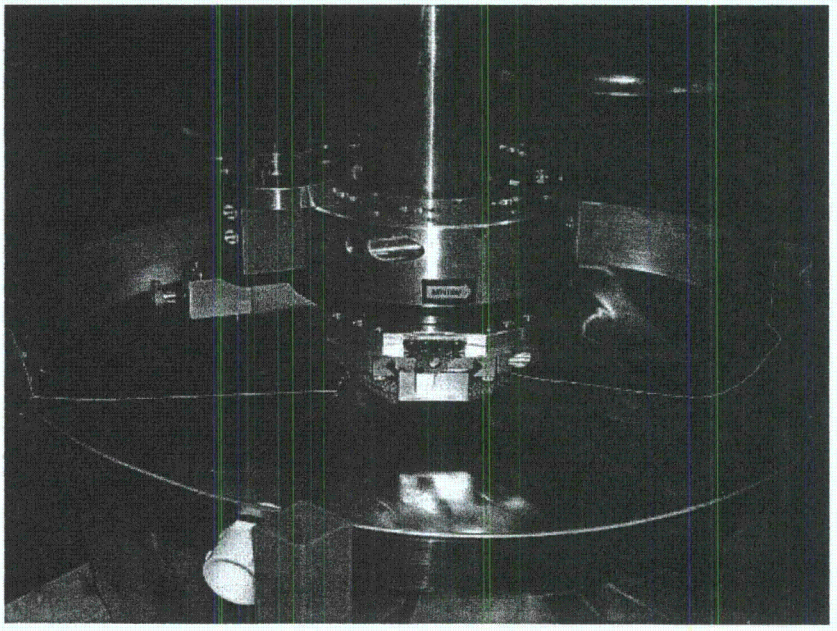

Figure 2.5 Nozzle 63 with Hydraulic Rotary Pipe Cutting Tool

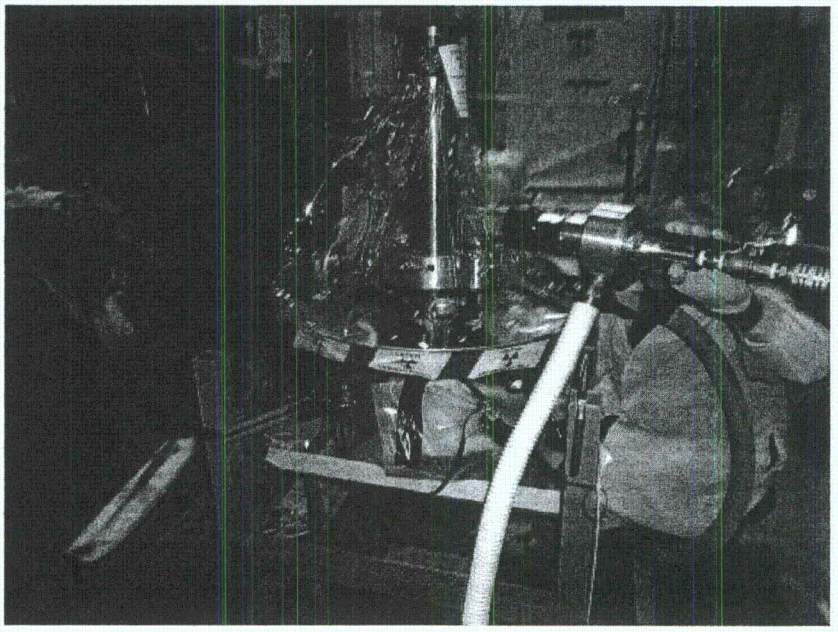

Figure 2.6 Cutting of Nozzle 63 Penetration Tube

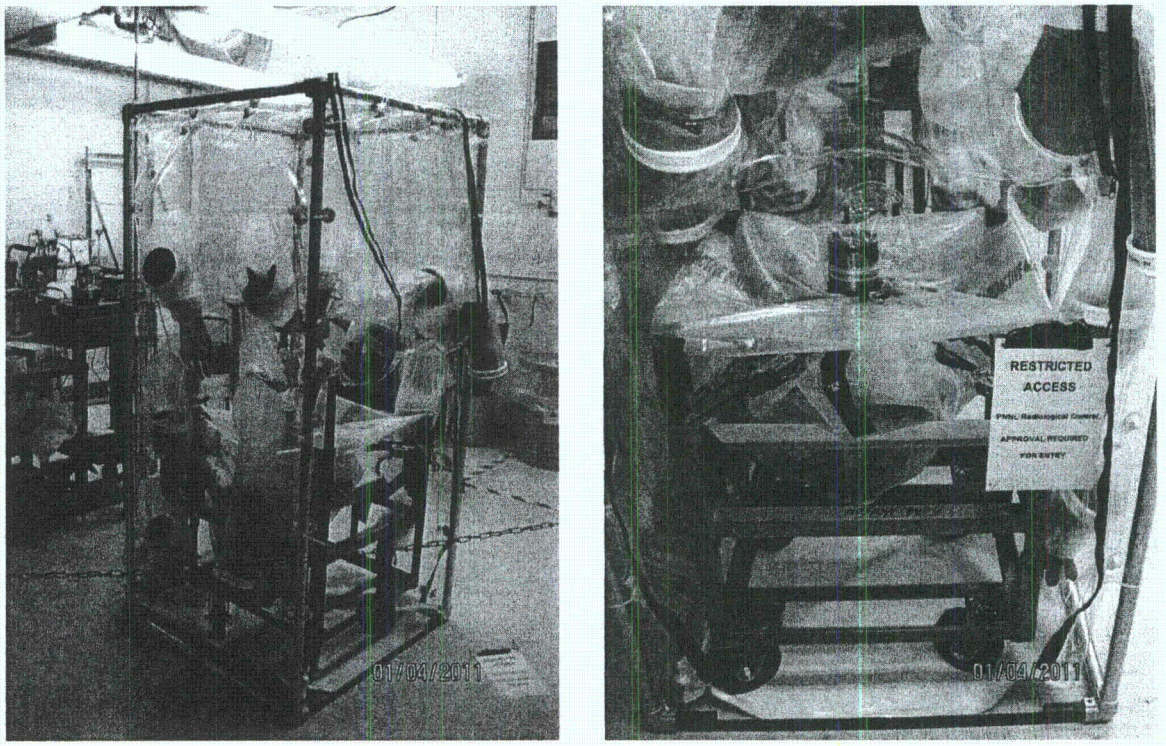

Figure 2.7 CRDM Installed in Containment Glovebag

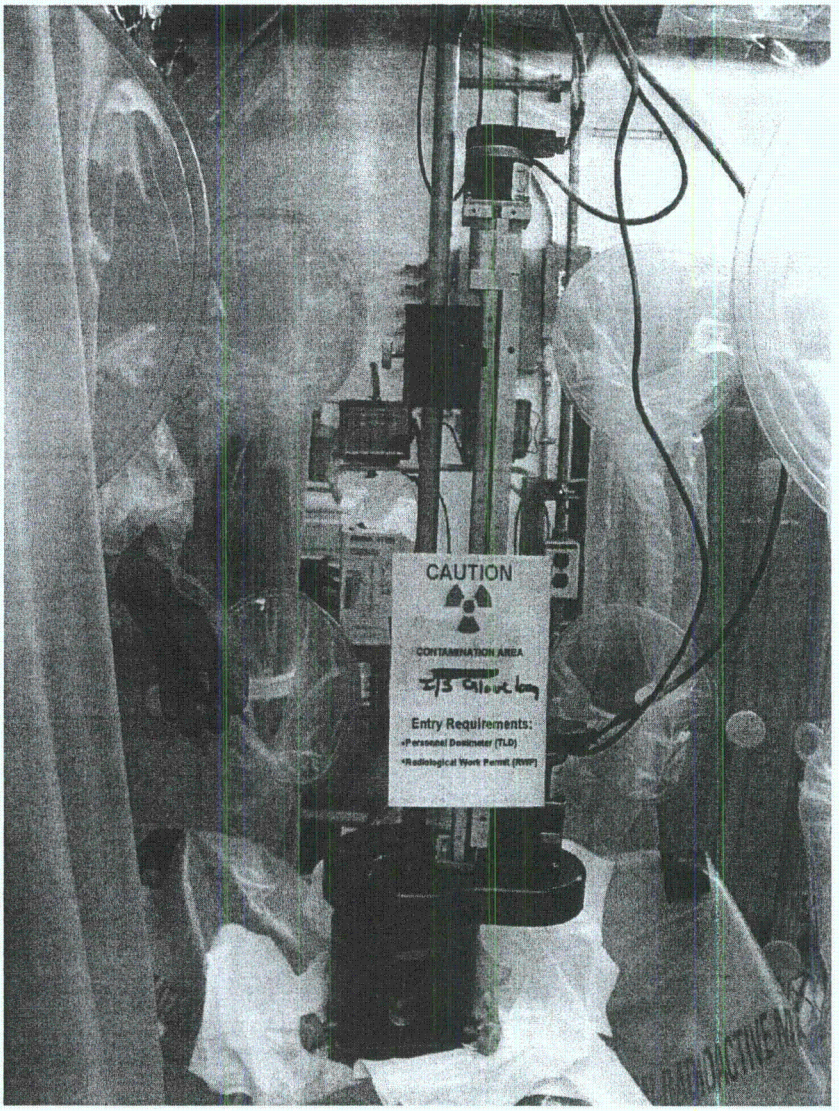

Figure 2.8 Final Configuration of CRDM Nozzle 63 for Examination

3 ULTRASONIC TESTING EQUIPMENT FOR NOZZLE 63 EXAMINATION

The nondestructive leak path assessment of Nozzle 63 was performed at the Pacific Northwest National Laboratory (PNNL) with an ultrasonic phased-array (PA) probe. A PA probe has multiple individual elements that are electronically fired at prescribed time delays to form a coherent and focused beam at a specified depth and angle in the material under examination. The equipment used for this investigation was selected because it is similar to or better than equipment used by industry for in-service inspections of upper reactor pressure vessel (RPV) nozzle penetrations in pressurized water reactors (PWRs). A detailed description of the equipment is provided in this section.

3.1 Phased-Array Electronics

Ultrasonic data acquisition for Nozzle 63 was accomplished using the ZETEC Tomoscan III phased-array system to control the PA probe employed in this study. This commercially available system was equipped to accommodate a maximum of 64 channels of data from PA probes and was operated with UltraVision 1.2R4 software. Its frequency pulsing electronics can drive probes in the 0.7–20 MHz range. The system is capable of accepting multiple axis positional information from external encoders to map ultrasonic data to spatial location on a specimen. The data acquisition system is shown in Figure 3.1.

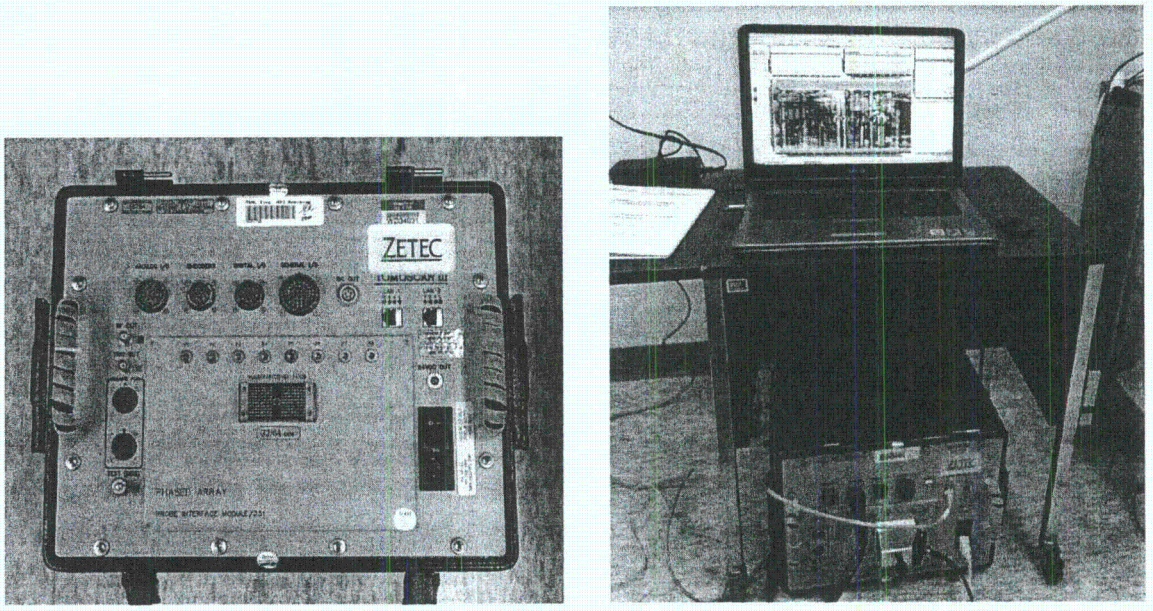

Figure 3.1 Data Acquisition System and Laboratory Workstation. Left: Tomoscan III phased-array data acquisition system. Right: Laboratory workstation/laptop computer for both data acquisition and data analysis, with the Tomoscan III system below.

3.2 Phased-Array Probe and Software Simulations

Nozzle 63 was examined with a pulse-echo (PE) longitudinal-wave immersion phased-array probe with a center frequency of 5 MHz, as shown in Figure 3.2. The PA probe was designed in a 1-D annular configuration using eight elements. The probe contained elements in a Fresnel radius pattern starting with a radius of 3 mm (0.12 in.) up to the final element radius of 9.72 mm (0.38 in.). Thus, the total aperture was 296.81 mm^2 (0.46 $in.^2$). As characterized by the manufacturer, Imasonic, the probe exhibited an overall 71% bandwidth at −6 decibels (dB) with all eight elements and an overall central frequency of 5.4 MHz. This design was chosen for enhanced depth focusing capabilities. Its beam-forming capabilities showed a satisfactory insonification of the interference fit region of interest as well as the ability to propagate a coherent ultrasonic beam deep into the weld region. Figure 3.3 shows the probe attached to the scanning arm.

Before the PA probe was used for the examination, a set of focal laws was produced to control the firing of individual elements. The focal laws were inputs to the UltraVision control software, which determined specific elements to excite at specific times to allow for proper beam-forming in the material. The focal laws may also contain details about insonification angles, the focal depth of the sound field, the delays associated with the wedge and electronics, and the orientation of the probe. For this investigation, a software package contained in the UltraVision software program suite, known as the ZETEC Advanced Focal Law Calculator 1.2R4, was used to produce the focal laws. The software program generated focal laws and simulated the ultrasonic field produced by the probe when using the generated laws. The user entered the physical information about the PA probe and wedge into the program, including the number and size of probe elements, and the wedge angle and size. After the desired angles and focal distances were entered, the software generated the needed delays for each element to produce the desired beam steering and focusing in the material. The software beam simulation produced a simple ray-tracing image of the probe, wedge, and material under evaluation, as well as a density mapping of the modeled sound field. The sound field mapping enabled the user to see how well the sound field was formed with the given input parameters. The probe was also evaluated for the generation of grating lobes that may be detrimental to the examination. It should be noted that the software simulation was performed using an isotropic material assumption; namely, that the velocity of sound is maintained throughout any angle for a particular wave mode. The simulations enabled the user to estimate sound field parameters and transducer performance to optimize array design and focal law development.

Typical control rod drive mechanism (CRDM) nozzles made from Alloy 600 have a tube wall thickness on the order of 15–17 mm (0.59–0.67 in.). Because the targeted area of interest in this study was the interference fit in the annulus between the outer diameter (OD) of the nozzle and the RPV head, it was important to design a PA probe capable of depth focusing into this region. Prior to probe fabrication, sound field simulations were conducted using the Phased Array Calculator 1.2R4 software program and the design parameters to simulate a projected sound field into an isotropic material with acoustic properties of Alloy 600. Figure 3.4 shows a side view representation of the focal laws generated on the left and a sound field simulation on the right for a target depth focus of 15 mm (0.59 in.). The gray-green regions at bottom represent the Alloy 600 material and the dark blue regions represent water as labeled. In this

immersion scanning setup, water was used as the 'wedge' material. The red horizontal line at 15.1 mm (0.59 in.) represents the target focal region. The simulation showed a favorable sound field density at the desired focal depth.

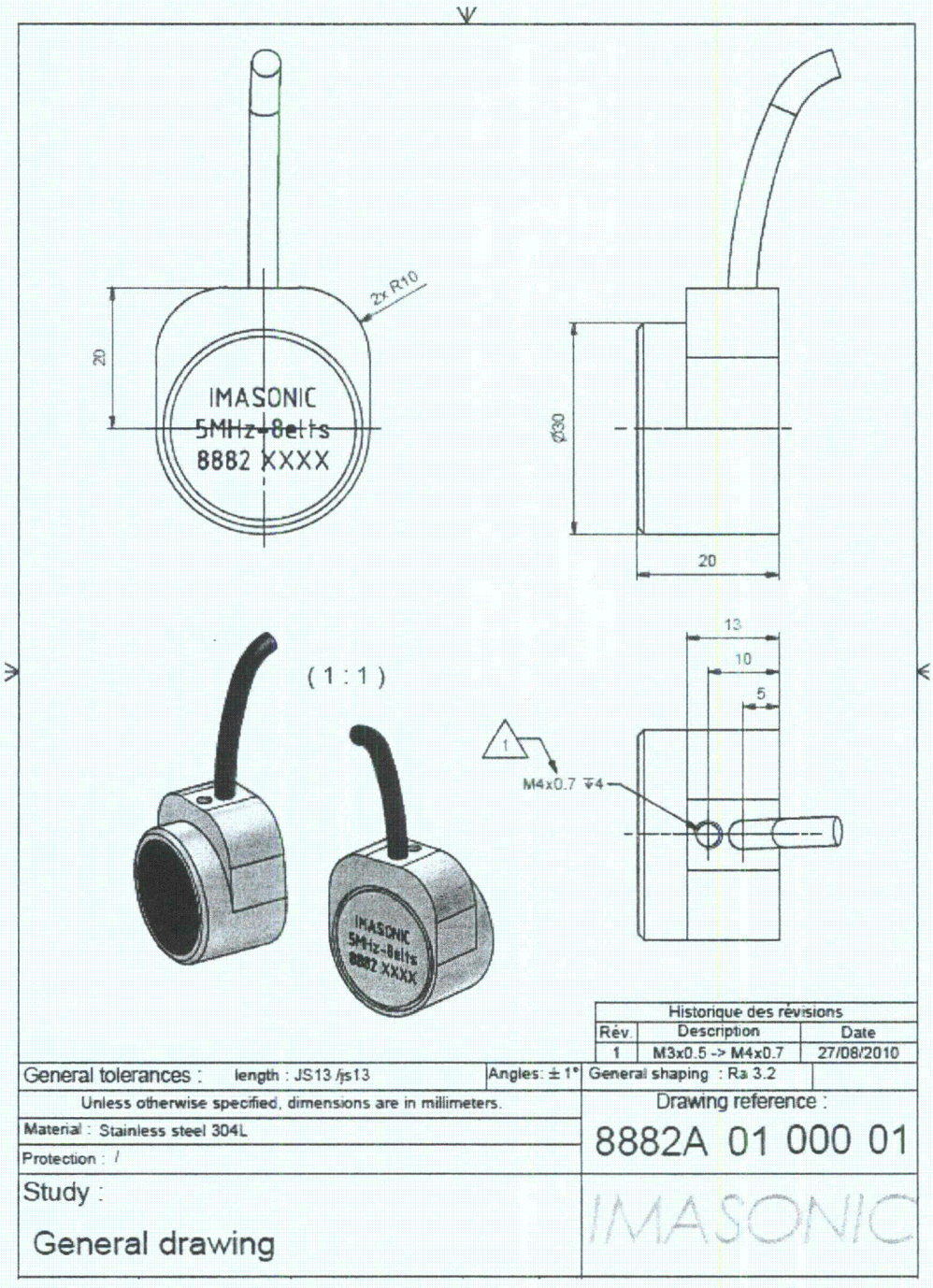

Figure 3.2 5.0-MHz Phased-Array Probe

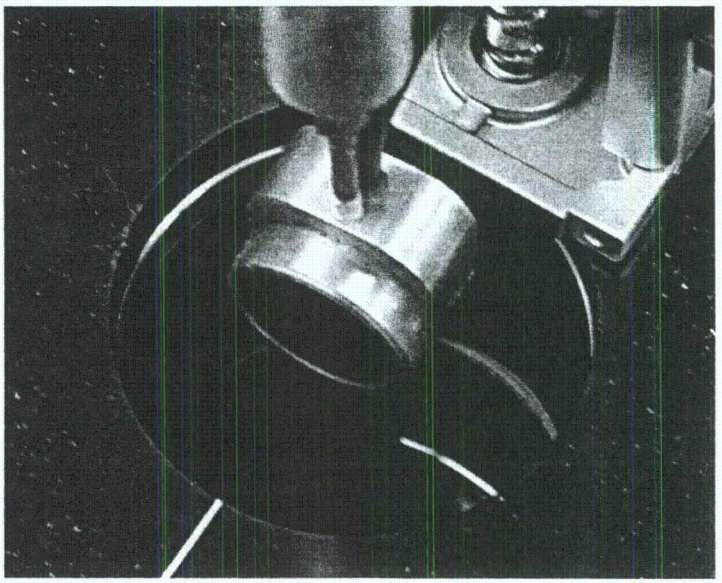

Figure 3.3 Annular Phased-Array Probe Attached to Scanner Arm

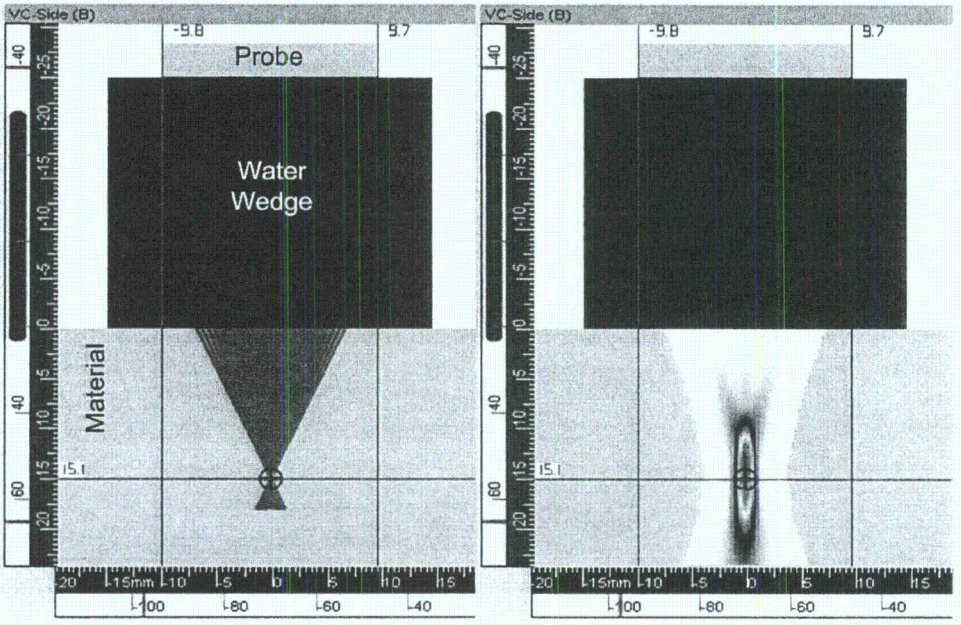

Figure 3.4 Side View—Left: Law Formation. Right: Sound Field Simulation for a Depth Focus of 15 mm (0.59 in.). Blue and red lines are measurement cursors from the origin defined as center of probe in X,Y and material face in Z.

The simulations viewed from the top or C-scan view gave information on the overall spot size in the scan and index axes of the formed beam at a particular depth. As seen in Figure 3.5, the predicted −6 dB (50%) and −3 dB (70.7%) spot sizes for the phased-array probe focused at a

depth of 15 mm (0.59 in.) in Alloy 600 material were 1.2 × 1.2 mm (0.047 × 0.047 in.) and 1.0 × 1.0 mm (0.04 × 0.04 in.), respectively. Additional sound field simulations were modeled at 1.0 mm (0.04 in.), corresponding to the tube inner diameter (ID) and 30 mm (1.18 in.) (15 mm [0.59 in.] into the J-groove weld region). The −6 dB spot size for depth foci of 1 and 30 mm (0.04 and 0.59 in.) were 0.6 × 0.6 mm (0.024 × 0.024 in.) and 2.0 × 2.0 mm (0.079 × 0.079 in.), respectively. The −3 dB spot sizes were 0.4 × 0.4 mm (0.016 × 0.016 in.) and 1.4 × 1.4 mm (0.055 × 0.055 in.), respectively.

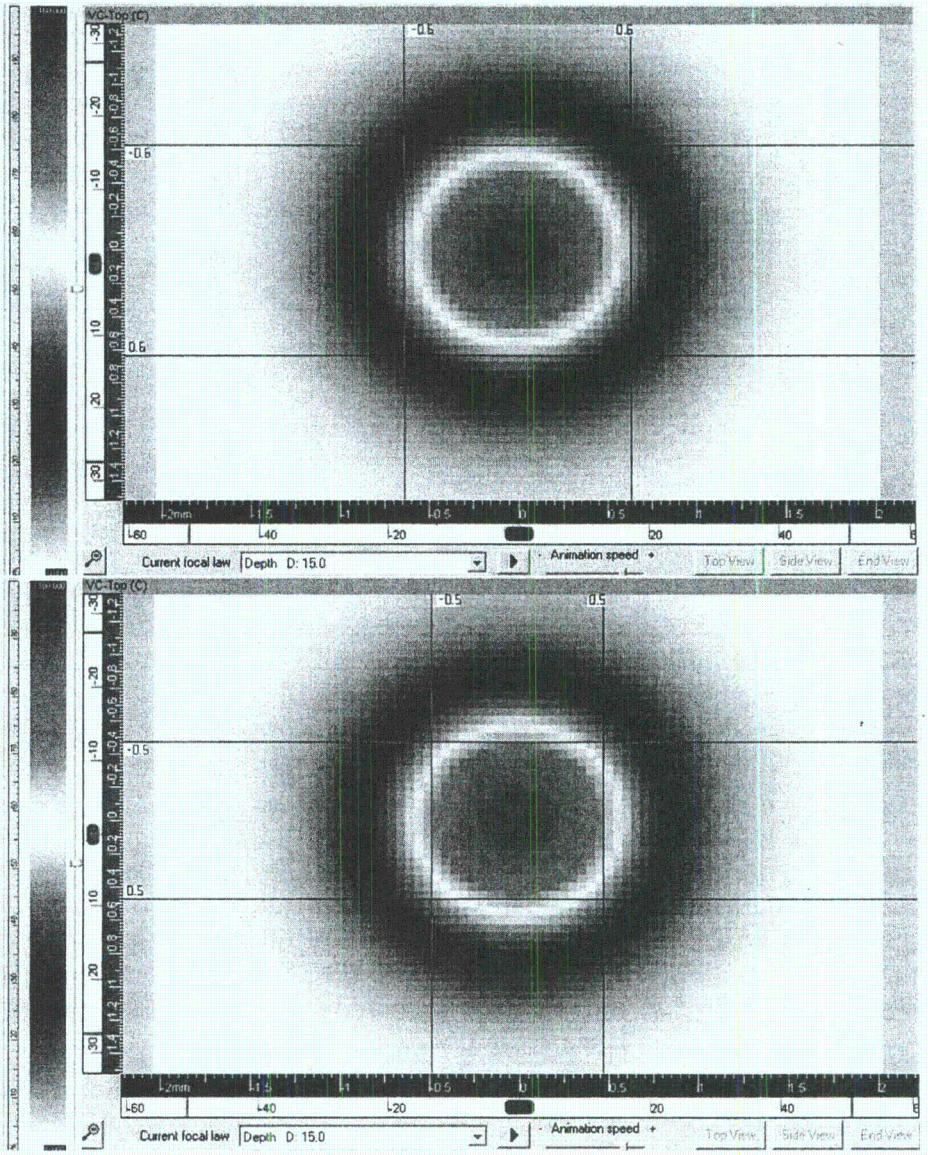

Figure 3.5 C-Scan View at a Depth Focus of 15 mm (0.59 in.). Top: −6 dB spot size. Bottom: −3 dB spot size. Blue and red lines are measurement cursors from the origin defined as center of probe in X,Y. The cursors are positioned at the -6 and -3dB locations.

3.3 Scanner

The theta-Z scanning apparatus for examining the annulus region of the nozzle from the ID of the penetration tube was constructed by Brockman Precision Machine and Design located in Kennewick, Washington. The ID scanner was designed for inner-surface scanning with ultrasonic probes but could be adapted and used with other sensor technologies. The scanner system was built to attach directly and securely onto the nozzle, centered by three set screws spaced evenly around the collar of the scanner. Figure 3.6 shows photographs of the scanner sitting on a nozzle mockup specimen. The scanner had a linear, Z or vertical axis for movement along the length of the nozzle and a rotational or theta axis for rotation around the nozzle. Motion of the scanner was controlled by two pulse-counter or stepper motors. Optical eye shaft encoders with a sensitivity of 2500 counts per revolution were attached to each motor. The calibrated positional information attained via the slave encoders was routed directly into the ultrasonic system and correlated with the ultrasonic testing (UT) data. The maximum range of motion along the nozzle length was 457.2 mm (18 in.). The rotational motion was continuous with no fixed limits, but was practically constrained to approximately 1.5 revolutions by the cables attached to the motor drivers, encoders, and the PA probe.

The scanner system was controlled using a custom-designed software program interfaced with a pulse-counter motor control system. A menu in the program allowed the user to 'jog' the scanner to a desired position. This feature was useful for setup, mapping the desired scan bounds as well as calibrating the UT signal response at certain locations. The customizable scanning sequence menu allowed the user to specify the scan and index range and resolution settings. Additionally, speed settings were tailored to acquire data with consistency and within the UT data acquisition system limits.

Prior to scanning, the nozzle was oriented vertically, plugged with a water-tight seal in the bottom end, and then filled with distilled water. In immersion scanning, water serves as both the wedge material and the ultrasonic couplant material. The water was given 24 hours or more to degas/de-bubble. Next, the ID of the nozzle specimen was gently brushed to remove bubbles that formed and attached to the ID wall region. Because air bubbles have a strong ultrasonic impedance mismatch to water or steel, it was important to remove them from the ID surface prior to scanning to minimize reflection or distortion of the ultrasonic energy.

The scanner was lowered onto the top of the nozzle specimen, centered, and secured by uniformly tightening the three set screws in the collar. Centering the scanner apparatus allowed the transducer arm to be positioned at the center of the nozzle tube so that a constant sound path was maintained during a circumferential scan sweep to reduce signal walk. The phased-array probe was then affixed to the 762-mm (30-in.) scanner arm using an M4 threaded rod running directly into the transducer housing and attached to the vertical axis via a set screw, as shown in Figure 3.7. The transducer face was orientated such that the ultrasonic beam was propagating radially outward towards the annulus or weld region. Using a set screw to hold the scanner arm enabled manual positioning of the probe in the vertical axis for increased versatility.

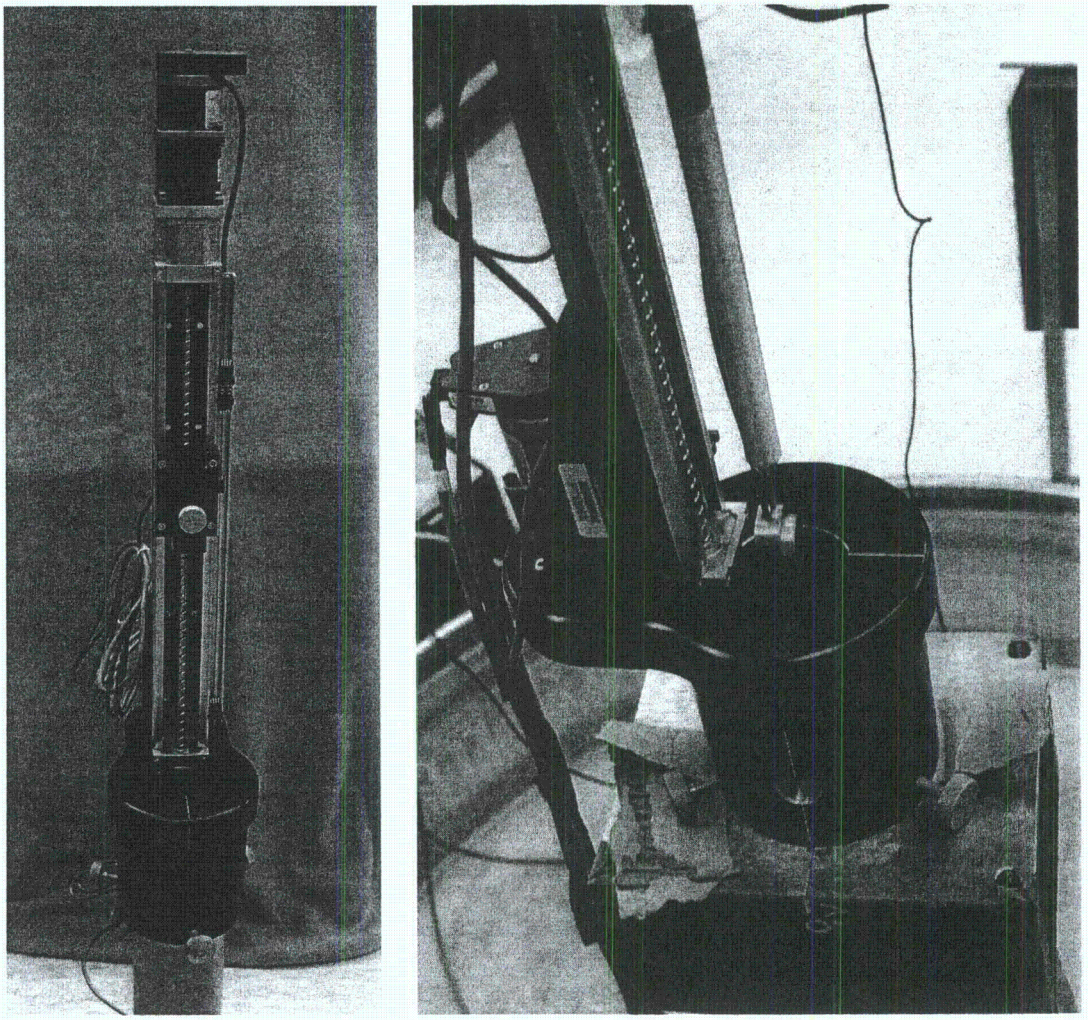

Figure 3.6 Scanner on Mockup Nozzle Specimen. Left: Scanner alone. Right: Scanner with PA probe attached sitting on the calibration mockup specimen.

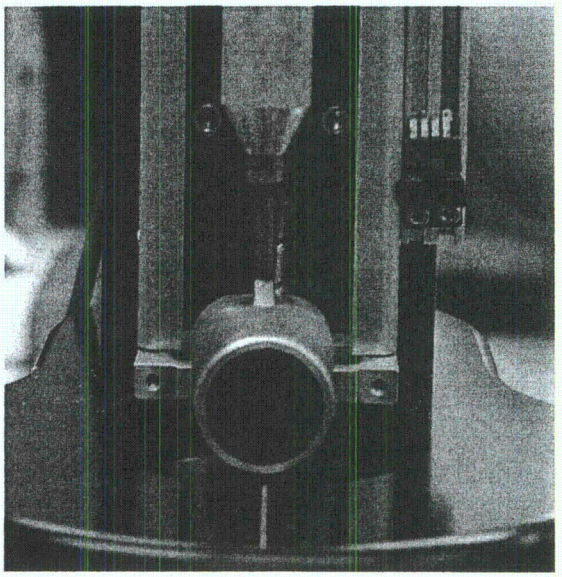

Figure 3.7 Transducer Attachment

The scanning sequence used the rotational or circumferential direction as the scan axis and the vertical direction as the index axis. The positive scan direction was established to be counter clockwise and the positive index was defined as vertically upwards. Positional resolutions were set to 0.25 degrees in the scan and 0.5 mm (0.02 in.) in the index directions for scanning the calibration mockup specimen. For output file size management, Nozzle 63 scanning protocol used 0.5 degrees by 0.5-mm (0.02-in.) resolutions in the scan and index directions, respectively. Figure 3.8 shows a detailed scanning setup schematic on a CRDM nozzle assembly.

For radiological control, a custom glovebag (details discussed in Section 2) was constructed around Nozzle 63 to reduce radiation contamination to persons or equipment. Setup in the glovebag required modifications to the glovebag so that scanner and phased-array cables and equipment could be passed in while maintaining connection to vital equipment such as the phased-array electronics and motor control units. Figure 3.9 depicts the scanner system fully assembled in the protective glovebag environment.

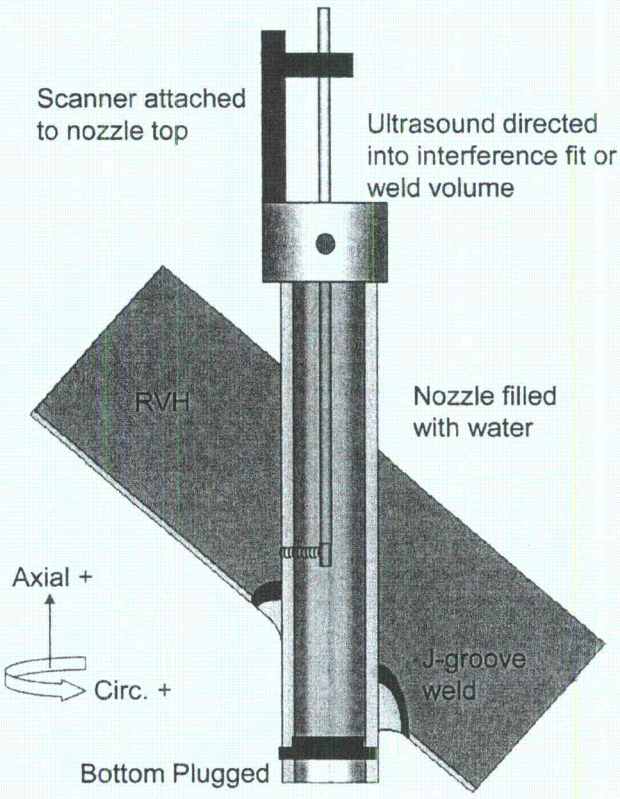

Figure 3.8 Scanning Setup/Orientation Schematic

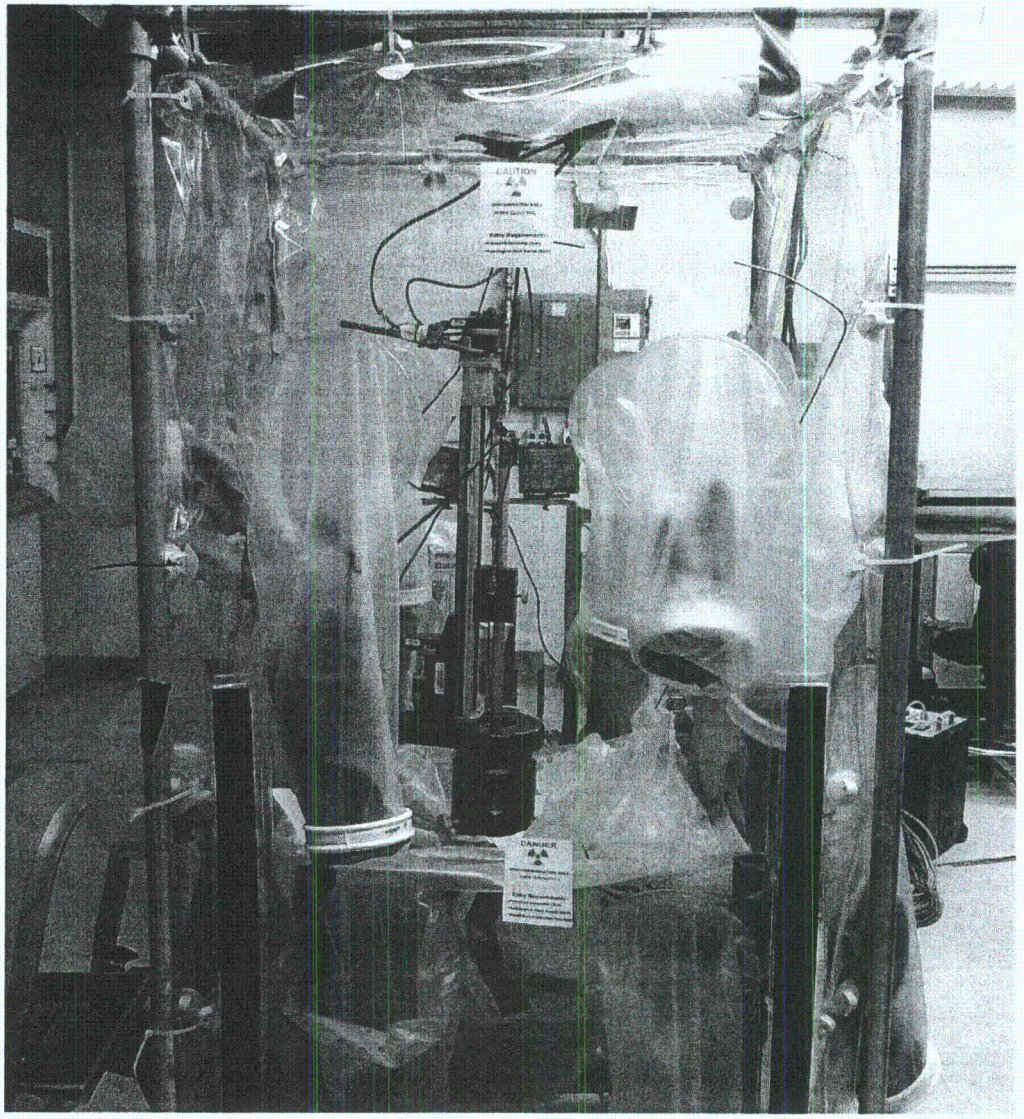

Figure 3.9 Scanner System on Nozzle 63 in the Custom Glovebag

4 CALIBRATION MOCKUP

Prior to performing the non-destructive leak path assessment of Nozzle 63, a control rod drive mechanism (CRDM) mockup was constructed at Pacific Northwest National Laboratory (PNNL) for calibration of the ultrasonic testing equipment and to assess its capability to identify features associated with primary water leakage. These include crystalline boric acid in the interference fit region, wastage or corrosion of the low alloy steel reactor vessel head material, and cracking or degradation of the Alloy 600 nozzle material. A description of the mockup and testing is presented in this section.

4.1 Mockup Design and Fabrication

The CRDM mockup was made from an Alloy 600 tube fitted with two 152-mm (6-in.)-thick carbon steel blocks. The mockup was designed to simulate the interference fit between the CRDM nozzle and the reactor pressure vessel (RPV) head material in a pressurized water reactor (PWR), using similar materials and fabrication techniques. The mockup had two interference fit regions as shown in Figure 4.1. In the top interference fit, notches were made on the outer diameter (OD) of the tube and on the carbon steel blocks with electric discharge machining (EDM) to simulate cracking, wastage, and degradation of the materials. In the bottom interference fit, crystalline boric acid was placed between the tube and the carbon steel blocks to simulate deposits left by primary water leakage. To prevent tipping of the mockup, the flange end of the tube was bolted to a larger plate for increased stability.

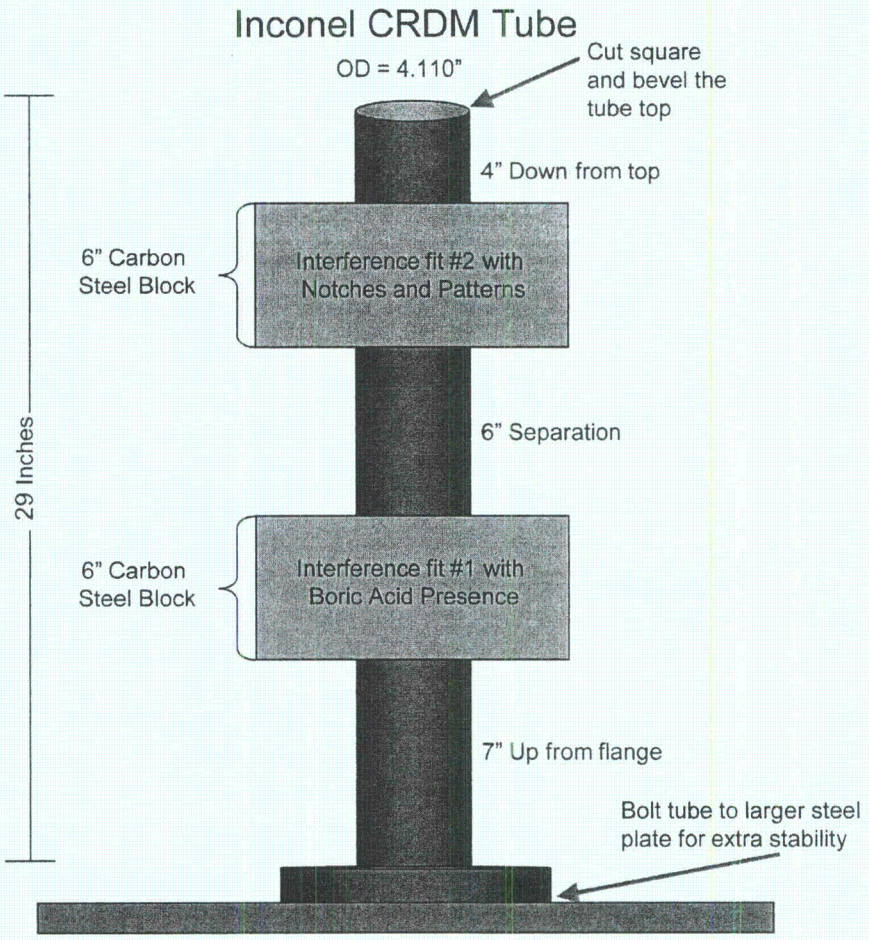

Figure 4.1 Assembled CRDM Interference Fit Mockup Specimen

4.1.1 Simulated Boric Acid Deposits

The lower interference fit on the CRDM nozzle mockup contained crystalline boric acid deposits in the region between the Alloy 600 tube and the carbon steel block. Boric acid deposits in the interference fit of an operating plant could indicate leakage of borated primary water through the J-groove seal weld. In-service-inspection data show that the presence of boric acid creates a unique ultrasonic transmission and reflection patterns in the fit regions (Cumblidge et al. 2009). The mockup was designed so that PNNL could evaluate and quantify this ultrasonic transmission and reflection phenomenon prior to examining Nozzle 63.

The lower interference fit mockup region was designed to have both regions where boric acid deposits were present and bare metal regions without boric acid, as shown in Figure 4.2. Ideally, the differences in ultrasonic transmission and reflection for the respective regions would allow them to be identified by the test system. The process of creating the boric acid deposit regions began with masking off regions with tape on the Alloy 600 tube OD to preserve the bare

metal surface, as shown in the left hand side of Figure 4.3. Simulated boric acid deposits were prepared by mixing a small amount of boric acid in solid form with a small amount of methanol. The two components were then sonicated into a paste with medium to high viscosity. A thin and even coat of the paste was applied with a compatible brush over the localized region on the OD of the tube between the masked-off sections. Upon evaporation of the methanol and solidification of the boric acid, the masking tape was removed. A snake-like pattern was scraped into one of the boric acid regions as indicated with the blue line in Figure 4.2 and the arrow in the right hand side of Figure 4.3.

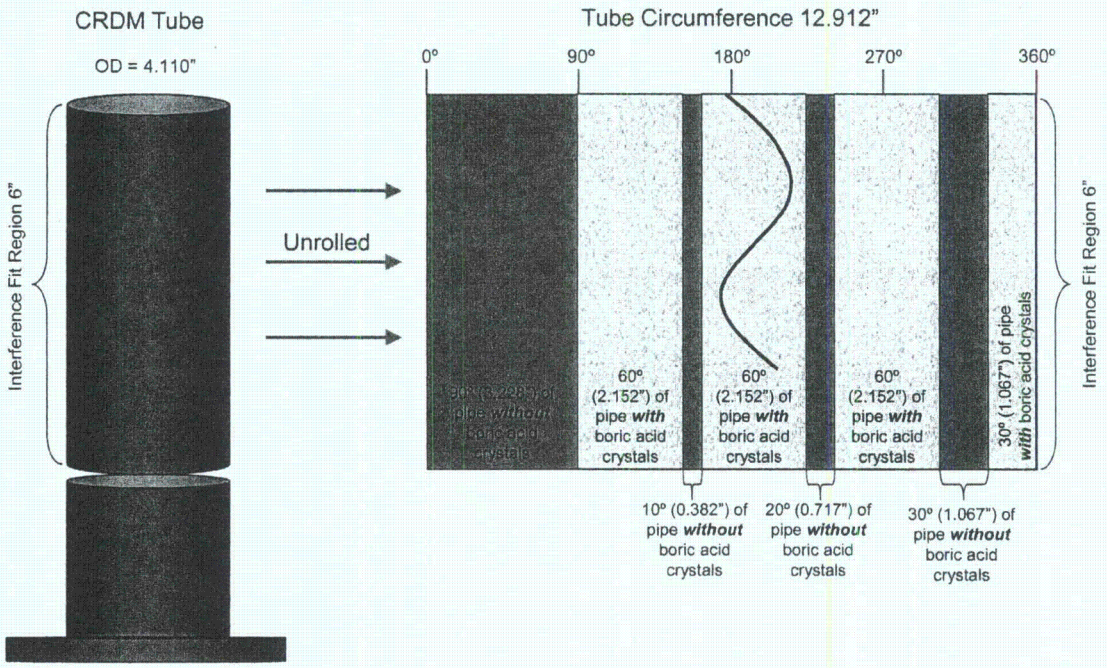

Figure 4.2 Boric Acid Pattern Conceptual Design

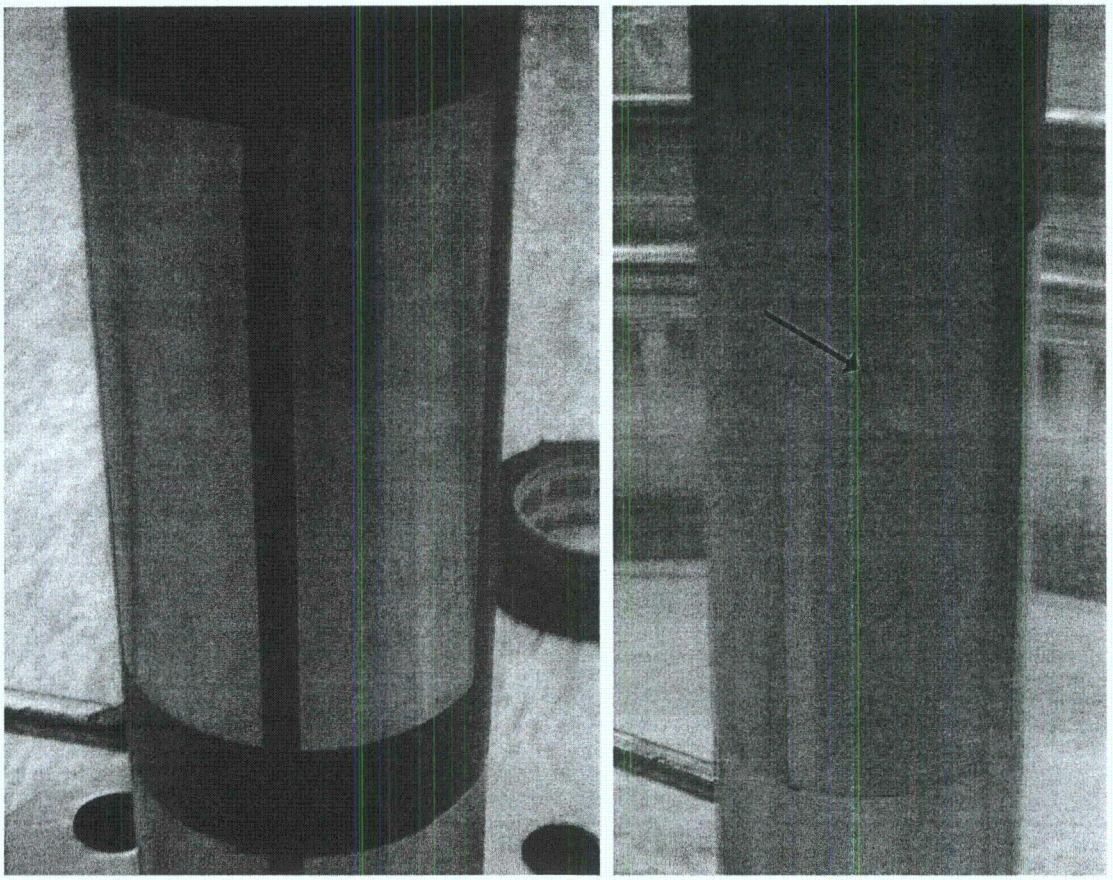

Figure 4.3 Boric Acid Application. Left: Blue painter's tape was used to mask off boric acid regions on the nozzle. Right: The arrow indicates a region where boric acid was intentionally removed.

4.1.2 Simulated Cracking, Cutting and Wastage

The upper interference fit in the CRDM nozzle mockup contained various precision-crafted EDM notches to create a small void region between the tube and the carbon steel block. This was intended to simulate regions in the assembly where a void was created by wastage of the carbon steel RPV or by anomalies in the CRDM tube such as machining marks, cracking, and steam cutting. The notches were machined by Western Professional, Inc., with the pattern shown in Figure 4.4, to provide ultrasonic detection limits and characterization information for voids in the interference fit region.

As shown in Figure 4.4, notches were put in both the Alloy 600 tube, which is the silver-colored region in the figure, and the carbon steel block, which is the brown/orange colored region. The tube and the carbon steel block had the same notch pattern, but the mockup was oriented so that the region with notches on the tube did not overlap the region with notches on the block. The first 180 degrees of the mockup had the notches cut into the tube OD, and the area from 180 to 360 degrees having the notches cut into the carbon steel block inner diameter (ID). The

notches were oriented both horizontally and vertically to assess probe resolution in the circumferential and axial directions. A theoretically determined spot size using the 5-MHz phased-array probe at the interference fit region is 1.0 mm (0.04 in.) in both theta and Z directions (circumferential and axial directions). For reference, the theoretical wavelength (λ) in the Alloy 600 tube material at 5 MHz is 1.1 mm (0.043 in.).

The probe resolution in both the circumferential and axial directions was measured by acquiring data on a series of like-sized notches (2-mm wide × 2-mm deep × 25-mm long [0.079-in. × 0.079-in. × 1.0-in.]) that were spaced 2, 3, and 5 mm (0.079, 0.12, and 0.20 in.) apart (approximately 2, 3, and 5 λ), respectively. One set of these notches was orientated circumferentially and the other was oriented axially, as represented by blue lines in the upper left area of the rectangular schematics in Figure 4.4. To measure width detection sensitivity, axially oriented notches with similar length and depth but varying width (0.79–6.35 mm [0.03–0.25-in.]) were machined into the tube and carbon steel block, as represented by the lines labeled 1 through 4 in the lower end of the schematics in Figure 4.4. To assess depth sensitivity, a series of axially oriented notches with similar length and width but varying depth (0.025–0.127 mm [0.001–0.005 in.]) were machined into the tube and carbon steel block, as represented by the lines labeled 5 through 8 in the upper right of the schematics in Figure 4.4. Complete as-built dimensional details for all of the notches can be found in Appendix A.

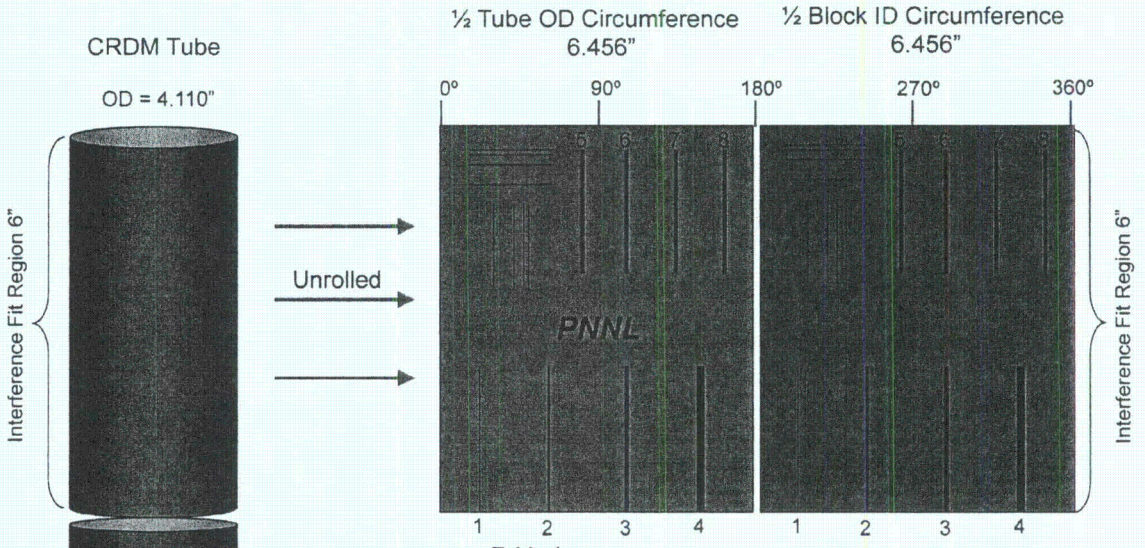

Table 1

Notch	Length (in)	Depth (in)	Width (in)
1	2.0	0.10	0.03125 (1/32)
2	2.0	0.10	0.0625 (1/16)
3	2.0	0.10	0.125 (1/8)
4	2.0	0.10	0.25 (1/4)

Table 2

Notch	Length (in)	Depth (in)	Width (in)
5	2.0	0.001	0.04 (1 mm)
6	2.0	0.002	0.04 (1 mm)
7	2.0	0.003	0.04 (1 mm)
8	2.0	0.005	0.04 (1 mm)

Figure 4.4 Interference Fit #2; Notch and Pattern Conceptual Design

The three sets or groupings of notches did not overlap, but were separated so that ultrasonic observations could be made independently on the ability to resolve two closely spaced indications, as well as width and depth sensitivity. The acronym 'PNNL' was also inscribed on the OD of the tube to provide an indication of off-axis sensitivity. Figures 4.5 and 4.6 show the EDM notch patterns as cut into the Alloy 600 tube and carbon steel block.

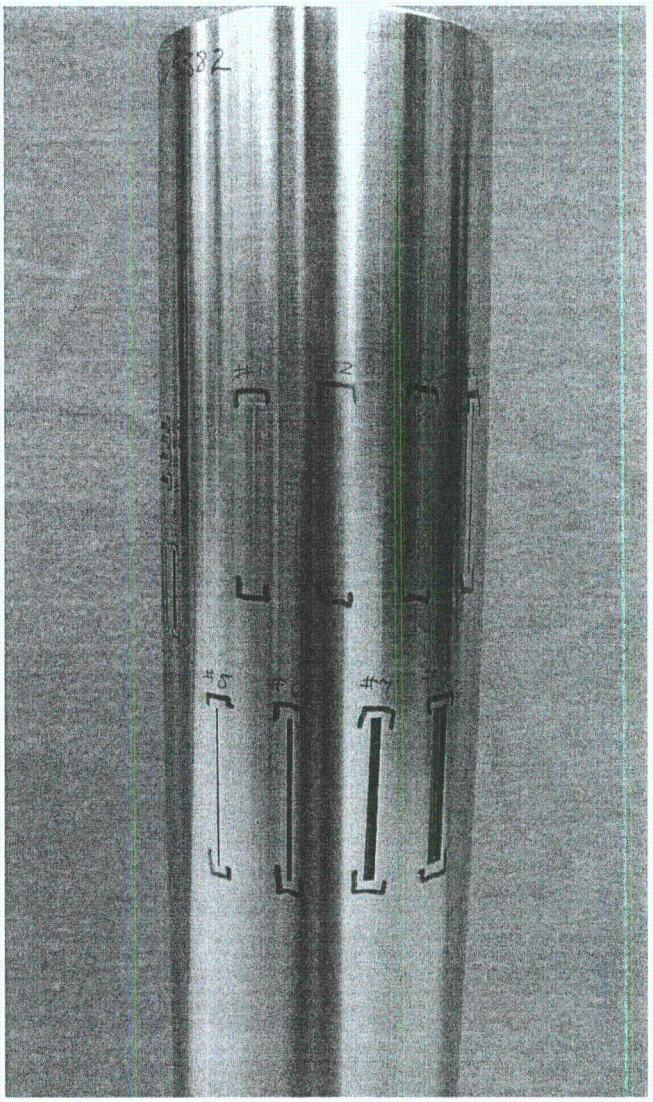

Figure 4.5 EDM Notches in Alloy 600 Tube

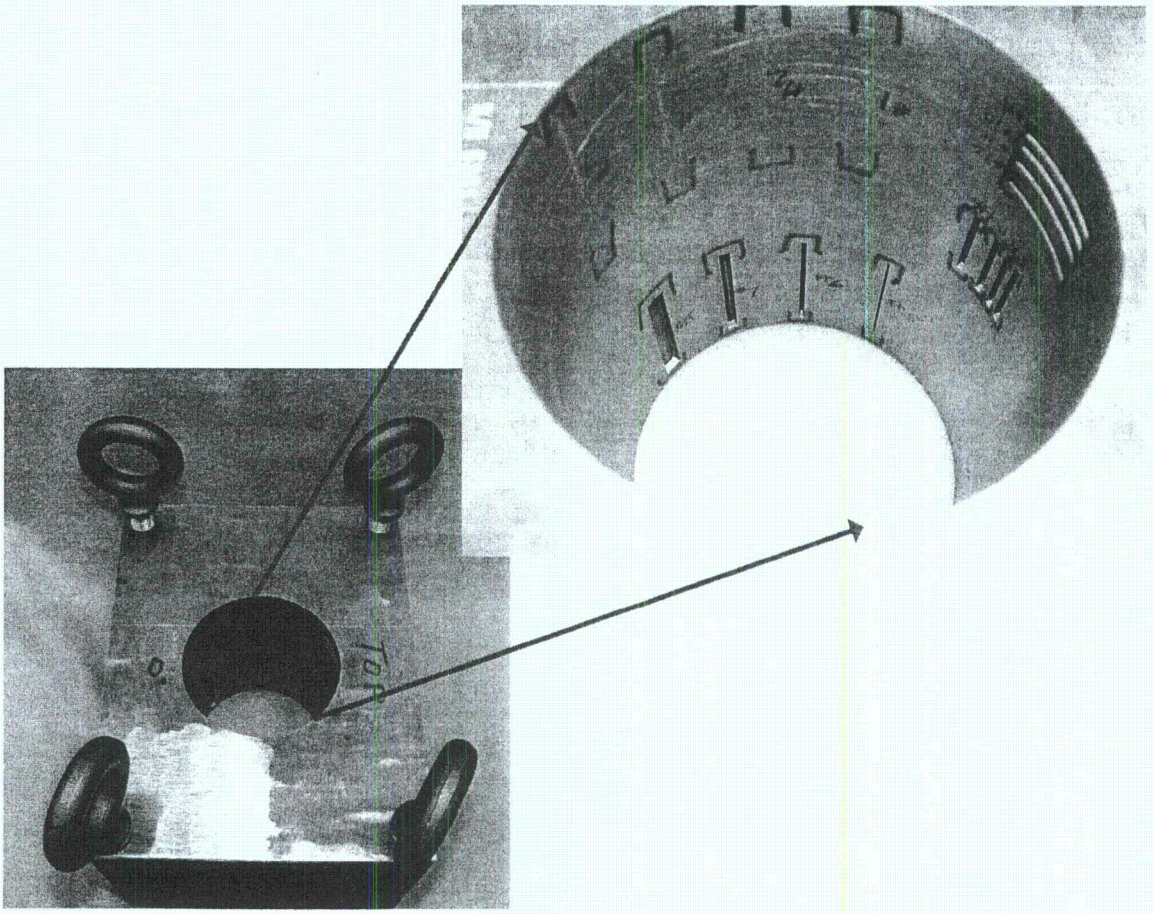

Figure 4.6 EDM Notches on Carbon Steel Block

4.1.3 Mockup Assembly

An interference fit is made by either heating the low alloy steel reactor pressure vessel (RPV) head or cooling the Alloy 600 nozzle, or both. PNNL choose to cool the nozzle. The other parameter considered was the size of the interference fit diameter. A suggested maximum fit was 0.102 mm (0.004 in.) (Gorman et al. 2009). Reported industry interference fit ranges were listed as 0.030 to 0.102 mm (0.0012 to 0.004 in.) (Hunt and Fleming 2002). PNNL decided to fabricate nominal 0.0762-mm (0.003-in.) interference fits.

The nozzle was lightly machined to remove any minor surface irregularities and its outer diameter was measured. Then the carbon steel blocks were machined with a hole that was 0.0762 mm (0.003 in.) in diameter smaller than the OD of the tube at room temperature of 22°C (72°F). The assembly of the CRDM mockup involved temporarily cold-shrinking the Alloy 600 tube with liquid nitrogen (LN), so that it could be fitted with the carbon steel blocks. This created an interference fit of 0.0762 mm (0.003 in.) after all components returned to room temperature.

To assemble the mockup, LN was used to shrink the 740-mm (29-in.) long Alloy 600 tube. As the tube rested vertically in a stainless steel secondary containment trough, LN was added in the tube to approximately 100 mm (approximately 4 in.) below the top, as shown in Figure 4.7. The LN was contained solely within the tube. A permanent end cap was seal welded at the flange end of the tube to prevent leakage of any LN. Towels were used to assist in insulating the tube to prevent unwanted heat transfer and/or ice formation on the OD of the tube. Once the tube cavity was full of LN, the OD of the tube was monitored with calipers until the maximum shrinkage level was achieved. As measured at the top of the tube, a diameter-shrinkage of 0.20 mm (0.0079 in.) was achieved. Additional details regarding shrinkage fits are found in Appendix B.

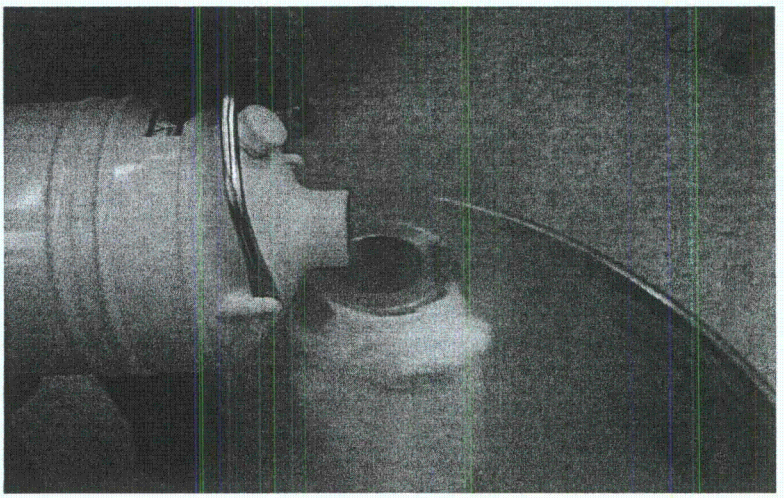

Figure 4.7 Filling Alloy 600 Tube with Liquid Nitrogen

The first fit to be made was the lower one with simulated boric acid deposits. Oversized polyvinyl chloride (PVC) piping was cut to length and fitted over the Alloy 600 tube and served as a hard stop for the carbon steel block to rest on while the specimen returned to room temperature, as seen in Figure 4.8. Next, the insulation towels were removed and the machined carbon steel block was hoisted over top of the tube and aligned accordingly. The block was lowered rapidly and slid down the Alloy 600 tube, but came to rest approximately 64 mm (2.5 in.) above the targeted resting place. Thus, the boric acid deposits were only under the bottom half of the carbon-steel block. Upon return to room temperature, the PVC piping was no longer needed and was removed.

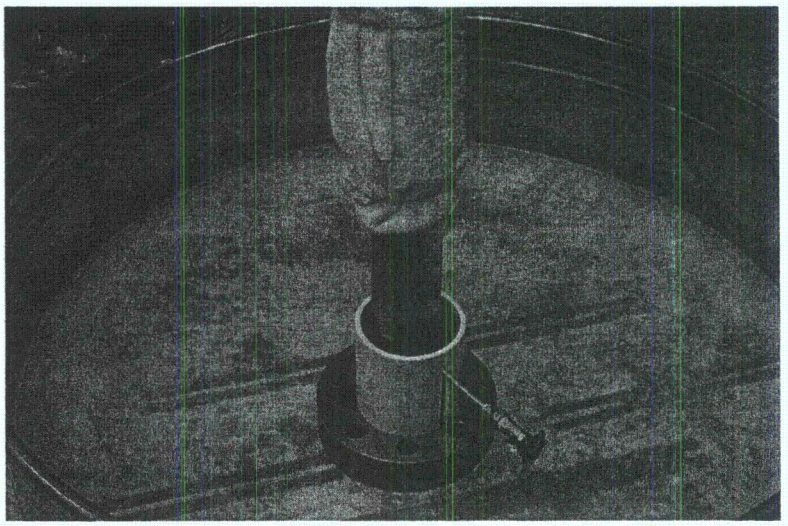

Figure 4.8 PVC Spacer Shown at Bottom of Specimen

The second interference fit with machined notches was created following a similar protocol. For this fit, it was critical to align the zero degree point of the carbon steel block with the zero degree point stamped on the Alloy 600 tube so as to not overlap the notch patterns created in the two materials. The assembly of this fit went according to plan using the PVC piping separator during assembly to maintain separation between the two fit regions. Figure 4.9 shows the completed and assembled calibration specimen.

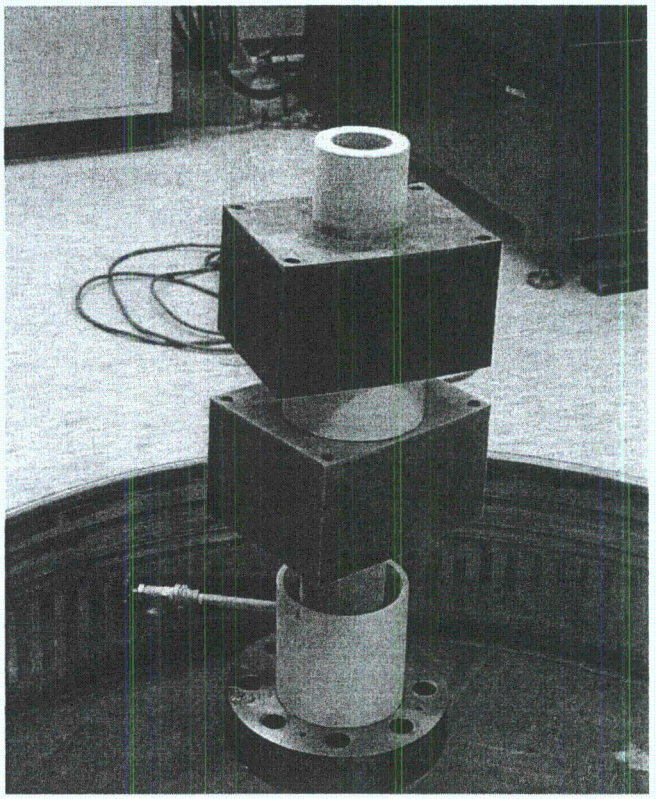

Figure 4.9 Assembled Calibration Specimen

4.2 Ultrasonic Evaluation of Mockup

The CRDM nozzle mockup was examined with the annular ultrasonic phased-array probe described in Section 2. The results of the mockup examination are presented in the following sections.

4.2.1 Alloy 600 Tube Notches

The machined notches in the Alloy 600 tube of the CRDM nozzle mockup simulated potential cracks or degradation of the nozzle penetration. The notched area shown in Figure 4.4 was scanned over approximately a 0 to 170 degree range in the circumferential direction (horizontal axis) and 0 to 180 mm (7.1 in.) in the axial direction (vertical axis) with the data image shown in Figure 4.10. This top view, plan view, or C-scan image shows the resolution notches in the upper-left portion of the image. The variable depth and width notches are also seen as well as the letters "PNNL." The color scale is displayed on the left with lowest amplitudes at the bottom represented by white and the highest amplitude at the top of the color bar represented by red. In this pulse-echo data, the low amplitude signals (blue and green) indicate good transmission or low reflection of the ultrasonic energy at the interface of the tube to the carbon steel. Conversely, the high-amplitude signals (yellow and red) represent poor transmission or large

reflection at the interface. A large reflected signal would be generated at a tube-to-air interface as would be seen above and below the interference fit region or in the presence of a notch with large enough dimensions.

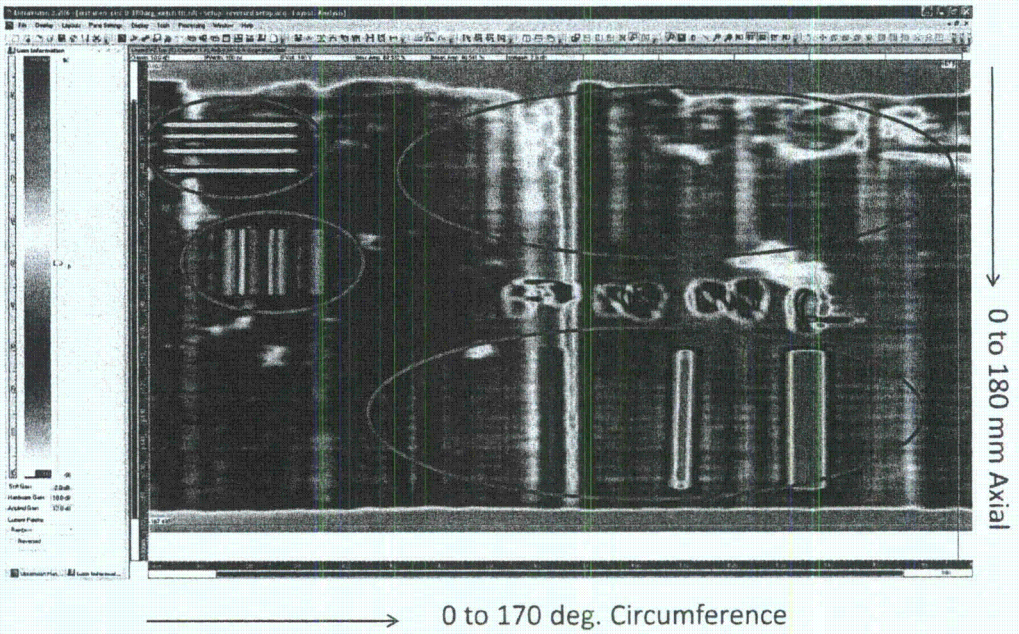

Figure 4.10 Top View, Plan View, or C-scan Ultrasonic Image of the Upper Interference Fit Region Containing Calibration Notches in the Alloy 600 Tube. Calibration notches are circled.

The data analysis software allowed electronic gating of signals in the time or depth dimension as well as positional dimensions Z and theta (axial and circumferential, respectively). The axial resolution notches were first gated or selected for analysis. An enlarged D-scan end view, as depicted in Figure 4.11 was used to measure the center-to-center spacing of the notches. This image was taken as viewed from the left edge of the image in Figure 4.10 and depicts depth into the material (along the sound path) in the vertical axis and the scanner index or nozzle axial direction in the horizontal axis. From this end view, an "echodynamic" curve or profile was generated along the red horizontal line drawn through the responses from the notches, and was plotted above the image. The measured notch widths, from left to right, as measured at the half-amplitude points, were 2.0, 2.0, 2.5, and 2.5 mm (0.08, 0.08, 0.10, and 0.10 in.), respectively. This represents only 4 or 5 pixels with each pixel equal to 0.5 mm (0.02 in.). The actual notch widths were 2.08, 2.06, 2.16, and 2.11 mm (0.082, 0.081, 0.085, and 0.083 in.), respectively. Notch depths were measured as 2.06, 2.06, 2.03, and 2.03 mm (0.081, 0.081, 0.080, and 0.080 in.), respectively. Actual depths were 2.06, 1.95, 2.00, and 2.00 mm (0.081, 0.077, 0.079, and 0.079 in.), respectively. The data suggested that cracks as small as approximately 1 mm (0.04 in.) in depth could be accurately measured. Also, the notches could be clearly distinguished from each other, providing an indication of lateral probe resolution in the nozzle axial direction. In this set of notches, the actual center-to-center separations were 7.11,

5.08, and 4.06 mm (0.28, 0.20, and 0.16 in.), respectively. The measurements from the ultrasonic data gave separations of 7.0, 5.5, and 4.0 mm (0.28, 0.22, and 0.16 in.), respectively. These highly correlated data values and the data image indicated that an axial resolution of better than 4.0-mm (0.16-in.) was achievable.

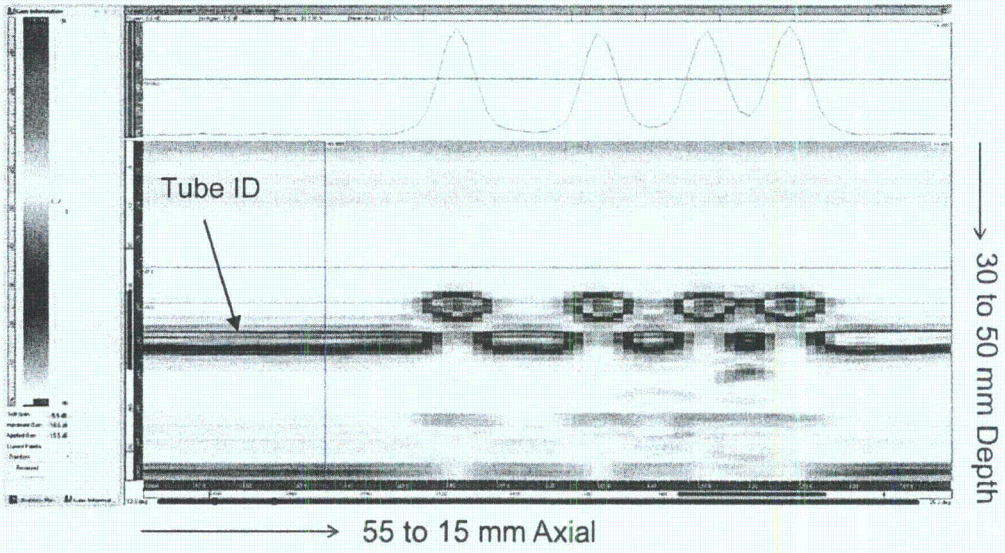

Figure 4.11 D-scan End View of the Axial Resolution Notches in the Inconel Tube

The gated circumferential resolution notch set is shown in Figure 4.12. This image was taken as viewed from the bottom edge in Figure 4.10. Notice that the closely spaced two notches on the left are overlapping but they are still resolvable. Peak-to-peak values gave measured notch separations of 4.36, 5.18, and 6.82 mm (0.17, 0.20, and 0.27 in.), respectively. The actual separations were 4.06, 5.08, and 7.11 mm (0.16, 0.20, and 0.28 in.), respectively. This is greater error than was observed for the axial direction. This test demonstrated a circumferential probe resolution of approximately 4.4 mm (0.17 in.).

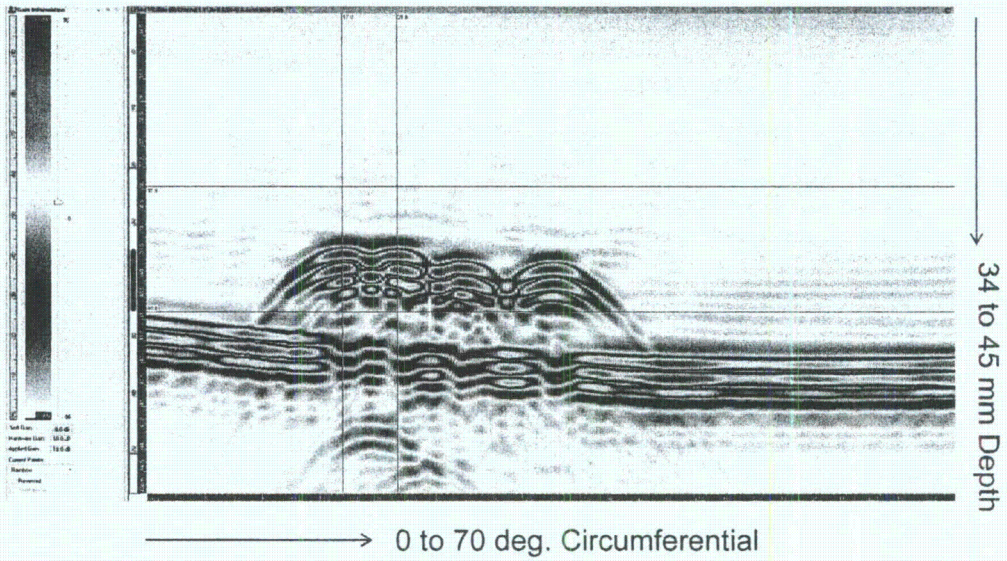

Figure 4.12 B-scan Side View of the Circumferential Resolution Notches in the Inconel Tube

The set of notches in the upper right portion of the scanned image in Figure 4.10 varied in depth but had constant width. These very shallow notches were recognized because their shape and location were known, but they could have been missed based on amplitude response alone. Machining marks on the tube as well as variations in the interference fit produced a non-uniform background response for the fit region, complicating the detection. The center-to-center separations of these notches as ultrasonically measured were 23.84, 24.29, and 23.61 mm (0.939, 0.956, and 0.930 in.), respectively, whereas the actual spacing was 25.4 mm (1.0 in.) between each notch. Flaw depth information was not discernible in the first interference fit echo, but the second echo gave some indication of a flaw tip as noted by the red arrows in the upper part of Figure 4.13. This image represents the B-scan side view of the data while the lower image is a C-scan top view. A higher inspection frequency could have better resolved the small depth variations in these notches. The current second-echo ultrasonic data showed an approximate depth of 0.15 mm (0.006 in.) for all four notches, whereas the actual depths were 0.028, 0.051, 0.76, and 0.13 mm (0.001, 0.002, 0.003, and 0.005 in.), respectively. While these very shallow notches each presented a discontinuity that was ultrasonically detected, their depths were below the system depth or range resolution. For a greater than 50% bandwidth probe, the range resolution is on the order of one wavelength, which in Alloy 600 is approximately 1.1 mm (0.043 in.) at a 5-MHz inspection frequency.

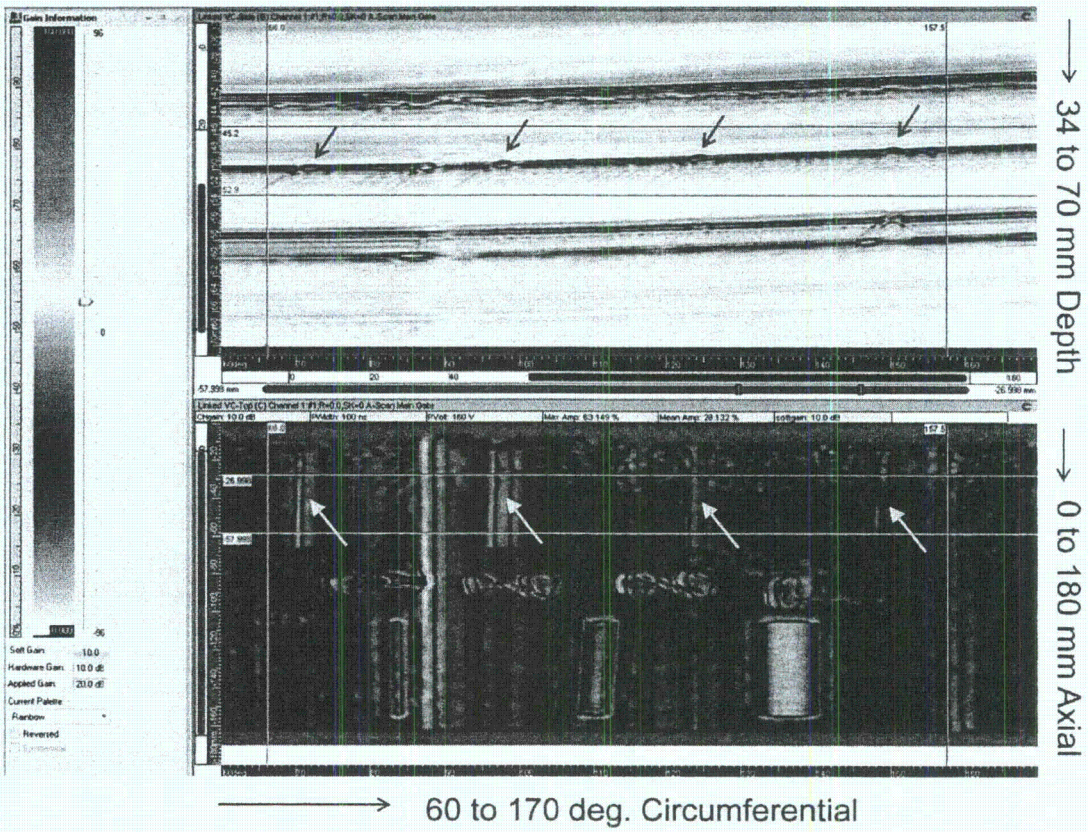

Figure 4.13 The Second Echo is Gated in the Side View Image in the Top of Figure with the Horizontal Lines. The corresponding C-scan top view is displayed in the bottom image. This second echo captures a disturbance in the back-wall echo showing some depth information, noted by the red arrows at top. The yellow arrows note the depth-varying notches.

The final set of notches contained width variations and are shown in Figure 4.14. These flaws were ultrasonically measured with depths of 2.2, 2.5, 2.7, and 2.9 mm (0.09, 0.10, 0.11, and 0.11 in.), respectively, left to right in the image, while the actual depth was 2.53 mm (0.10 in.) for all notches. The measured center-to-center spacings were 23.1, 24.8, and 23.8 mm (0.91, 0.98, and 0.94 in.), respectively, while actual spacings were all 24.5 mm (1.00 in.). Finally, the widths of the flaws were measured in two ways. The first method used the width of the upper part of the flaw response, and the second method used the width of the loss of back-wall signal. The loss of back-wall signal technique was more accurate with measured widths of 3.91, 3.36, 5.00, and 8.82 mm (0.099, 0.126, 0.154, and 0.298 in.), respectively. Actual widths were 0.80, 1.61, 3.24, and 6.42 mm (0.031, 0.063, 0.127, and 0.253 in.), respectively. When measured from the second ultrasonic back-wall echo, the loss of signal measurements gave notch widths of 1.36, 2.73, 3.82, and 7.00 mm (0.054, 0.107, 0.150, and 0.276 in.), which were closer to the actual values. The probe spot size when focused at the interference fit, or 15 mm (0.59 in.) into the Alloy 600, was modeled at 1.2 ×1.2 mm (0.047 × 0.047 in.) at the −6 dB points. Flaw width

sizing values are typically oversized by the probe spot size so these measured width values were well within the error expected with this probe.

In summary, the system resolution for defects as represented by notches in the Alloy 600 tube was better than 4 mm (0.16 in.) in the axial direction and 4.4 mm (0.17 in.) or greater in the circumferential direction. The depth or range resolution notches, as small as 0.028 mm (0.0011 in.), were beyond the system limits for depth sizing but the notches were detected. Range resolution was estimated at 1 mm (0.039 in.). Notches as narrow as 0.80 mm (0.031 in.) in the circumferential direction were detected and sized but the limits were somewhat dependent on the machining marks and other anomalies in the materials and interference fit that also gave ultrasonic indications.

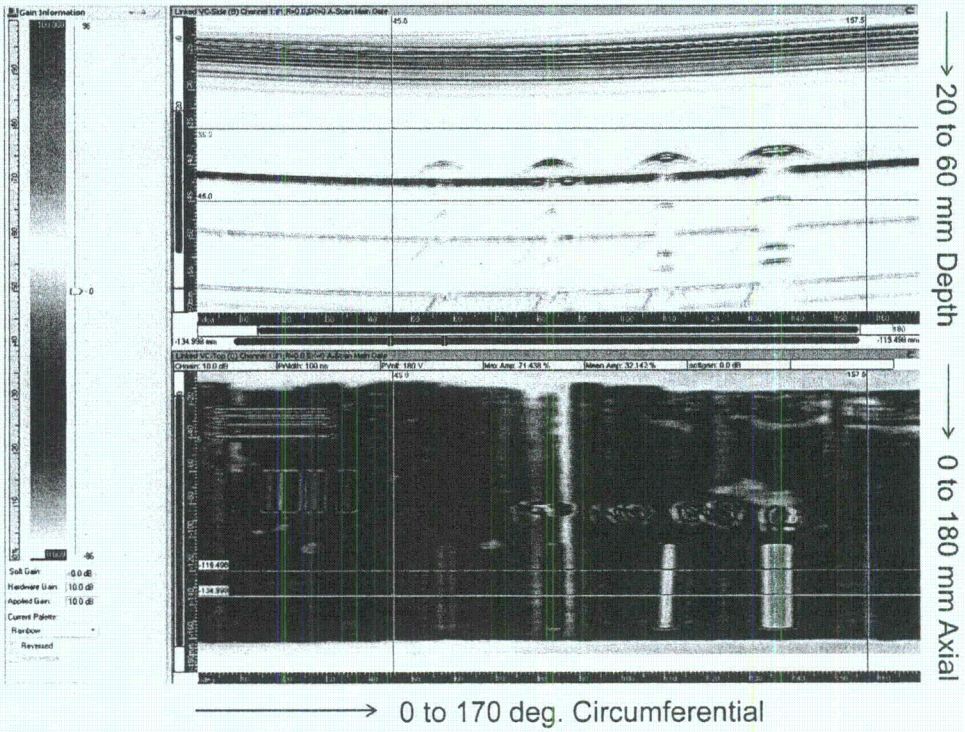

Figure 4.14 B-scan Side View on Top and C-scan Plan View on Bottom of the Width Varying Notches in the Inconel Tube

4.2.2 Carbon Steel Notches

The 180–360 degree portion of the upper fit region in the CRDM mockup contained notches in the carbon steel block to simulate degradation or wastage of the RPV head material. These notches were on the far side of the interference fit relative to the location of the probe. Because the interference fit was not uniform, the notch responses were not as clear as those for notches in the tube, as evident in Figure 4.15.

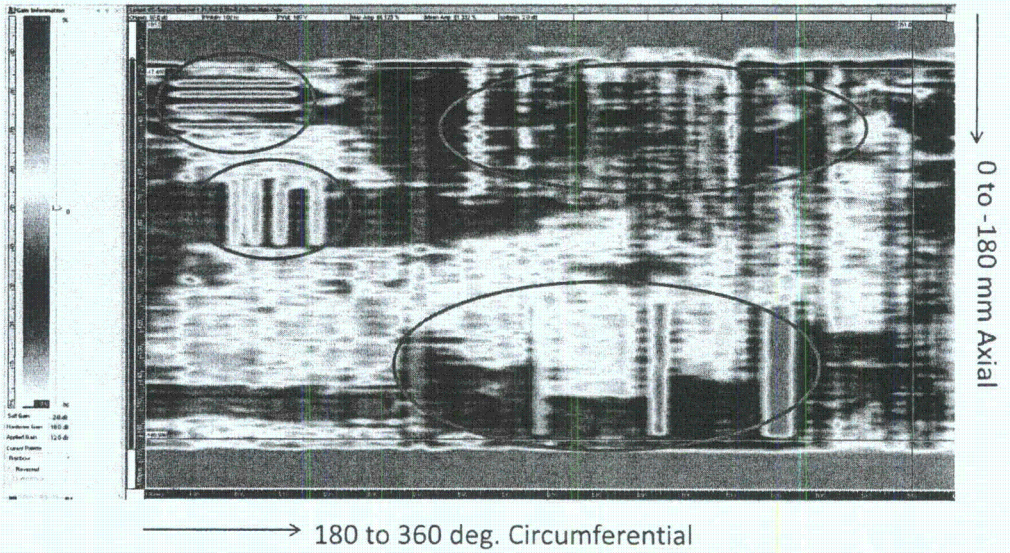

Figure 4.15 C-scan Plan View of the Notches in the Carbon Steel from the First Ultrasonic Echo. The calibration notches are circled.

The axial resolution notches in the top left of the figure were resolved, but the lower notch was on the edge of a high-amplitude region. The measured center-to-center spacings were 3.90, 4.58, and 6.88 mm (0.15, 0.18, and 0.27 in.), respectively, while actual spacings were 4.06, 5.08, and 7.11 mm (0.16, 0.20, and 0.28 in.), respectively. Axial resolution was therefore approximately 4 mm (0.16 in.) or better.

Measurements from the circumferential resolution notch pattern showed center-to-center spacings of 3.82, 5.00, and 7.54 mm (0.15, 0.20, and 0.30 in.), respectively, with actual spacings of 4.06, 5.08, and 7.11 mm (0.16, 0.20, and 0.28 in.). Circumferential resolution was also approximately 4 mm (0.16 in.) or better.

The variable depth notches in the top right of Figure 4.15 were detected but depths could not be measured. First and second echo images are shown in Figures 4.16 and 4.17, respectively. Center-to-center spacing was ultrasonically measured at 23.9, 22.4, and 24.4 mm (0.94, 0.88, and 0.96 in.), respectively, with an actual spacing of 25.4 mm (1.00 in.) for all notches.

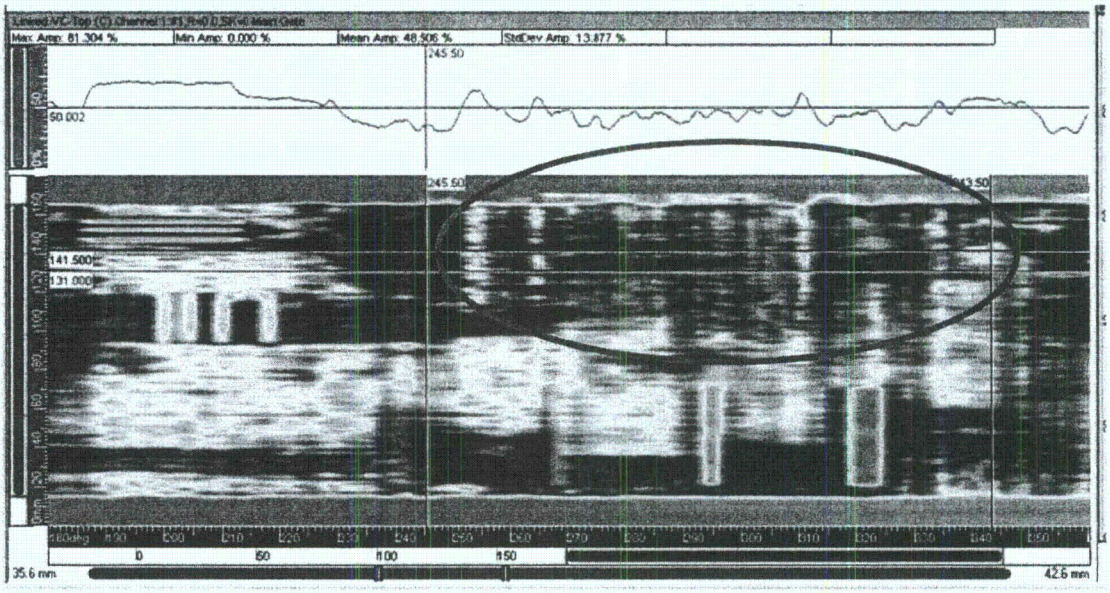

Figure 4.16 C-scan Plan View of the Depth Notches in Carbon Steel, Circled on the Upper Right. This image was acquired from the first ultrasonic echo.

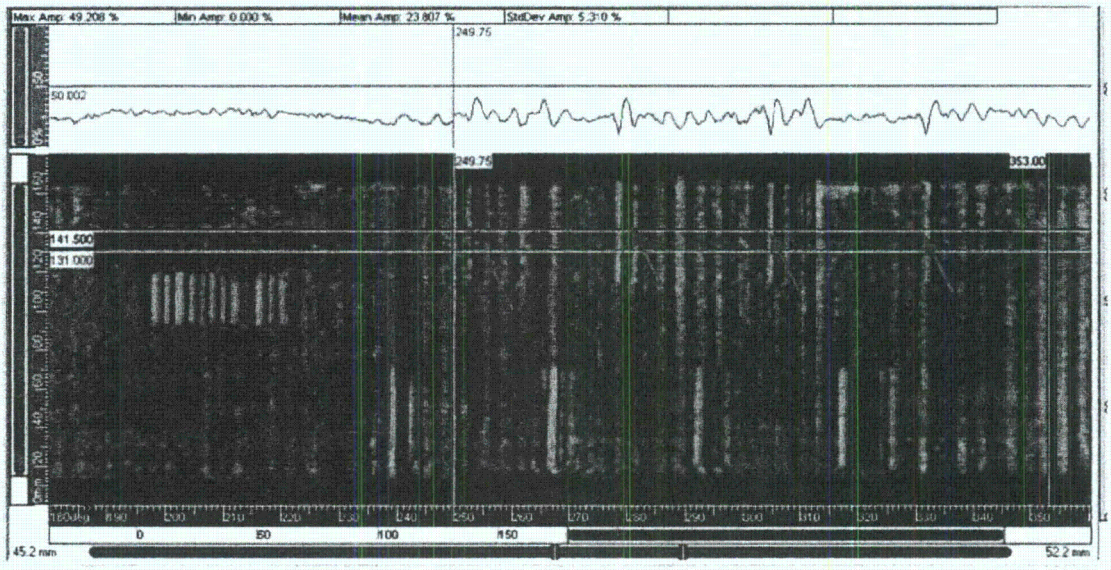

Figure 4.17 C-scan Plan View of the Depth Notches in Carbon Steel, Noted by Red Arrows on the Upper Right. This image was acquired from the second ultrasonic echo.

The set of notches with variable widths is shown in Figure 4.18 with the notches marked by red arrows at the bottom of the image. This image represents the second echo. The center-to-center spacing measurements were 25.4, 23.2, and 25.0 mm (1.00, 0.91, and 0.98 in.),

respectively, left to right, with actual spacing of 25.4 mm (1.00 in.). Measured notch width values were 1.82, 2.27, 4.27, and 6.82 mm (0.072, 0.089, 0.168, and 0.268 in.), respectively, with actual values of 0.80, 1.59, 3.18, and 6.39 mm (0.032, 0.062, 0.13, and 0.25 in.), respectively. The notch widths were also measured from the first echo (refer to Figure 4.15, a first ultrasonic echo image) with slightly poorer results.

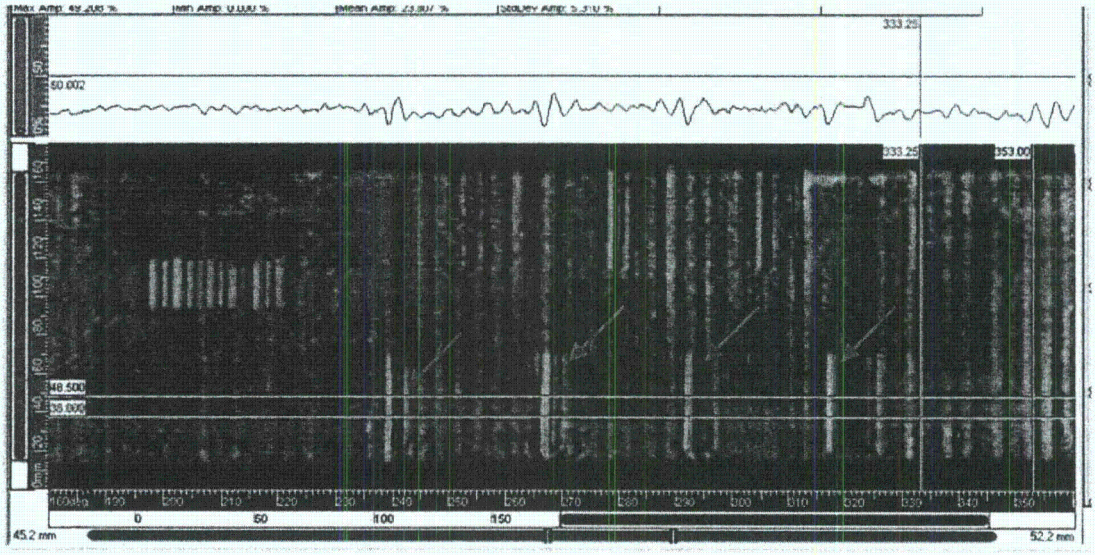

Figure 4.18 C-scan Plan View of the Width Notches in Carbon Steel, Noted by Red Arrows on the Bottom. This image was acquired from the second ultrasonic echo.

In summary, the system resolution for defects as represented by notches in the carbon steel was better than 4 mm (0.16 in.) in both the axial and circumferential directions. The depth or range resolution notches, as small as 0.028 mm (0.0011 in.), were beyond the system limits for sizing but the notches were detected. In general, the notch depth into the carbon steel is not measureable because the sound beam is reflected at the first tube-to-air interface and does not travel through the air gap to the back of the cavity in the steel. Notches as narrow as 0.80 mm (0.10 in.) in the circumferential direction were detected.

4.2.3 Simulated Boric Acid Deposits

The top view, C-scan images from the mockup with boric acid deposits in the interference fit region are displayed in Figures 4.19 and 4.20. The first image represents the 60 to 240 degree circumferential region and the second image represents the 240 to 60 degree circumferential region, both as captured by the first echo. The boric acid regions were readily detected as lower amplitude response and are outlined with red boxes. Again, notice machining marks and non-uniformity in the interference fit response. The amplitude relevance is discussed in the next section.

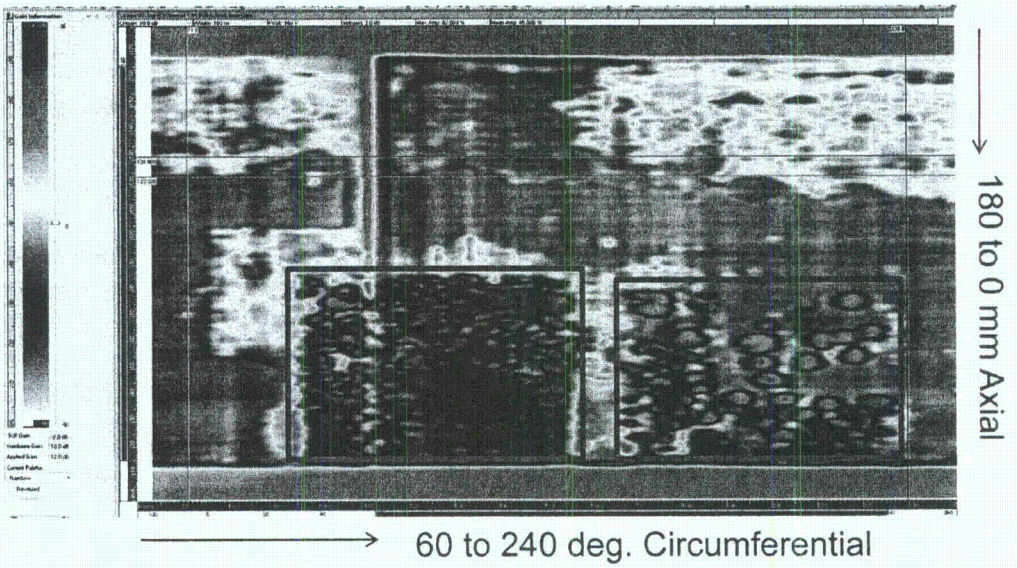

Figure 4.19 C-scan Plan View of the Boric Acid Deposits, Boxed in Red, in the Lower Interference Fit Region. The horizontal axis represents the circumferential range of 60–240 degrees. This image is from the first ultrasonic echo.

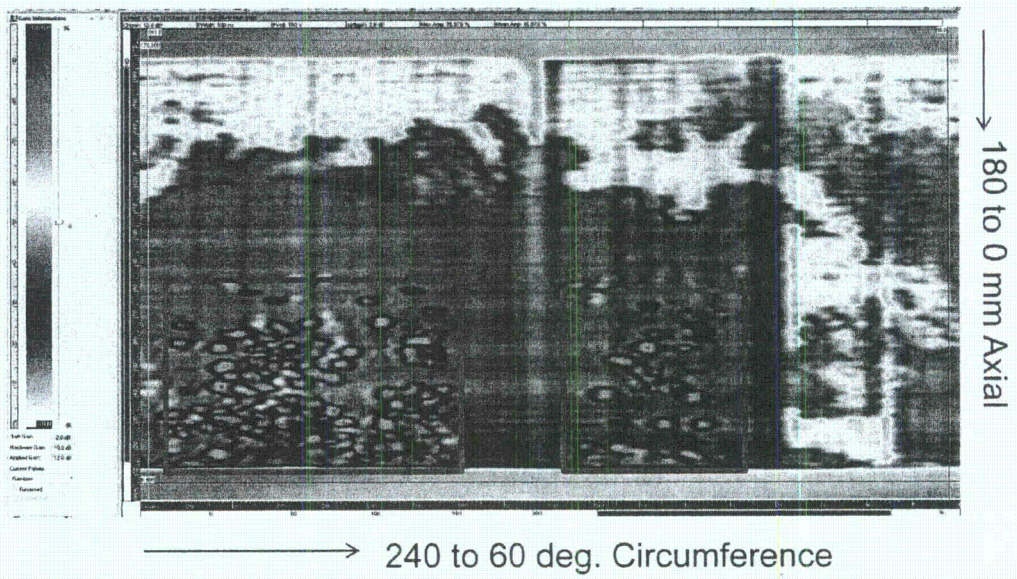

Figure 4.20 C-scan Plan View of the Boric Acid Deposits, Boxed in Red, in the Lower Interference Fit Region. The horizontal axis represents the circumferential range of 240–60 degrees. This image is from the first ultrasonic echo.

4.2.4 Amplitude Response

In addition to characterizing the notch response data for probe spatial and range resolution and flaw detection capability, an analysis of the acoustic response from the different regions was performed based on the reflected signal strength in the lower boric acid mockup section. The three categories represented in the data were the interference fit region where no boric acid was present, the interference fit region where boric acid was present, and the tube region outside of the interference fit area. These areas are represented in Figure 4.21 for the 60 to 240 degree boric acid image. The portion of the image outlined with the red box represents the interference fit region where boric acid deposits were present, the black dashed boxes represent the tube regions above and below the interference fit, and the black dotted boxes represent regions in the interference fit without boric acid deposits. The mean and peak amplitudes were measured in each of these boxed areas from the C-scan image. Similar measurements were also acquired for the 240 to 60 degree boric acid image.

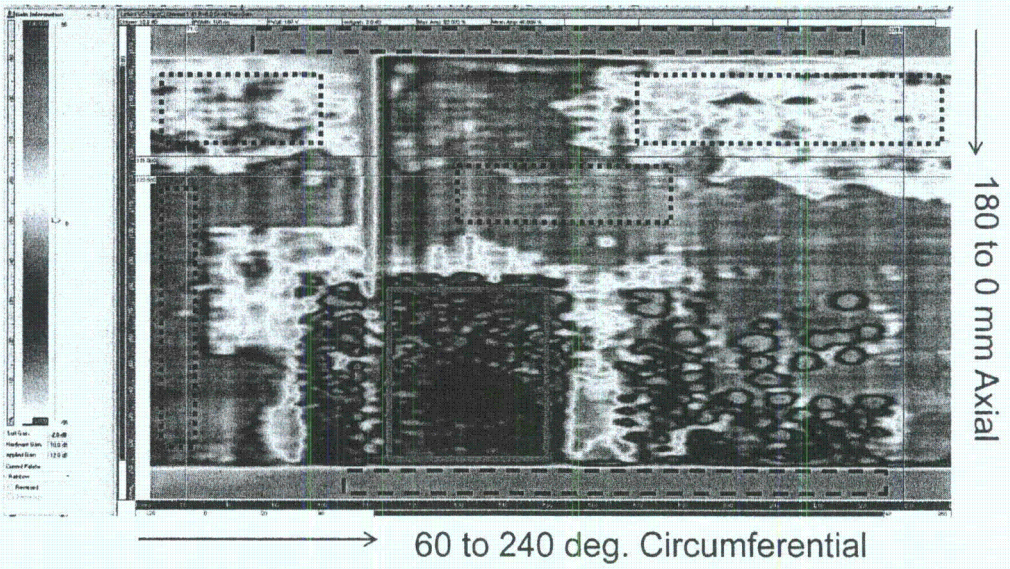

Figure 4.21 The Interference Fit Region Containing Boric Acid is Subdivided into Three Regions. The red box represents the presence of boric acid in the interference fit region, the black dashed boxes represent the tube region, and the black dotted boxes represent the interference fit region.

The data images were analyzed with a total image gain of 12 dB. This represented 10 dB of hard gain applied during acquisition and 2 dB of soft gain applied during analysis. The mean responses from the interference fit regions without boric acid deposits were in the range of 40 to 55 percent of full-screen amplitude. This range of values was due to the variability in the fit itself. Some regions of the fit were tight, giving lower reflected amplitude and more transmitted energy. This condition is represented by the green color in the image. Other regions of the fit showed higher reflected energy (not tight), thus less transmitted energy, and this state is represented by the yellow-to-orange colors. Machining marks were evident and also lead to

response variability. The mean responses of the interference fit regions with boric acid deposits were in the range of 24 to 30 percent range of full-screen height (FSH). This shows more energy transmitted (less reflected) through the interference fit region with the presence of boric acid than in the regions without boric acid. The boric acid crystals filled gaps in the fit and efficiently coupled the ultrasonic energy into the carbon steel material. Finally, the mean responses of the tube regions above or below the interference fit were 60 to 75 percent of FSH, demonstrating greater reflectance of energy at the outside tube surface-to-air interface. These measurements established a baseline for the Alloy 600 tube-to-air interface reflectivity level. It also indicated that orange-colored regions in the interference fit represented an air gap. These mockup data images showed that interference fit region where no boric acid is present, the interference fit region where boric acid is present, and the tube region above or below the interference fit area are distinguishable by their mean ultrasonic response.

A final study was conducted as a result of discussions with John P. Lareau of WesDyne International on industry-style CRDM inspections and practices. He reported that the presence of boric acid was simulated with clay on a nozzle mockup specimen and gives an ultrasonic response that is 2 dB lower than the nozzle without clay. To evaluate the PNNL inspection system under a similar scenario, putty was placed on the outside of a blank nozzle specimen. The presence of putty was clearly seen with the mean response from the putty region measured at 64.8 percent of FSH and the clean nozzle response measured at 72.0 percent. This represents a 0.9 dB drop in amplitude. This smaller response difference is possibly due to the type of clay used in the WesDyne testing as compared to the putty used at PNNL.

5 NOZZLE 63 NONDESTRUCTIVE LEAK PATH ASSESSMENT

After calibration and testing on the control rod drive mechanism (CRDM) mockup, the phased-array ultrasonic equipment was transported to the Radiochemical Processing Laboratory (RPL/33) for the examination of Nozzle 63. The results of the examination are presented in this section.

5.1 Scanner Setup

A CRDM nozzle was used to assess the functionality of the probe, scanner, and electronics after they were moved to RPL/33 where Nozzle 63 was housed. A simple scan on the nozzle was performed in the ultrasonic laboratory where the mockup was tested and then in RPL/33 after transporting and reassembling all of the equipment. The maximum and mean amplitude responses were within 0.23 and 0.08 dB, respectively, of each other. Typically calibration data that fall within ±2 dB of each other are acceptable so the equipment functionality was validated.

After equipment verification, the scanner was placed on Nozzle 63 in the glovebag. The wetted side of the nozzle assembly was facing down. A plug was inserted in the wetted side of the nozzle several months earlier. Water was added several days prior to mounting the scanner on the nozzle. With the scanner in place, the glovebag was examined for any leakage points in the bag walls and glove ports. No leaks were found and the glovebag was sealed. Any materials entering the glovebag from this point forward were passed through an access port in the bag wall.

5.2 Data Acquisition

Before the start of a scan, the probe was manually lowered to the bottom of the interference fit region and the data were collected while indexing the probe upwards. Two data channels were recorded during acquisition—one with a focus at the front surface (1 mm or 0.04 in.) and the other focused at the interference fit interface (15 mm or 0.59 in.). The front surface reflection represented the interface between the water inside the tube and the Alloy 600 tube inner diameter (ID), and provided an indication of the surface condition of the tube. This data would reveal bubbles, pitting, and other surface anomalies, if present. The second data channel recorded the reflection from the interface between outer diameter (OD) of the Alloy 600 tube and the carbon steel RPV head material, and represented the interference fit region. The first coarse scan data showed the need to laterally adjust the scanner to more accurately center the phased-array probe in the nozzle. Results from data acquired towards the top of the tube before and after centering the scanner are displayed in Figure 5.1. The horizontal axes in each image represent a circumferential distance from −90 to +90 degrees. The vertical axes represent approximately 20 mm (0.79 in.) of travel in depth or distance from the probe. Before centering the scanner, the front surface signal travel or difference from high to low point was measured at 10 mm (0.39 in.) on the left image. After centering, the signal travel was only 1 mm (0.04 in.) with the data displayed on the right of Figure 5.1. In addition to showing centeredness of the probe, the coarse scans also verified that the areas of interest were captured in the data file.

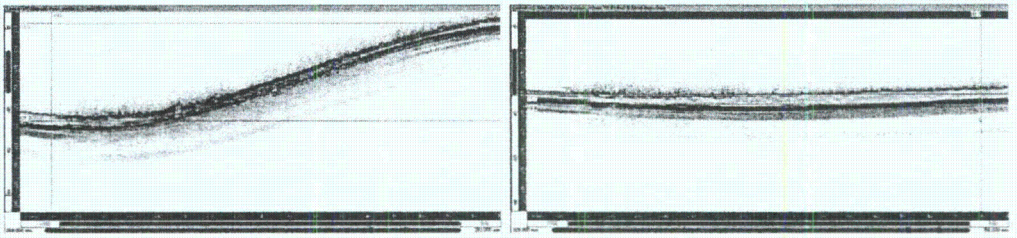

Figure 5.1 Alloy 600 Tube ID Response Before (left) and After (right) Centering the Scanner on the Nozzle. The horizontal axis represents approximately 180 degree and the vertical axis 20 mm (0.79 in.).

Once the areas of interest were bounded, the scanner step sizes were reduced for more detailed imaging. A resolution of 0.5 degree in the circumferential (scan) direction and 0.5 mm (0.02 in.) in the axial (index) direction were selected. The ZETEC UltraVision software limits the data files to 1 gigabyte in size. Working within this constraint, data in a file were collected over a range of approximately 180 degrees circumferentially and 380 mm (14.96 in.) axially. A previous examination of Nozzle 63 by industry indicated a leakage path at the low point or downhill side of the nozzle, which is the 180-degree location on the coordinate system established for this investigation. Therefore, data were acquired over an approximate −90 to +90 degree region and a 90 to 270 degree region to capture the possible leakage path in the center of an image. The actual circumferential scan regions were slightly larger than 180 degrees to provide some overlap in the data.

The first data covering the 90 to 270 degree area are shown in Figure 5.2. The front surface echo is displayed on the top and the interference fit echo on the bottom. These C-scan top view images show approximately 180 degrees across the horizontal axis and 360 mm (14.17 in.) on the vertical axis. The color bar on the left shows low-amplitude signals in blue/white, which represent good transmission or poor reflectance. High-amplitude signals in orange/red conversely represent poor transmission and good reflectance. The weld region is shown in the white-to-light-blue color at the bottom of the interference fit image. The interference fit or shrink-fit zone is located between the counter bore regions as was shown in Figure 1.1. The data above the interference fit (dry-side annulus region) represent a tube-to-air interface and should provide a strong and uniform reflection. Such a strong reflection was only evident in the orange-colored regions in the right side of the images. The tube OD-to-air interface is a good reflector, so a uniform orange color would be expected across the top of the image. Therefore, the lack of uniformity across the upper portion of the image (tube OD) was unexpected. The lack of uniformity across the entire front surface echo (upper image in the figure) was also unexpected.

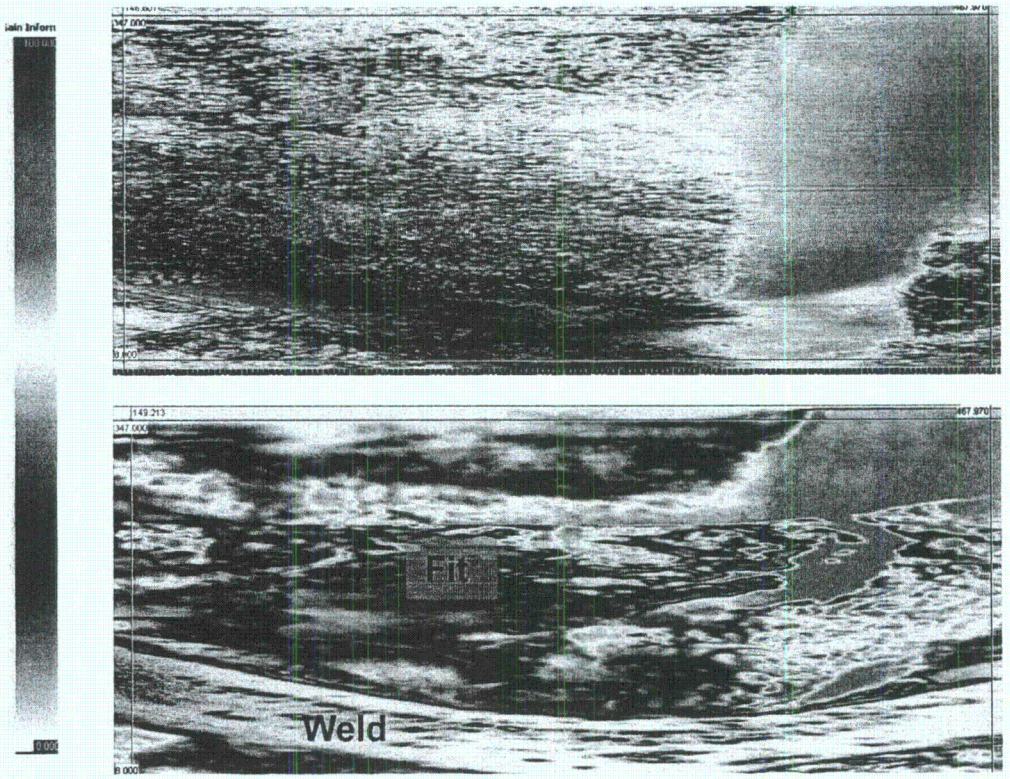

Figure 5.2 First PA Ultrasonic Data from Nozzle 63. The front surface or nozzle ID echo is on the top and the interference fit echo on the bottom. The horizontal axis represents the 86 to 274 degree area and the vertical axis represents 360 mm (14.17 in.). The color scale is represented on the far left.

After the first scanning attempt, the probe was lifted above the water line and found to be dirty. The probe face was carefully wiped with a dry cloth. It was also suspected that bubbles on the ID tube surface could be partly responsible for the degraded image. After carefully brushing the inside of the tube several times, a good data set was obtained.

Data acquired after brushing from the two scans were pieced together to form the composite image of the interference fit region in Figure 5.3. This image displays a full 360-degree representation of the weld and interference fit region with −90 degrees at the left and 270 degrees at the right. The suspected leakage path at the low point, near 180 degrees, is marked with arrows. Also observed from the weld region response below the annulus are suspected inclusions or fabrication flaws.

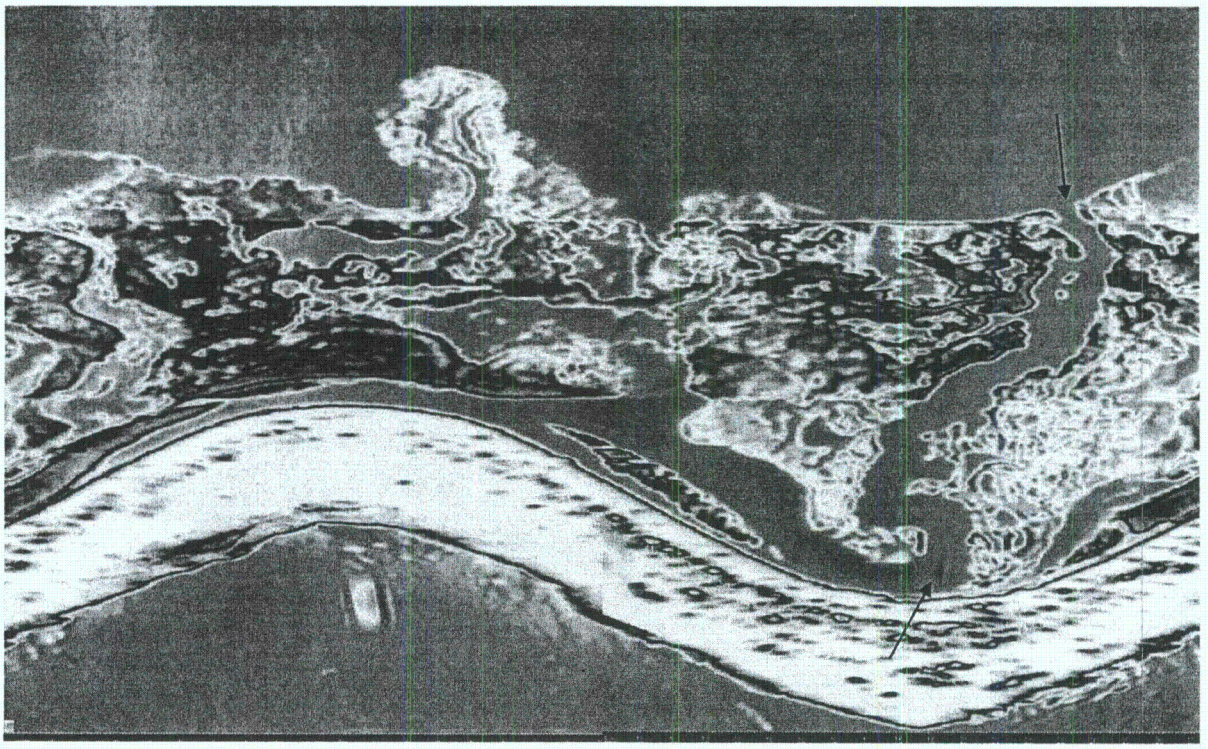

Figure 5.3 PA Ultrasonic Data from the Interference Fit in Nozzle 63 Acquired After the Second Brushing of the Nozzle ID. The horizontal axis represents the full 360-degree area and the vertical axis represents 360 mm (14.17 in.). Black arrows indicate primary leak path. The left edge marks the –90 degree location and the right edge the 270 degree location.

5.3 Amplitude Analysis

An analysis based on amplitude responses was conducted on the data images. The first such analysis was conducted on the 90 to 270 degree data acquired after the first brushing. The image was segregated into regions as depicted in Figure 5.4. The peak and mean amplitude responses were measured in each boxed region. Regions 1 through 6 are suspected leakage path zones. Regions 7 through 11 represent the response from the tube. The interference fit and lower counter bore areas are represented by regions 19 through 22 while regions 24 through 26 represent the interference fit with suspected boric acid present. The same procedure was used on the –90 to +90 degree data with the boxed regions shown in Figure 5.5. These suggested associations were based on the mockup data results and need to be confirmed by destructive analyses. Next the mean amplitudes within each boxed region were plotted with results in Figure 5.6. The suspected leakage path and tube responses all were in the range of 60 percent of full screen height and greater. At the other extreme, the regions with suspected boric acid deposits had mean amplitudes 25 percent and below. Finally, the interference fit/counter bore region mean amplitudes were in the 41 to 58 percent range. A proposed segregation of the regions is denoted by the orange, green, and blue colored zones in

the plot. A 30 percent mean amplitude or less is thought to indicate the presence of boric acid in the interference fit while greater than 60 percent represents an air gap and possible leakage path if connected all the way through (top to bottom) the interference fit. These results will need to be verified with destructive testing.

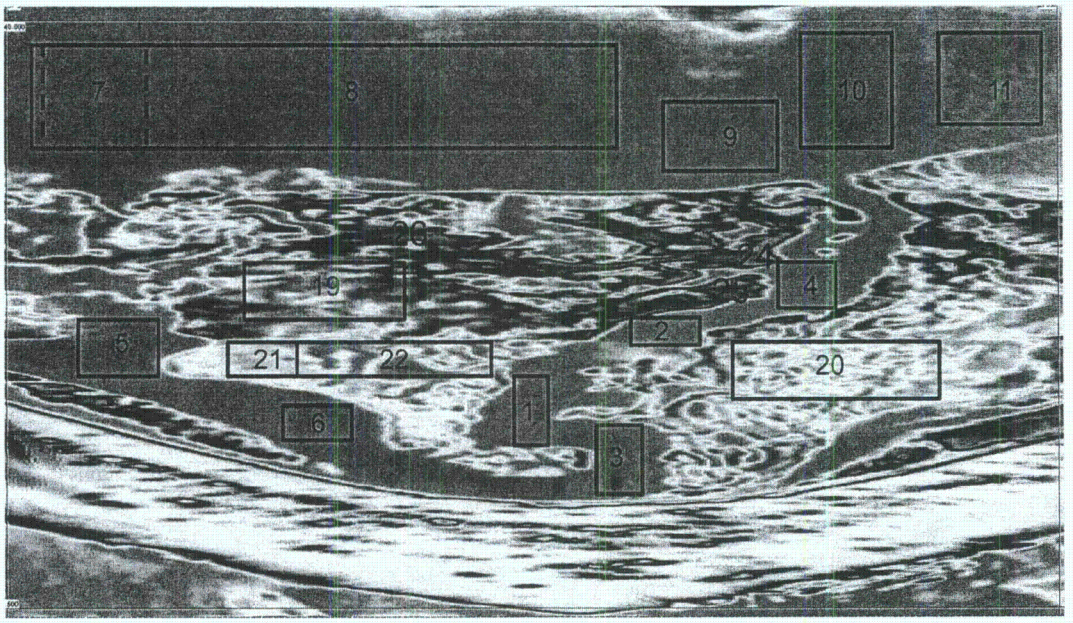

Figure 5.4 Interference Fit Data Image After First Brushing. The horizontal axis represents approximately 90 to 270 degrees. The vertical axis represents 360 mm (14.17 in.). Boxed regions were used in an amplitude analysis.

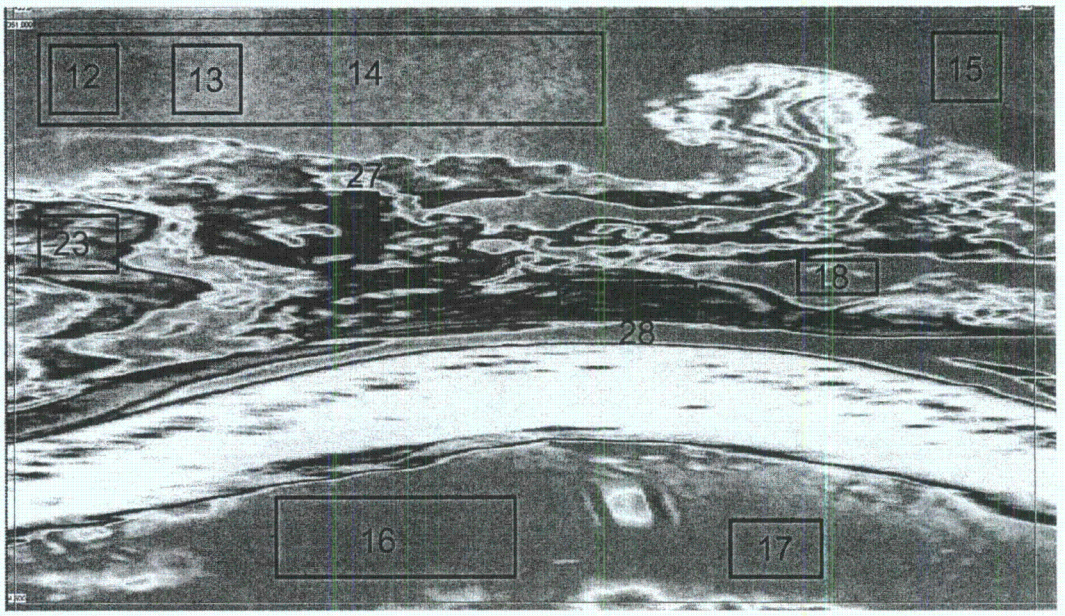

Figure 5.5 Interference Fit Data Image After First Brushing. The horizontal axis represents approximately –90 to +90 degrees. The vertical axis represents 360 mm (14.17 in.). Boxed regions were used in an amplitude analysis.

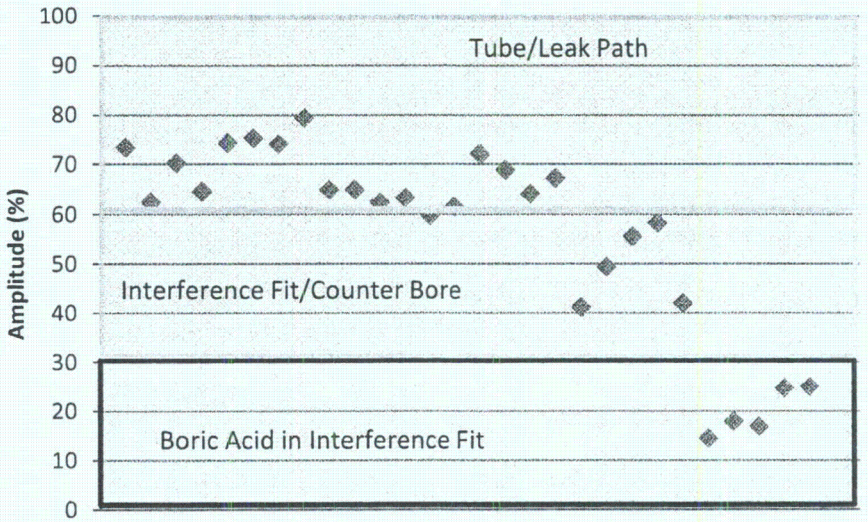

Figure 5.6 Mean Amplitude Response from the Regions Indicated in Figures 5.4 and 5.5

In summary, the mean amplitude responses from the different regions in the data image were measured. Based on this analysis, the regions are separable and compare favorably to the responses measured previously on the calibration mockup specimen. A comparison of the responses is presented in Table 5.1. Note that the Nozzle 63 data were acquired with 1 dB

more gain (13 dB as opposed to 12 dB) than the calibration mockup data and this difference was accounted for in the analysis.

Table 5.1 Mean Amplitude Responses (%)

Region	Calibration Mockup	Nozzle 63
Tube/Leak Path	60–75	60–79
Interference Fit/Counter Bore	40–55	41–58
Interference Fit – with Boric Acid	24–30	14–25

In a color-coded qualitative sense, the C-scan image analysis is also divided into three categories. The orange color implies that an air gap exists in the interference fit or counter bore response and presents a large reflected signal. Orange also represents the tube response outside of the interference fit region. The interference fit and counter bore regions with some contact between the tube OD and the low alloy steel are represented by the green-to-yellow colors and the interference fit region with greater contact is represented by the blue-to-white colors. This greater contact is assumed to be due to the presence of boric acid. Destructive analyses are needed to confirm these results.

Based on the amplitude analyses conducted, the data were also plotted with a tri-level color bar to represent the three categories previously discussed. The tri-level color bar implementation is shown in Figure 5.7. White represents the less than 30% amplitude range and indicates good transmission such as in the weld or possible boric acid in the interference fit region. Light blue represents the 30 to 60% amplitude range and indicates the interference fit and counter bore regions. Dark blue represents the above 60% amplitude range and indicates poor transmission such as in the tube above the interference fit or an air gap in the interference fit and counter bore regions. A leakage path exists if a gap in the interference fit region extends fully through the interference fit connecting the weld and annulus region immediately above the weld to the dry side of the tube. From this image as well as the rainbow color-coded images, one clear leakage path is visible. The leakage path starts in the vicinity of 180 degrees circumferentially, or the low point of the nozzle, and meanders upwards and toward the right in the image. Other leakage paths are also evident but may not connect all the way through to the dry side of the assembly. Destructive analyses are needed to confirm the cause of these regions of differing reflectivity.

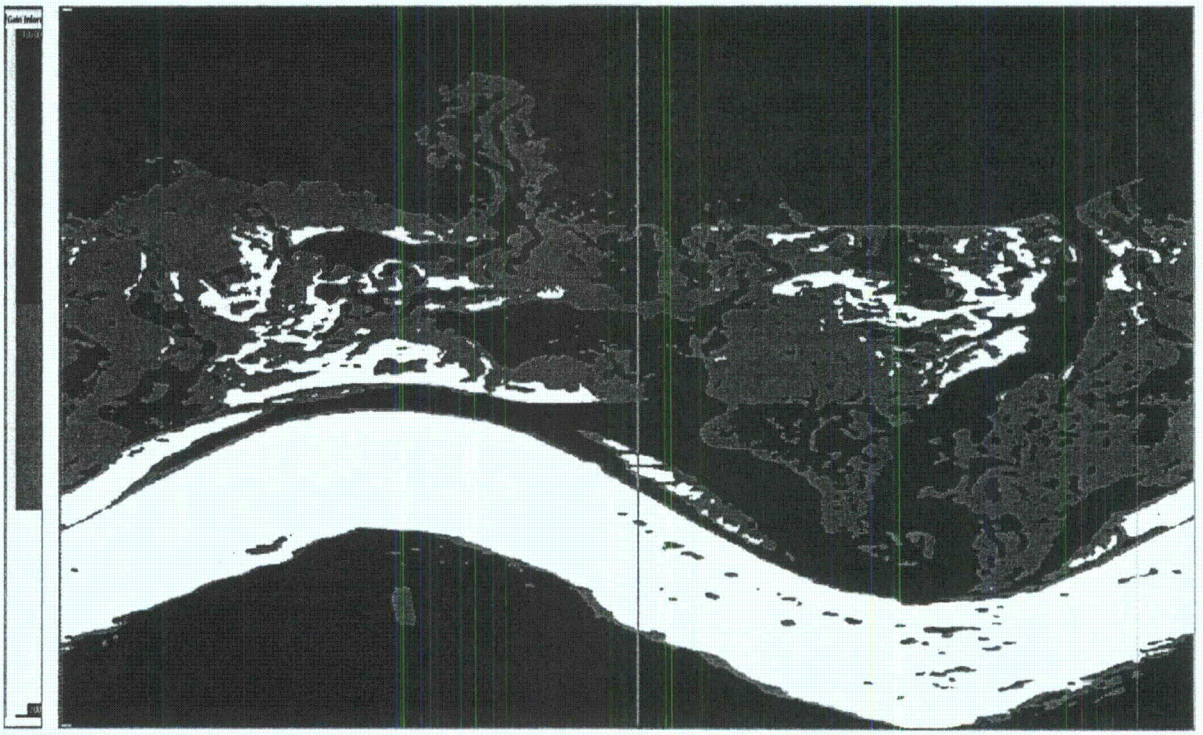

Figure 5.7 A Tri-Color Representation of the Interference Fit Data. The dark blue represents a leak path or gap, the light blue represents the interference fit and counter bore regions and the white represents the weld and suspected boric acid presence in the interference fit.

5.4 Industry Standard Nondestructive Evaluations

Standard ultrasonic evaluation techniques used by in-service inspection (ISI) vendors include time-of-flight diffraction (TOFD) for detecting cracks in both the circumferential and axial orientation and zero-degree pulse echo for an interference fit examination. Blade probes (low profile) and solid-probe head configurations are deployed depending on the access conditions of the CRDM assembly (EPRI 2005; IAEA 2007, and discussions with JP Lareau, WesDyne International). An examination conducted by ISI vendor, WesDyne International (data supplied by JP Lareau), discovered a probable leak path in Nozzle 63 during a 2002 outage. The data acquired with industry-standard 5.0- and 2.25-MHz probes are shown in Figures 5.8 and 5.9, respectively. The 2.25-MHz image in Figure 5.9 has a lower resolution than the 5.0-MHz image in Figure 5.8 as expected, but both data sets detect the leak path observed at the low point (industry's zero-degree position) of the interference fit region.

The Figure 5.8 image can be compared to the PNNL's laboratory results in Figure 5.3. Both data sets were acquired with probes having nominal center frequencies of 5 MHz and they show the main leak path as a high-amplitude signal. In the WesDyne data, this is represented by the magenta color. Both data images capture other partial leak paths and show similar areas of high and low reflectivity. Although these field data sets were acquired in 2002 and a technique

demonstration requirement did not come into effect until 2008, there have been only minor changes to the technique. The field procedure requires a minimum of a 5.1-cm (2-in.) scan above the weld, observation of a "river bed" pattern, and a nominal 2 dB difference in amplitude between the leak path response and the background.

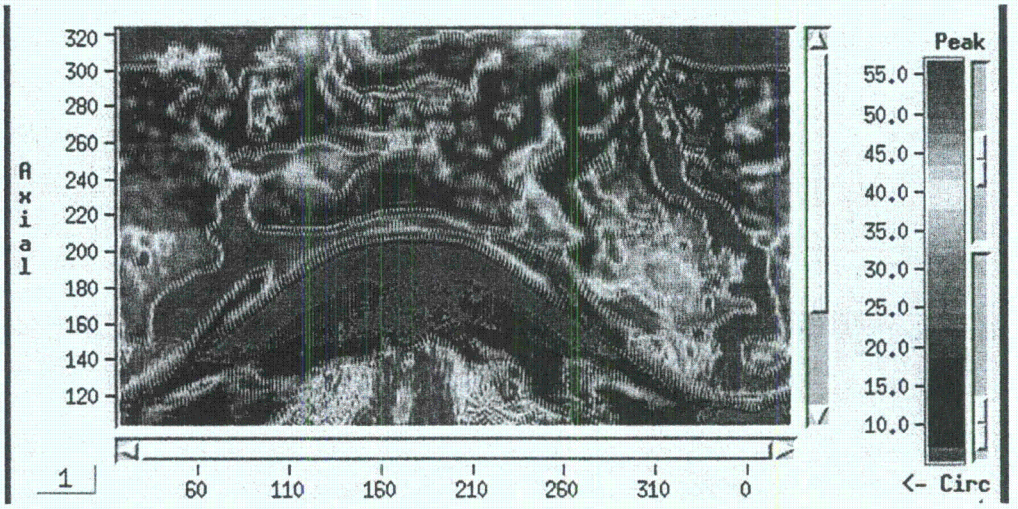

Figure 5.8 Ultrasonic Data from Nozzle 63 as Obtained by WesDyne International. The image was acquired with a 5-MHz probe. The horizontal axis represents the nozzle circumference in units of degrees. The vertical axis represents the nozzle axis in units of millimeters.

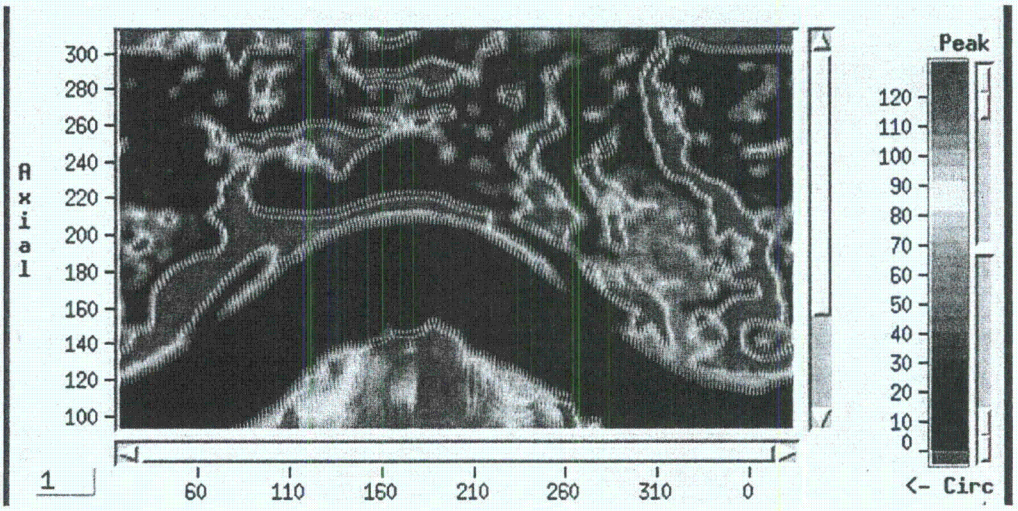

Figure 5.9 Ultrasonic Data from Nozzle 63 as Obtained by WesDyne International. The image was acquired with a 2.25-MHz probe. The horizontal axis represents the nozzle circumference in units of degrees. The vertical axis represents the nozzle axis in units of millimeters.

6 DESTRUCTIVE VALIDATION OF NOZZLE 63

Confirmatory destructive testing was necessary on Nozzle 63 to validate the ultrasonic characterizations of the leak path(s) and other areas of interest as described in Section 5. The destructive testing activity was conducted by Babcock and Wilcox Technical Services Group (B&W) located at the Lynchburg, Virginia, facility. This activity required the dismantling of the interference fit region with full separation of the Alloy 600 tube from the reactor vessel head (RVH) material to reveal true-state information with regard to the leak path(s), boric acid deposit regions, and wastage regions. Pacific Northwest National Laboratory (PNNL) personnel were on site during the critical sectioning activities to identify proper cutting locations. Additionally, the J-groove weld region was preserved and returned to PNNL for storage in anticipation of future work.

B&W used an industrial 19-ft CobraFab Industries, Inc. band saw model VH2532HD with 'Cobra Strike' and an interchangeable blade option for all cutting purposes associated with the destructive activity. The initial size reduction cuts were performed on the Nozzle 63 specimen using one of the coarse toothed blades prior to the arrival of PNNL staff. Non-essential material was removed to reduce weight and to facilitate proper blade placement on the specimen during critical cuts. Figure 6.1 shows images from the size reduction activity. All cuts in this activity were conducted without lubrication or coolant to minimize disturbance to the interference fit region.

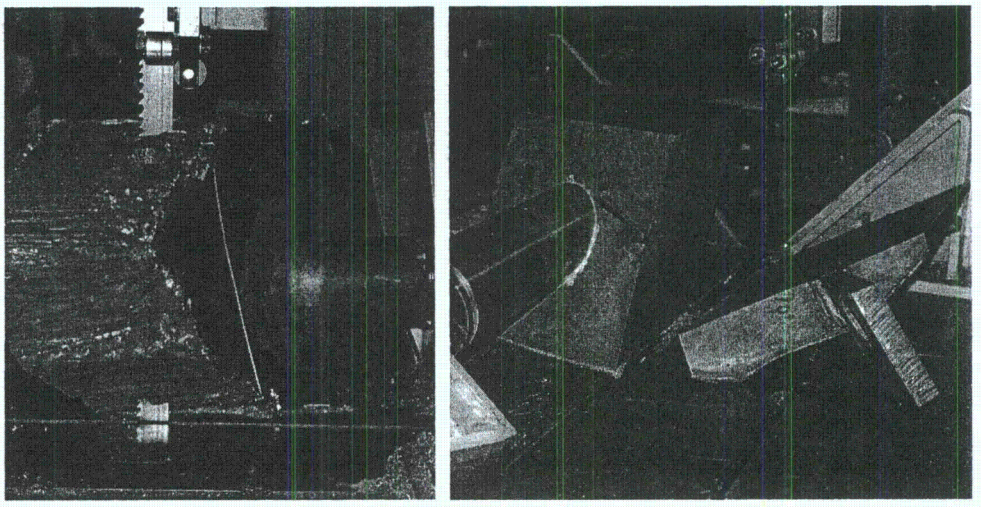

Figure 6.1 Size Reduction Cutting Activity

After size reduction, the nozzle assembly was prepared for the dissection cut that separated the high and low sides of the assembly. The cut line was selected to start at approximately the 95-degree mark (Figure 6.2), and follow through to the 275-degree mark. The line placement was based on the ultrasonic data and chosen to preserve the primary leak path previously identified in the ultrasonic images.

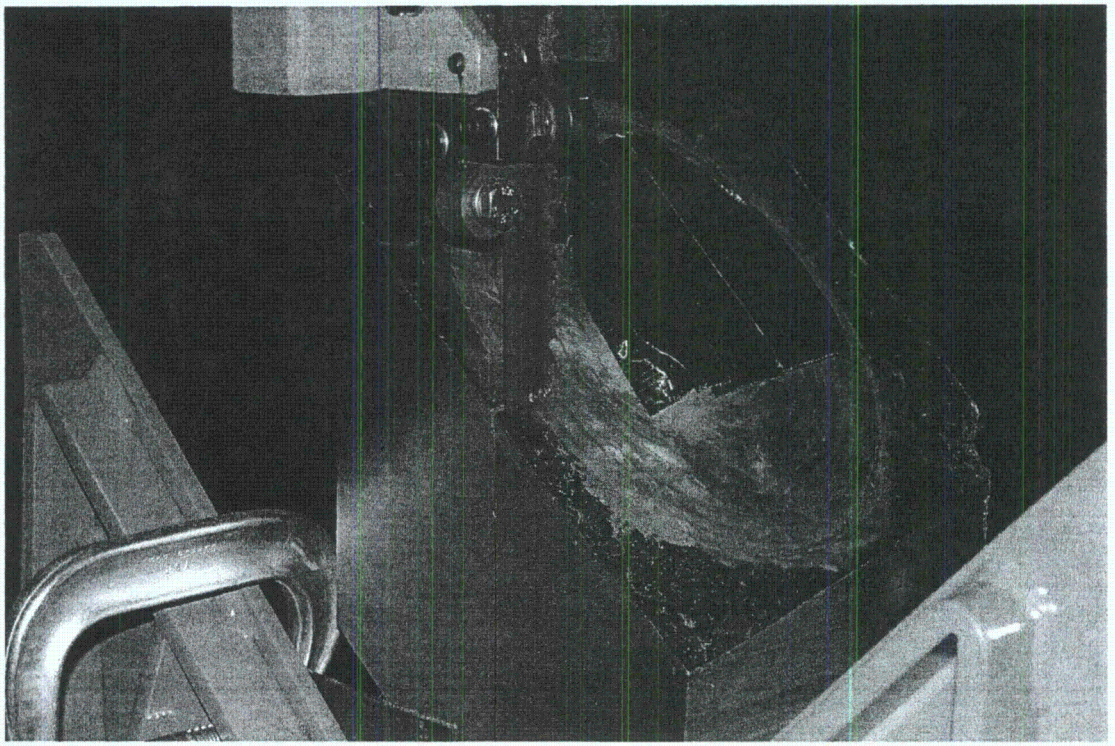

Figure 6.2 Start of the Dissection Cut

The cut to remove the J-groove weld was made 6.35 mm (0.25 in.) above the butter/triple point region in the reactor pressure vessel (RPV) head as seen in Figure 6.3. The high or uphill side half-portion was selected for the first cutting. As previously stated, the 'high' side has several potential leak paths whereas the 'low' or downhill side had the primary leak path as identified in the ultrasonic data. The specimen was secured and the band saw tilted to an approximate 43-degree angle to match the angle between the nozzle and head. Cutting at this angle maximized the annulus region that was exposed while keeping the weld and butter regions intact for future evaluation. As the cut was designed to pass only through the low-alloy RVH material, the fine toothed cutting blade was selected for use. However, other blades had to be used when cutting difficulties, as detailed in Appendix C, were encountered.

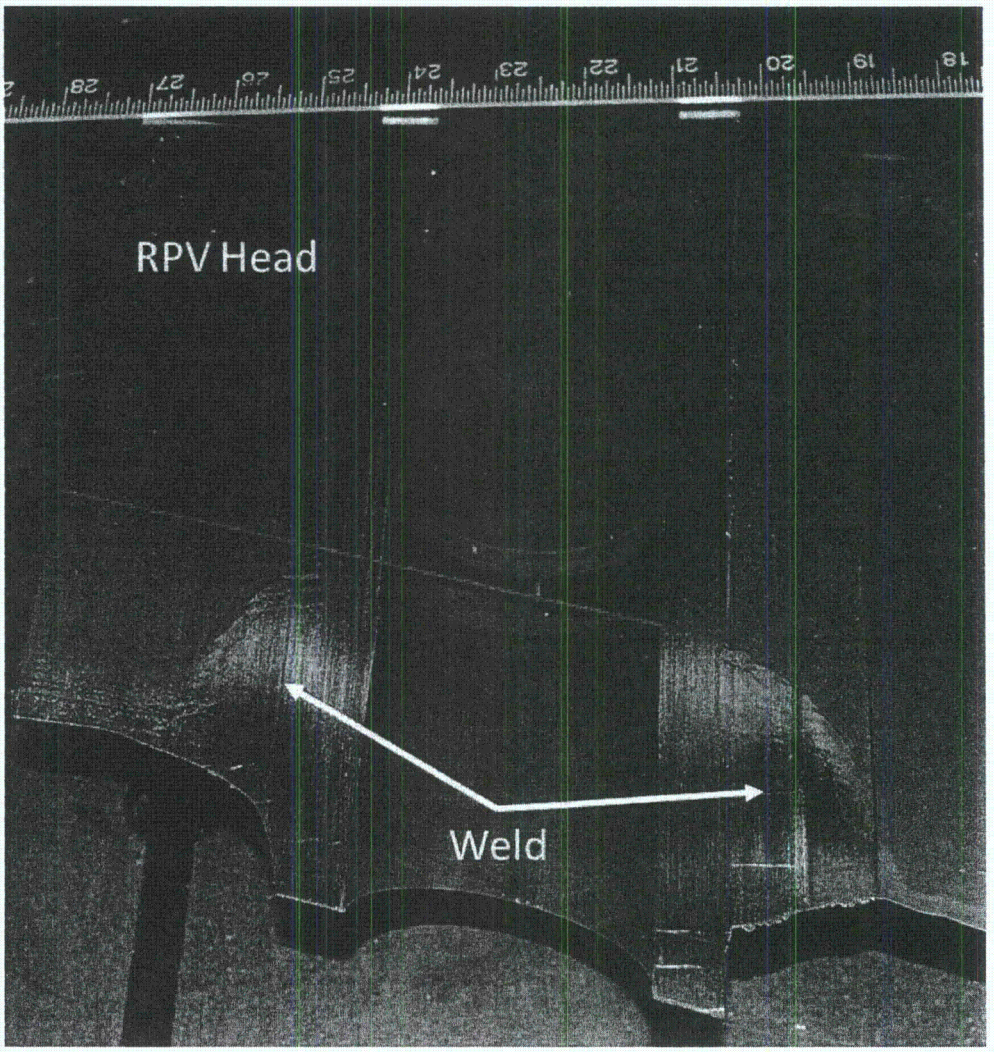

Figure 6.3 Nozzle 63 Assembly Cut in Half by Dissection Cut. The red line indicates where the weld removal cut was made.

The cutting continued until the entire nozzle was separated from the J-groove weld region as pictured in Figure 6.4. At this point, the nozzle region above the weld was freely released from the RPV head material. Removal of the nozzle exposed the annulus region of the high-side section as shown in Figure 6.5. A Nikon D40x camera was used to acquire high-resolution photographic documentation of the annulus region. This activity was provided by B&W. A subsequent cut was conducted on the low-side section to expose its annulus region containing the primary leak path (Figure 6.6). The nozzle freely released from this portion as well.

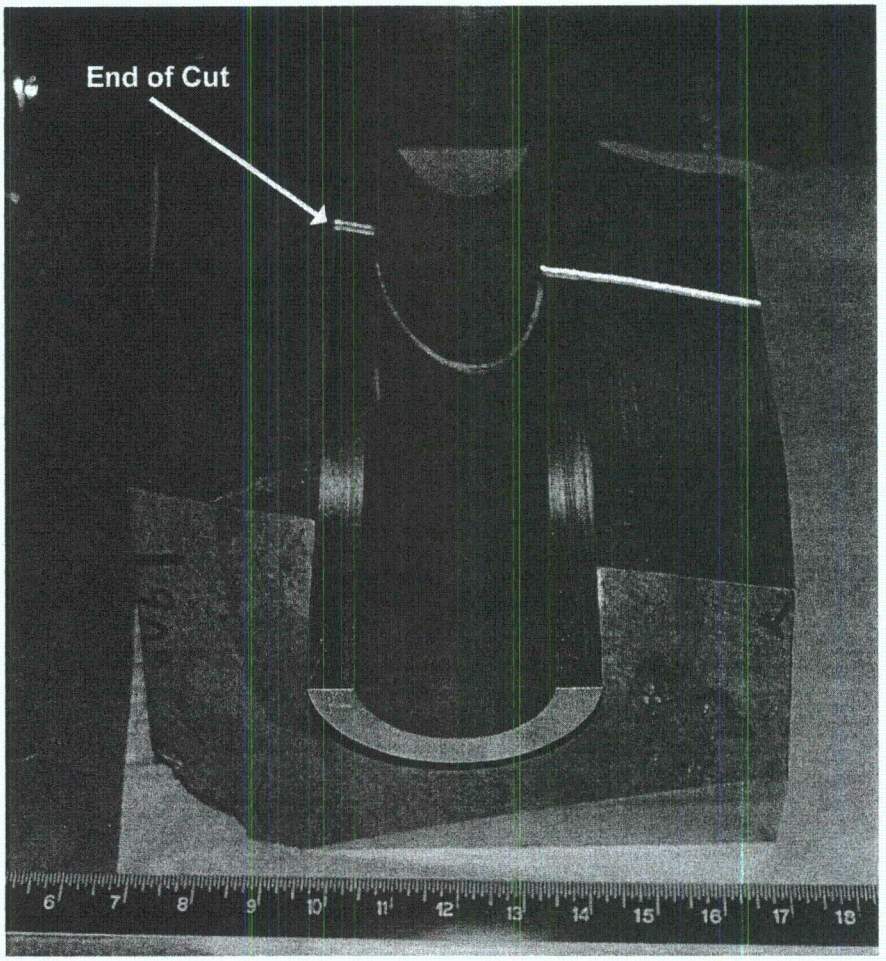

Figure 6.4 End of J-groove Weld Removal Cut

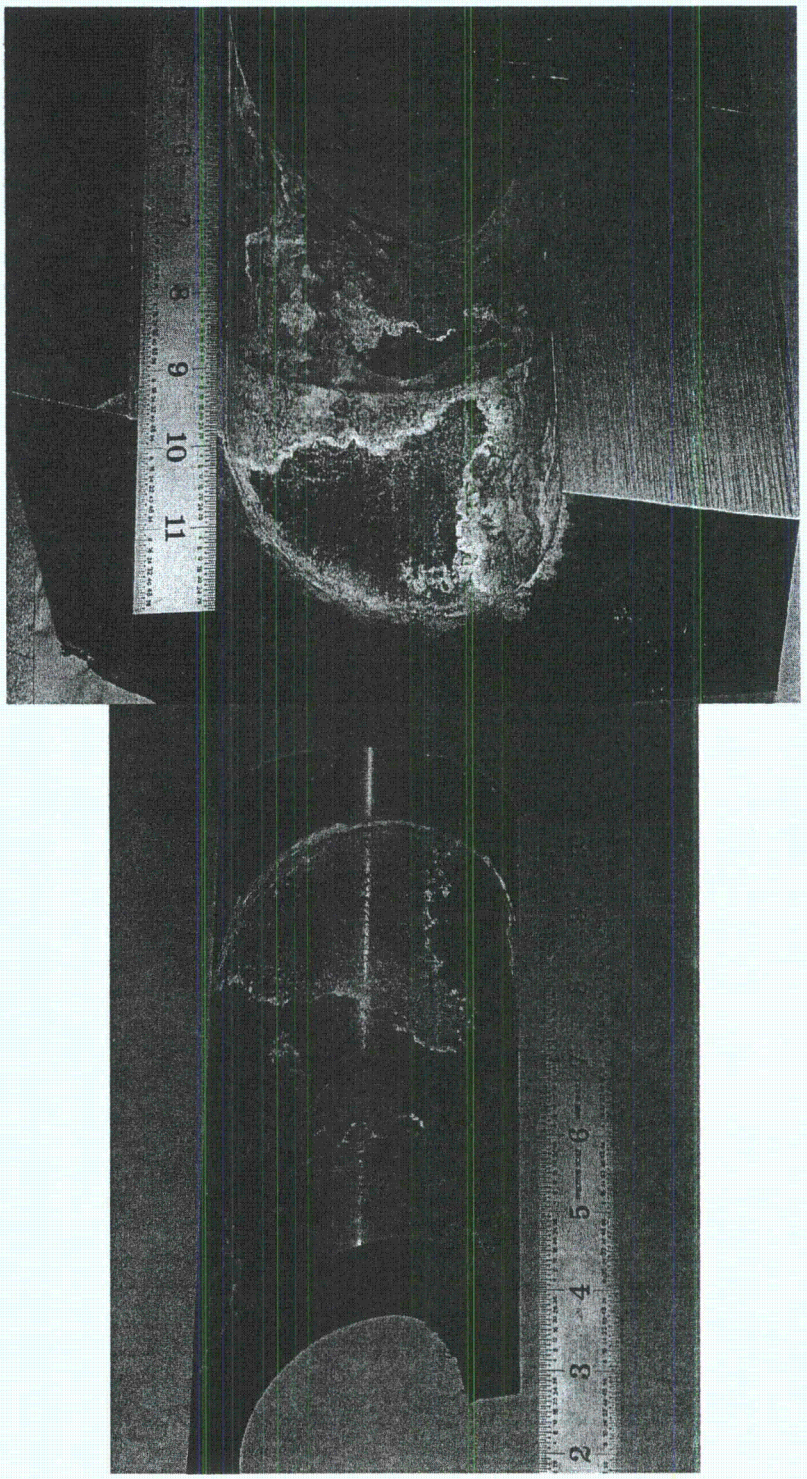

Figure 6.5 Exposed RPV Head and Nozzle from High Side Section

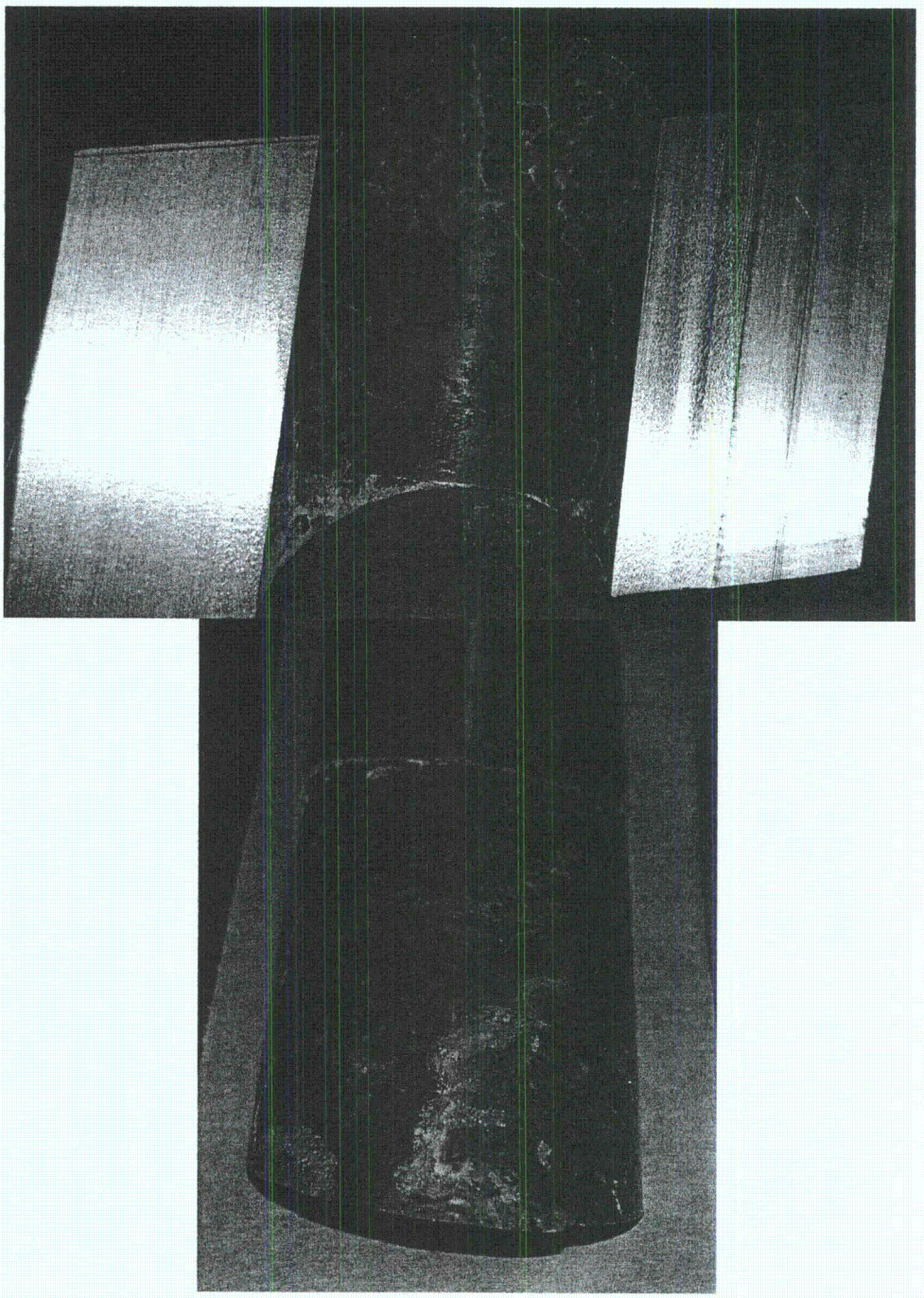

Figure 6.6 Exposed RPV Head and Nozzle from Low-Side Section

7 CORRELATION OF ULTRASONIC AND DESTRUCTIVE RESULTS

This section compares the phased-array ultrasonic results to the visual results obtained by cutting through the nozzle assembly to reveal the interference fit surfaces. The nozzle outer diameter (OD) surface was photographed in 45-degree increments with the individual photographs cropped and stitched together to form the montage image in Figure 7.1. Some evidence of thin boric acid deposits is visible in the white regions while a thin corrosion layer is seen in the rust-colored regions. The red line marks the interference fit region. The main leak path is identified by the two black arrows.

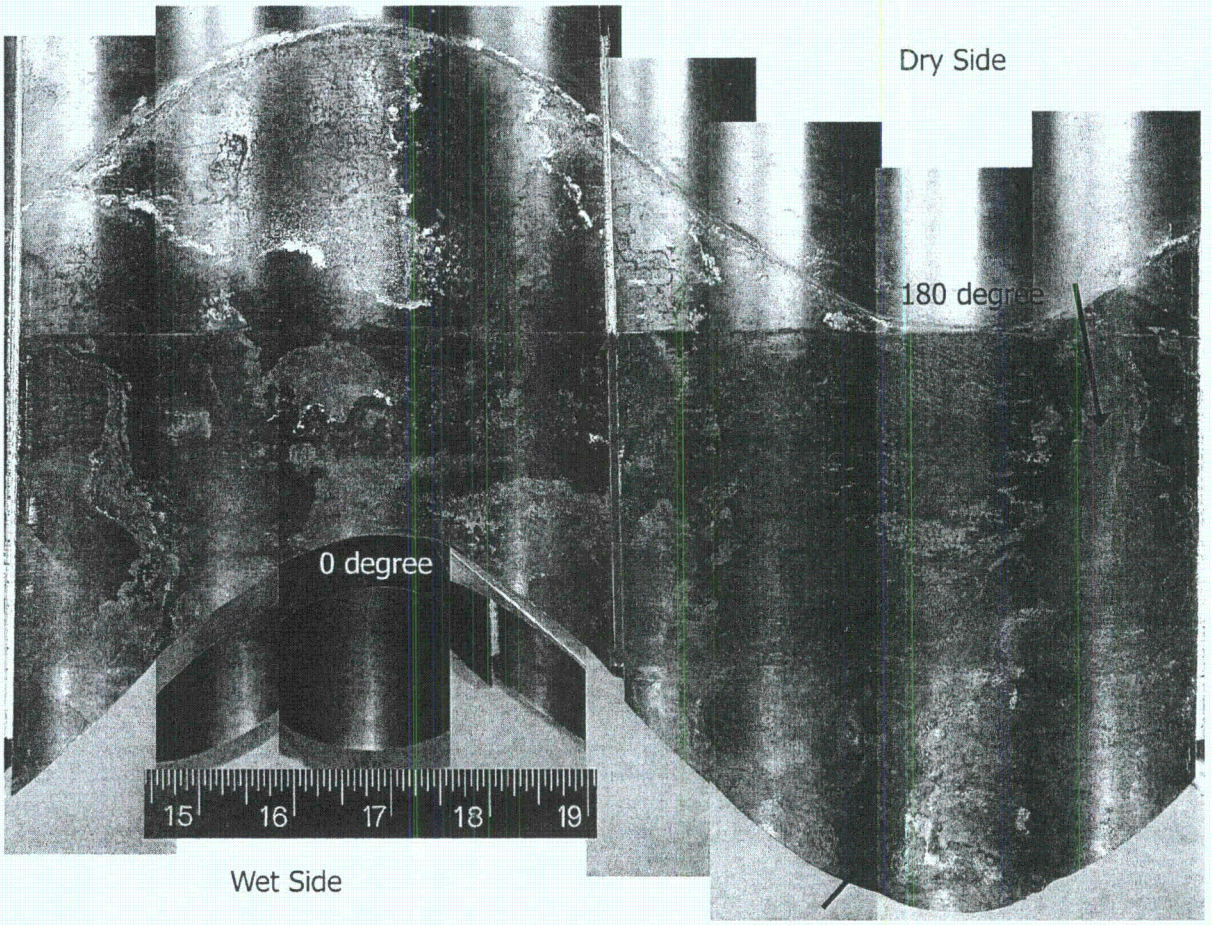

Figure 7.1 Nozzle Surface. The red line marks the interference fit region and the two black arrows identify the main leak path.

Similarly, the exposed reactor pressure vessel (RPV) head was photographed and the stitched image is displayed in Figure 7.2. The main leak path and other features seen in the ultrasonic images are clearly evident. Boric acid deposits are visible in white and corrosion products in the rust color. The interference fit region is evident in the photograph and is marked with the red line. For comparison, the ultrasonic data image with the same aspect ratio as the photograph is displayed in Figure 7.3. The ultrasonic image was stretched to best fit the visual data but the match is not perfect due to the curved surfaces. Nevertheless, the ultrasonic features well match the features seen visually on the RPV head annulus. Clearly, the main leak path was precisely imaged and other partial leak paths are evident and well imaged.

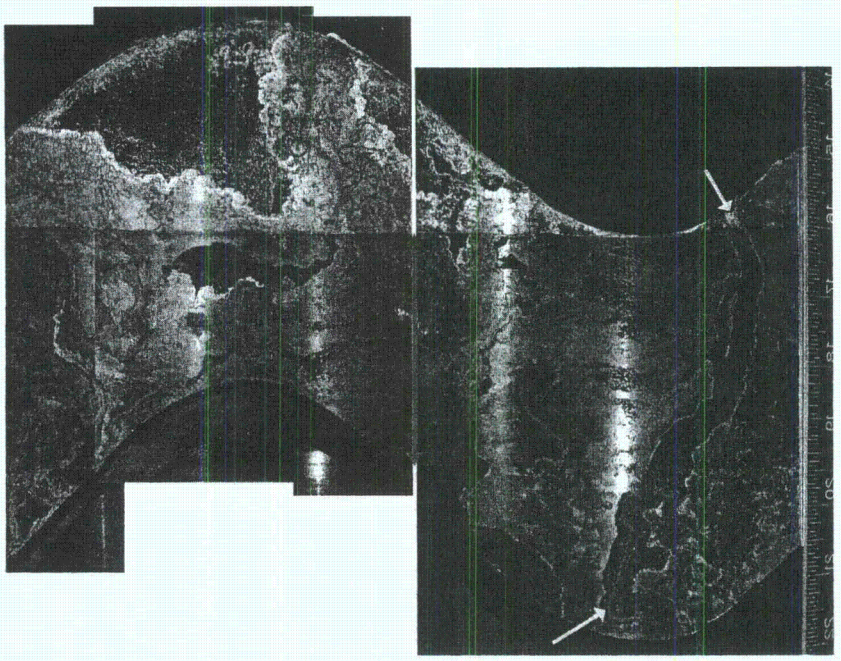

Figure 7.2 RPV Head Surface. The red line marks the interference fit region and the two yellow arrows identify the main leak path.

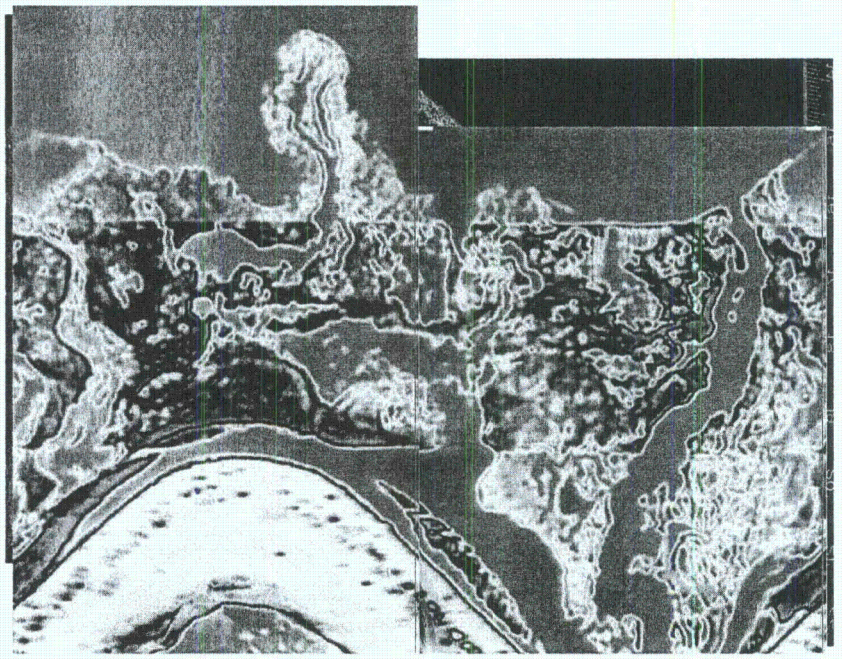

Figure 7.3 Ultrasonic Data Stretched to Best Match the RPV Head Photograph

8 ADDITIONAL PHYSICAL MEASUREMENTS ON THE REACTOR PRESSURE VESSEL HEAD

As part of a supplemental study, attempts were made at measuring the boric acid thickness in the annulus as well as the extent of corrosion of the reactor pressure vessel (RPV) head. These measurements were then compared to the ultrasonic data. The boric acid thicknesses were first measured at specific points using an eddy current thickness gage. Next the RPV head surface was replicated with a Microset material, and boric acid thickness measurements were made on cross-sectional slices through the replica in the main leak path area. Finally, the replicated sections were examined with a stereomicroscope providing an indication of the corrosion extent. Best-effort attempts within limited budget and time constraints were made to remove the boric acid deposits in order to then measure corrosion or material wastage under the deposits. This effort was unsuccessful, but replica observations indicated minimal corrosion and wastage of the low-alloy steel head.

8.1 Boric Acid Measurements – Thickness Gage

In addition to the comparison of the interference fit region photographs with the ultrasonic images, a further study was conducted to obtain boric acid thickness measurements on the RPV head in the annulus region and to compare these results to the ultrasonic data. This was done while recognizing that the ultrasonic response in terms of reflected ultrasonic amplitude from the interference fit region would likely not correlate solely to the boric acid thickness measurements on the RPV low-alloy steel material. The boric acid on the RPV head material was only part of the contribution to the ultrasonic response. Also contributing to the ultrasonic response was the boric acid on the nozzle material (refer to Figure 7.1), and this contribution was not measured. Additional factors not measured were the density of the boric acid deposits and the difference between boric acid and the visible low-alloy steel corrosion product. Both of these factors could cause differences in the reflection or transmission of ultrasonic energy. Nevertheless, a best-effort attempt was undertaken to quantify the boric acid in the annulus region and relate these measurements to the ultrasonic data.

An eddy current probe was selected (DeFelsko PosiTector 6000 Series coating thickness gage) to measure the boric acid deposit thickness at selected points in the annulus region on the RPV head material. The probe had a point contact area of 1 mm (0.040 in.) in diameter and spanned a measureable coating thickness range of 0 to 1.14 mm (0 to 45 mils). The thickness gage accuracy was verified by taking measurements on several plastic shims in the 24 to 507 micron (0.94 to 20.0 mils) range. Measurement error was less than or equal to 2.5 microns (0.098 mils). The selected measurement sites were chosen to represent the differing ultrasonic amplitudes in the interference fit that included the main leak path, other partial leak paths, the interference fit with and without suspect boric acid present, and areas outside of the interference fit. A total of 70 points were selected by both Pacific Northwest National Laboratory (PNNL) and U.S. Nuclear Regulatory Commission (NRC) personnel and are displayed in Figure 8.1 for the photographed uphill and downhill halves of the RPV head. The red dots represent leak paths or bare metal regions. The green dots represent areas with different reflectivity in the photo and

differing ultrasonic response. Lastly, the two yellow dot pairs represent points on either side of the upper interference fit border.

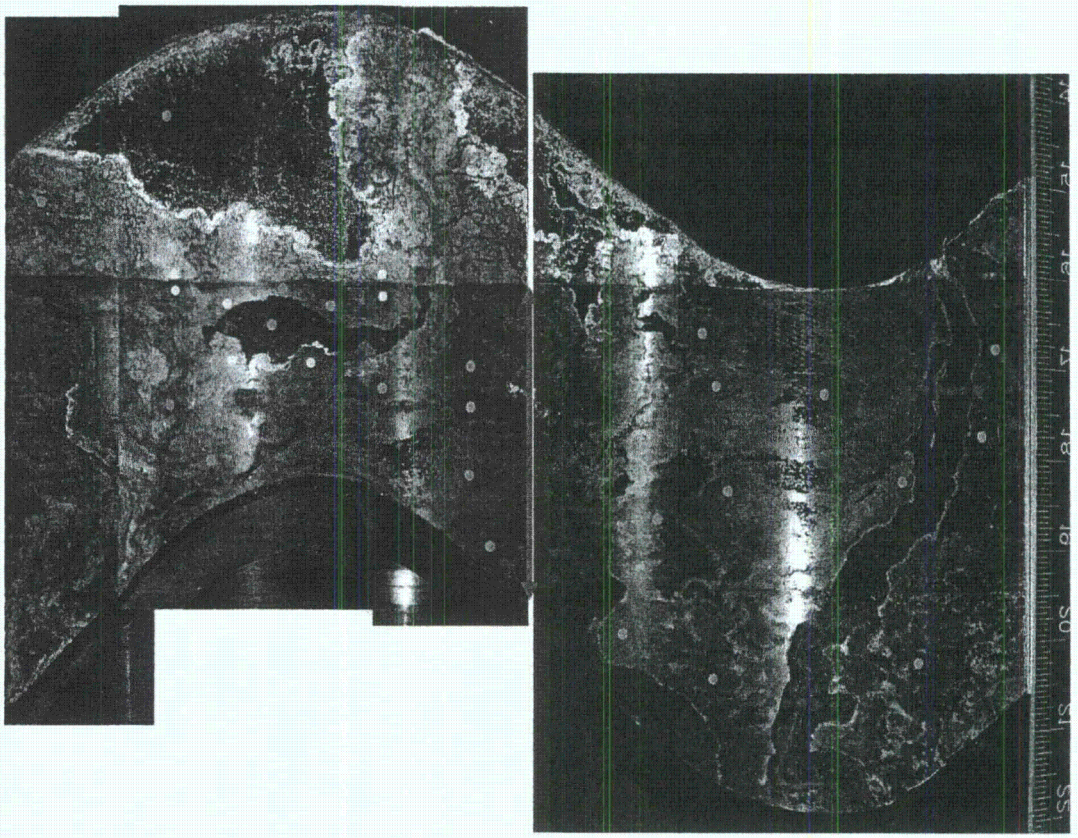

Figure 8.1 Photograph of the RPV Head Material with Boric Acid Measurement Points. The interference fit region is marked by the red line.

Each of the 70 data points was numbered and the boric acid measurements were entered into a spreadsheet. The thickness measurements in microns are displayed adjacent to the data points in Figure 8.2. Some general observations were:

1) Boric acid values above and below the interference fit region outside of leak path and bare metal or nearly bare metal regions are nominally in the 130 to 200 micron (5.1 to 7.9 mils) range.

2) The two pairs of data (yellow dots) on either side of the interference fit on the uphill section show boric acid values of 156 and 150 microns (6.1 and 5.9 mils) above the fit region and 62 and 74.5 micron (2.4 and 2.9 mils) in the fit region.

3) Leak path and bare metal or nearly bare metal points have a thin surface corrosion layer, not visible boric acid deposits, with deposits at 16 microns (0.63 mils) or less.

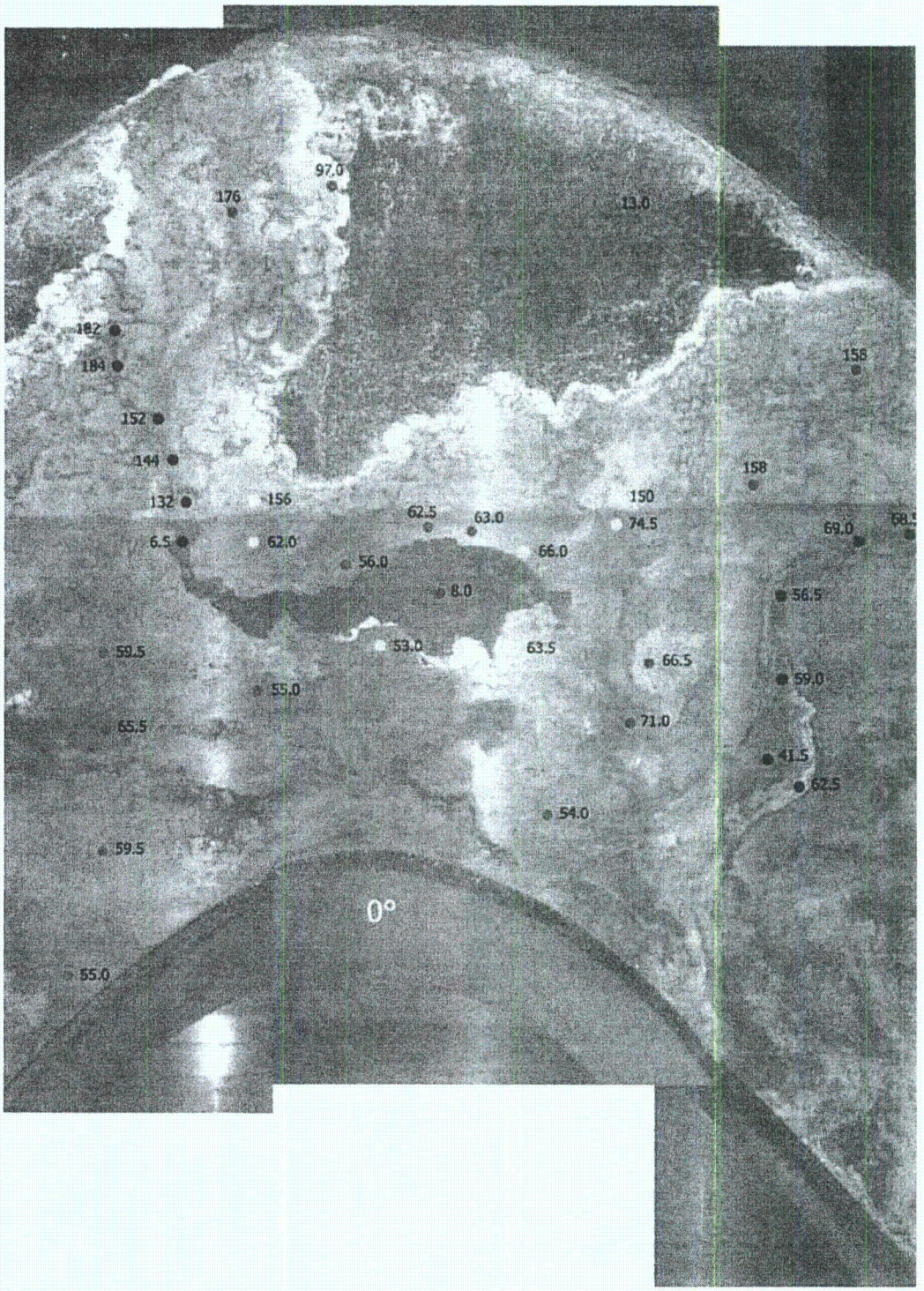

Figure 8.2 Boric Acid Thickness Values in Microns

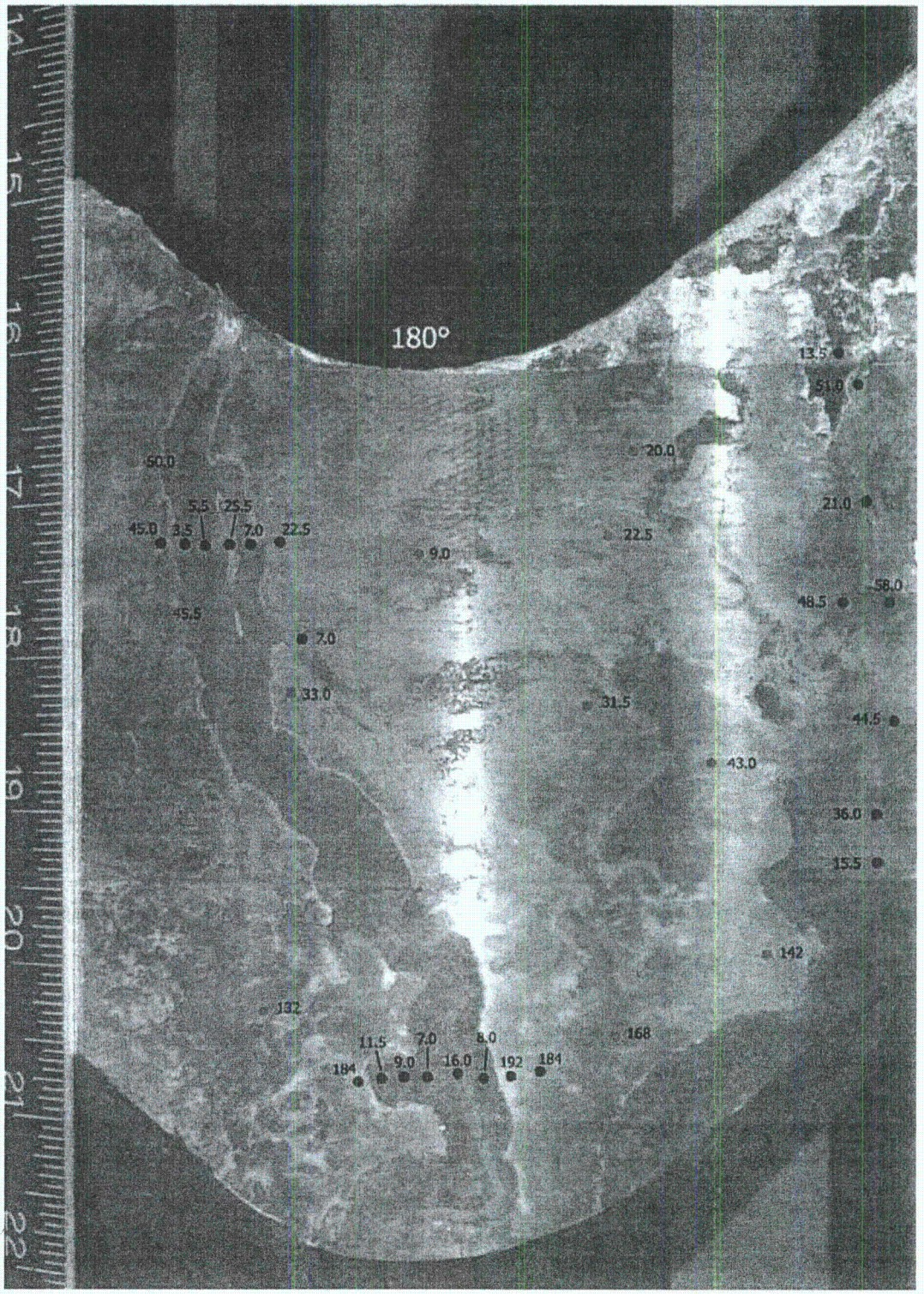

Figure 8.2 (Continued)

The relationship between the ultrasonic response values and eddy current (EC) thickness values was explored in more detail. As was previously demonstrated in the mockup evaluation, the large-amplitude ultrasonic data represent a gap in the interference fit. These data regions are represented by the color orange in the rainbow color bar previously shown in Figure 5.3, for example. Two horizontal profiles that display ultrasonic amplitude variations along the selected measurement line in the image are shown in Figure 8.3. The left image displays a profile taken along the red horizontal line located in the interference fit region. Clearly the high ultrasonic response is evident across the main leak path and then the response falls off on either side, of the leak path. The left side drop off is more severe in the profile and is associated with the blue color in the image, while the right side drop off is moderate and is associated with the yellow color in the image. The right image displays a profile taken along the red horizontal line in the image below the interference fit. The profile as well as the data image, again, shows a high-amplitude ultrasonic response for the leak path regions with signal drop off on both sides of the leak paths. At this axial position in the annulus, the drop off is smaller than that observed in the data from within the interference fit on the left.

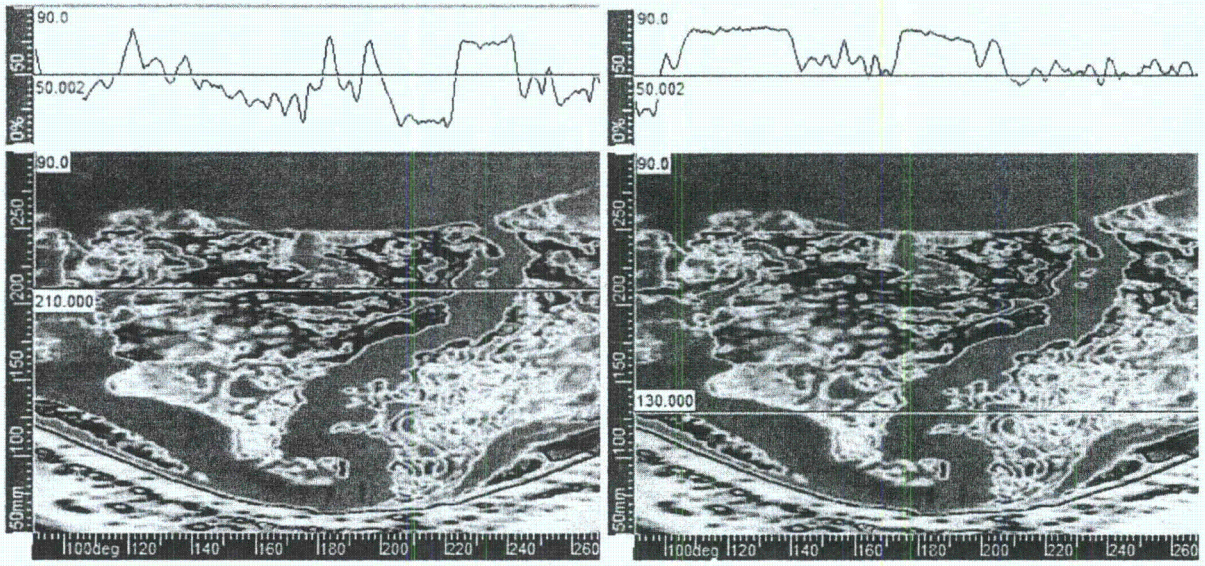

Figure 8.3 Ultrasonic Response Profile at Top, Acquired Along the Red Horizontal Line in the Image Below. The left image profile is in the interference fit and the right image profile is outside of the interference fit.

The inherent characteristic of a leak path in the ultrasonic image was suggested and verified as that of a high-amplitude response that traversed the entire interference fit (I fit) region. The primary leak path boric acid measurements obtained with the eddy current probe further show that the leak path was characterized by a region with a minimal or no boric acid/corrosion layer. This inverse relationship is represented in Figures 8.4 and 8.5. Eddy current data obtained at the red points spanning the primary leak path in Figure 8.1 are plotted as boric acid (BA) data in blue diamonds. The corresponding ultrasonic data at those same points are plotted as ultrasonic test (UT) data in red squares. Figure 8.4 represents data obtained in the interference

fit region and Figure 8.5 represents data outside of the interference fit from the primary leak path points, red in Figure 8.1. In each figure below, the leak path boundary is noted by two black horizontal lines. Both figures show that leak path data points are represented by this characteristic high ultrasonic response (above 70%) and low boric acid/corrosion layer thickness (approximately below 20 microns [0.79 mils]). More specifically, the BA/corrosion layer thickness within the interference fit is below 7 microns (0.28 mils) with the exception of the data point acquired at the island position in the main leak path. Here a larger thickness value of 25.5 microns (1.0 mils) was measured. Similarily, for data outside of the interference fit but still in the primary leak path, the layer thickness values were below 12 microns (0.47 mils) except for the data point at the rust-colored streak in the middle at 16 microns (0.63 mils). Moving outside of the leak path, the ultrasonic response drops and the BA/corrosion layer increases. Within the interference fit, Figure 8.4, this increase in BA/corrosion layer thickness is much smaller as can be expected. The interference fit region has little to no gap between the nozzle and RPV head but this condition is variable throughout the fit (Hunt and Fleming 2002). Boric acid presence in this region would likely be a thin layer and more compacted as noted by the low (blue-colored) ultrasonic response. Outside of the interference fit, the BA/corrosion layer increases more dramatically on either side of the main leak path, to nominaly 185 microns(7.28 mils). A wider gap was present in the annulus region outside of the interference fit due to a machined counter bore (refer to Figure 1.1). The data suggest that this gap fills with boric acid. Note that the ultrasonic response shows a smaller drop on either side of the leak path possibly indicating that the boric acid was less compacted in this region.

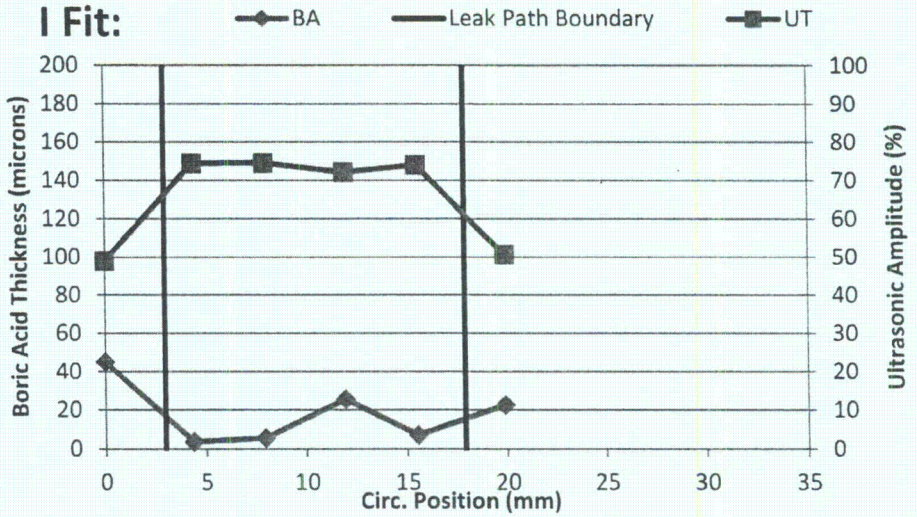

Figure 8.4 Ultrasonic and Boric Acid/Corrosion Layer Thickness Along a Line Across the Main Leak Path in the Interference (I) Fit

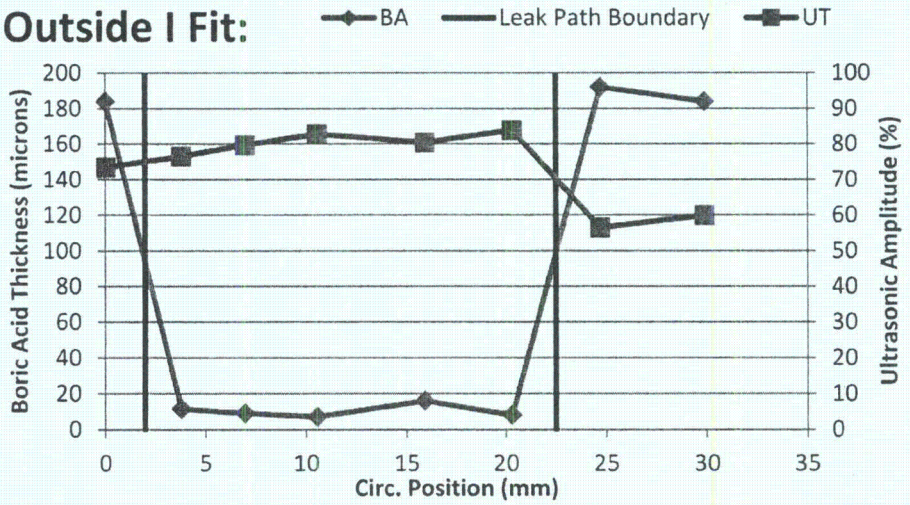

Figure 8.5 Ultrasonic and Boric Acid/Corrosion Layer Thickness Along a Line Across the Main Leak Path Outside the Interference Fit

Lastly, an attempt was made to correlate the ultrasonic and eddy current measurements at all 70 data points. In this analysis, the data points were segregated as the interference fit region and outside of the interference fit region. Initially, all of the points were plotted with results shown in Figure 8.6. Points with high ultrasonic response and BA/corrosion thickness, upper left, are primarily associated with the main leak path region and represent areas where any potential deposits are flushed out and not allowed to remain. In addition to the primary leak path, other partial leak paths and regions with possible bare metal, lacking deposits, were identified. All of these leak path and bare metal points are plotted in Figure 8.7. These points represent a gap in the annulus, noted by the high ultrasonic response. Deposits as measured with the EC probe could be present but are not compacted throughout the annulus thickness. The remaining points (70 original points minus the leak path and bare metal points) represent the nominal annulus condition and are plotted in Figure 8.8. An ultrasonic amplitude level of approximately 50% divides the data between an interference fit response and one outside the interference fit region. For this nozzle, the BA/corrosion layer thickness values in the interference fit are less than 75 microns (3.0 mils), and outside the interference fit are greater than 130 microns (5.12 mils). The center point, with a layer thickness of 97 microns (3.82 mils) in Figure 8.8, can be excluded as it was obtained at a location where there is a noticeable boric acid deposit on the nozzle side. This additional deposit, though not quantitatively known, would increase the layer thickness value moving the point to the right and likely in the range of the other "Outside I Fit" data points. The other outlier point (EC value of 9 microns [0.35 mils] and UT value of 73%) is from the interference fit data and was obtained at a rust-colored region so it was not included in the bare metal points. This outlier is possibly explained by positional registration error of the data points. For example, ultrasonic data in a narrow secondary leak path varied from a value of 83 to 44% within and outside the leak path, respectively. Also the accuracy in acquiring EC data at the exact points specified on the photograph varied as definitive local boundary markers on the component were not always present. This is to say that these measurements have some positional error that cannot be eliminated. Nevertheless,

a clustering of the data is evident. These results are specific to this nozzle, Nozzle 63, as the fabrication of each nozzle represents a unique geometrical condition; however, these data likely show expected trends for nozzles in general. A summary of the Nozzle 63 results is listed.

- Leak paths
  a. High UT response, >60%
  b. Minimal boric acid/corrosion layer EC measurement, <16 microns (0.63 mils)
- Outside the leak path
  a. Inside the interference fit region
     i. UT response <50%
     ii. EC measurement low, 15–75 microns (0.59–3.0 mils)
  b. Outside the interference fit region
     i. UT response >50%
     ii. EC measurement larger, 130–190 microns (5.12–7.48 mils)

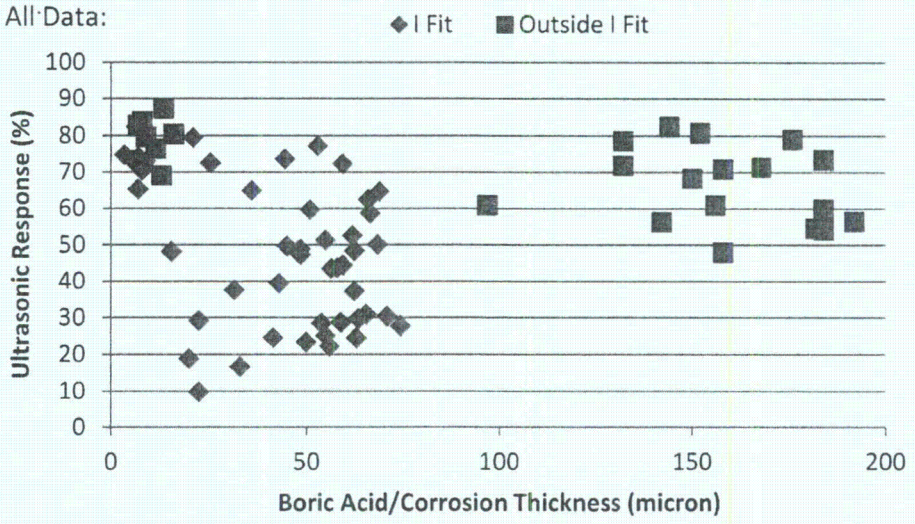

Figure 8.6 Comparison of Ultrasonic Response and Boric Acid/Corrosion Layer Thickness at all 70 Acquired Data Points

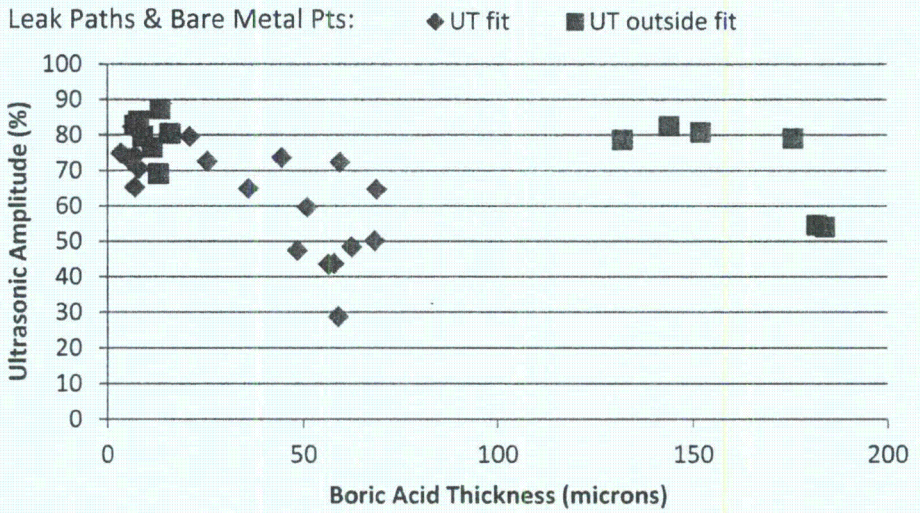

Figure 8.7 Comparison of Ultrasonic Response and Boric Acid/Corrosion Layer Thickness at the Leak Path and Bare Metal Data Points

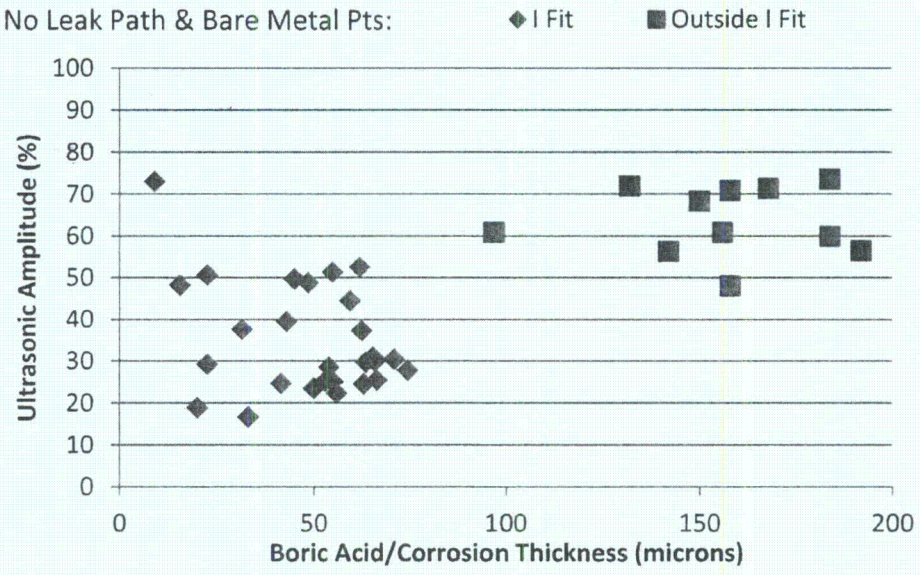

Figure 8.8 Comparison of Ultrasonic Response and Boric Acid/Corrosion Layer Thickness at Data Points Not in the Leak Paths Nor at Bare Metal Points

8.2 Boric Acid Measurements – Microset Cross Sections

Confirmatory boric acid measurements were also visually made on Microset replicas of the RPV annulus in the main leak path region. This replicating material has better than 0.1 micron (0.004 mils) resolution. Eight areas of interest across the main leak path, as shown in

Figure 8.9, were selected for these additional and confirmatory measurements. The sliced and annotated replica is shown in Figure 8.10. Boric acid measurements were made on the edges of the slices with the white arrows showing the cut surfaces that were measured. Several of the measurement values obtained by these surface cross sections were compared to the thickness gage measurements. While only a few data points were compared, the root mean squared error (RMSE) between measurements was 14 microns. This error is assumed to be primarily due to data registration.

8.3 Replicated Surfaces – Stereomicroscope

Lastly the replicated surfaces from Figure 8.10 were viewed with a stereomicroscope to better document the surface conditions and to attempt to quantify the corrosion or erosion of the low-alloy steel in the annulus region. Machining marks were observed on the replicated surfaces indicating minimal corrosion, erosion, or wastage throughout the leak path region. These observations further indicate a low flow rate during plant operation. Interesting areas are discussed.

Figure 8.11 shows replica pieces 2 and 3 in the main leak path in the region below the interference fit. Both pieces show double streaks from corrosion product staining but no or minimal actual corrosion or wastage. The machining marks are intact across the images.

The transition from below the interference fit to the interference fit region is captured in Figure 8.12 on piece 4. Machining marks are clearly evident and were observed in most of the bare areas examined on the RPV head surface. The surface finish within the interference fit region was approximately equivalent to a turned finish of 1.6 micro-meters (63 microinches). The finish below the interference fit region was approximately equivalent to a milled 1.6 micro-meters- (63 microinch-) finish.

Piece 5 contained an angular feature or anomaly with an approximate length of 2.3 mm (0.090 in.) and is shown in Figure 8.13. The right image is at a twice the magnification as the image on the left and shows more detail. This feature appeared to be more of a dent or scrape and not corrosion. Piece 5 lies in the interference fit region.

The only corrosion observed in the replicated surfaces was in the region above the interference fit in piece 9. The piece is shown in Figure 8.14 with the two areas of interest circled. The circled region on the left was in the main leak path and covered an area of approximately 6.4 mm (0.25 in.) in diameter with a depth of 0.25 mm (0.01 in.). The corroded area on the right was approximately 12.7 by 1.6 mm (0.5 by 0.06 in.) with a depth of 0.25 mm (0.01 in.).

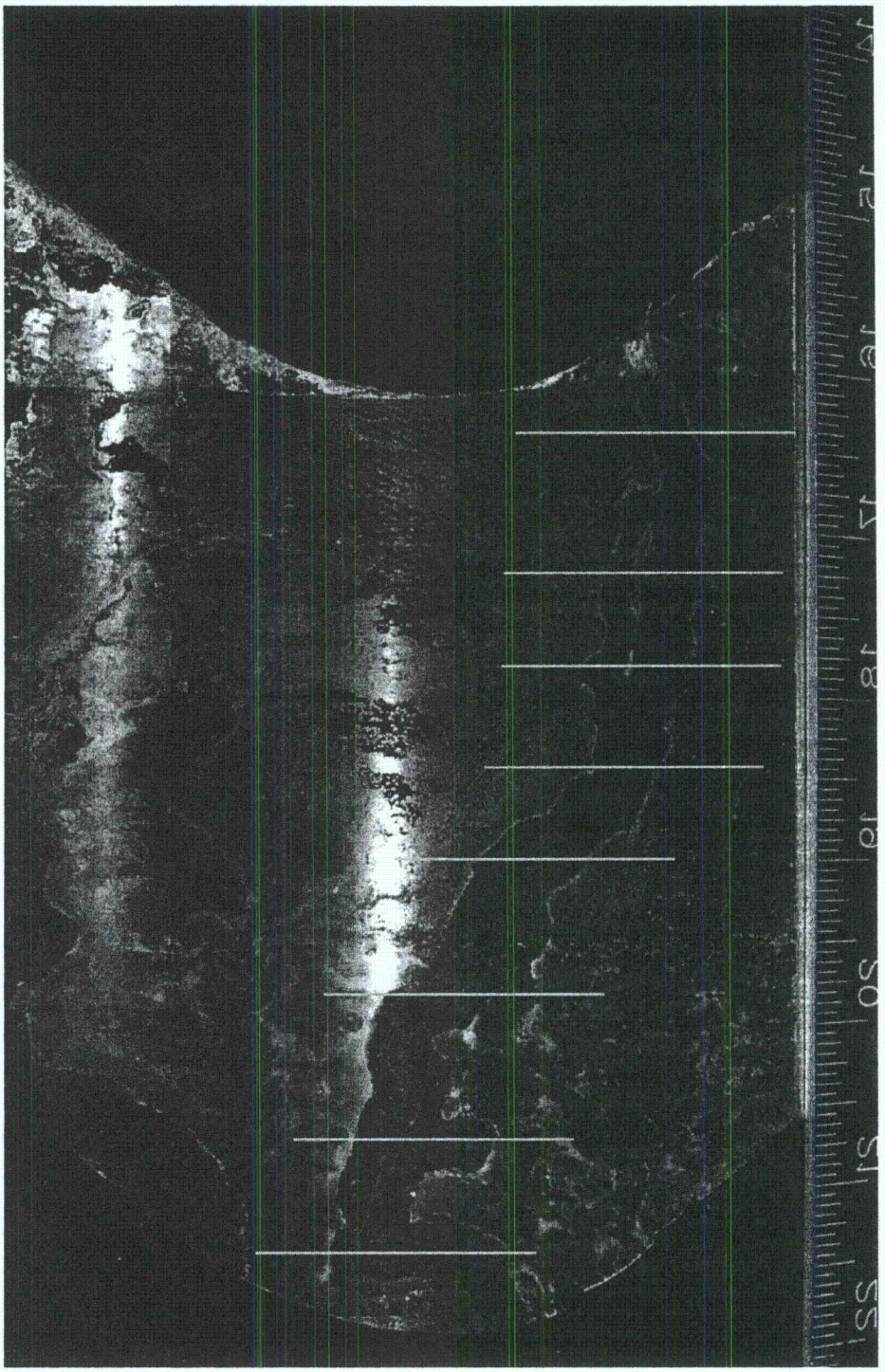

Figure 8.9 Eight Areas Selected for Boric Acid Thickness Measurements on Cross-Sectional Slices of Microset Replica

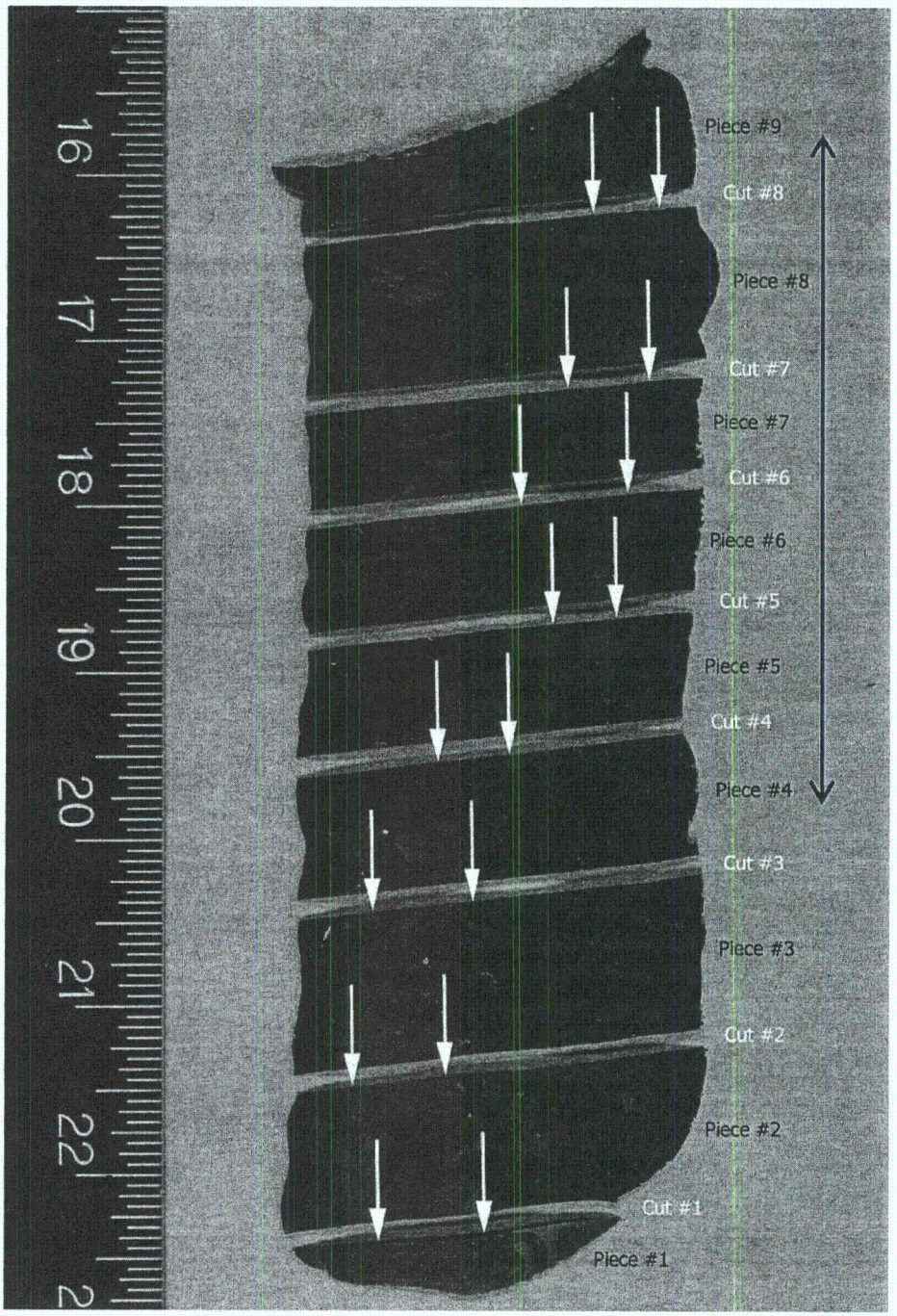

Figure 8.10 Leak Path Replica with Cuts and Pieces Identified. The interference fit region is noted with the black line and is contained in pieces 4 through 9.

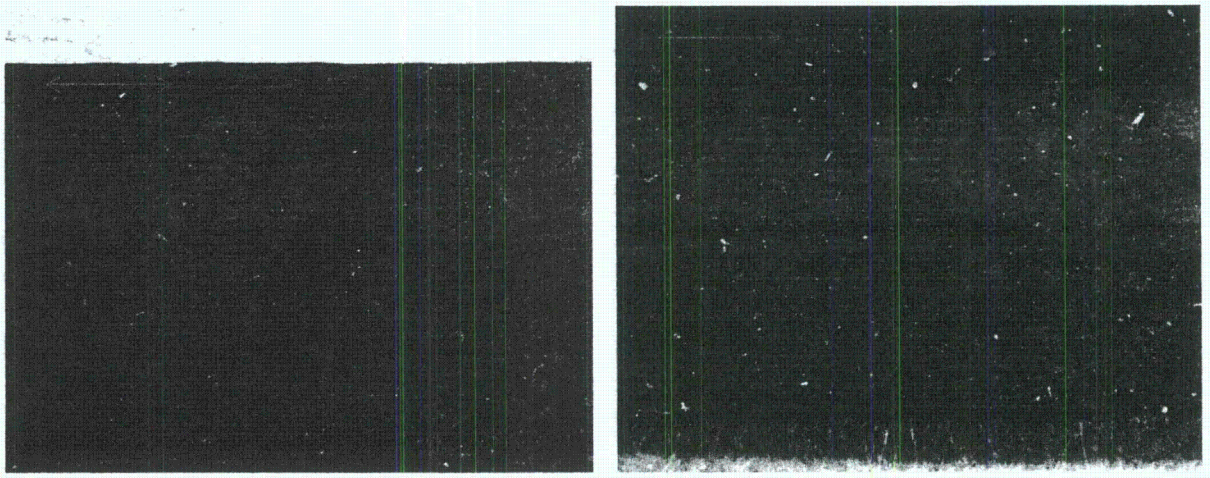

Figure 8.11 Staining Streaks in the Leak Path Below the Interference Fit from Replica Pieces 2 and 3, Left and Right, Respectively. The red line represents 2.0 mm (0.80 in.) in length.

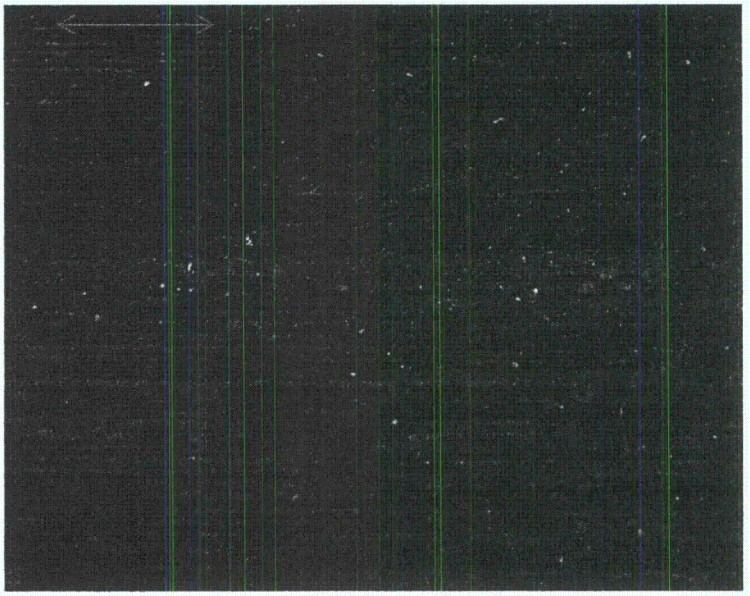

Figure 8.12 Transition from Below the Interference Fit to the Interference Fit Region. Machining marks are evident in this replica piece 4. The red line represents 2.0 mm (0.80 in.) in length.

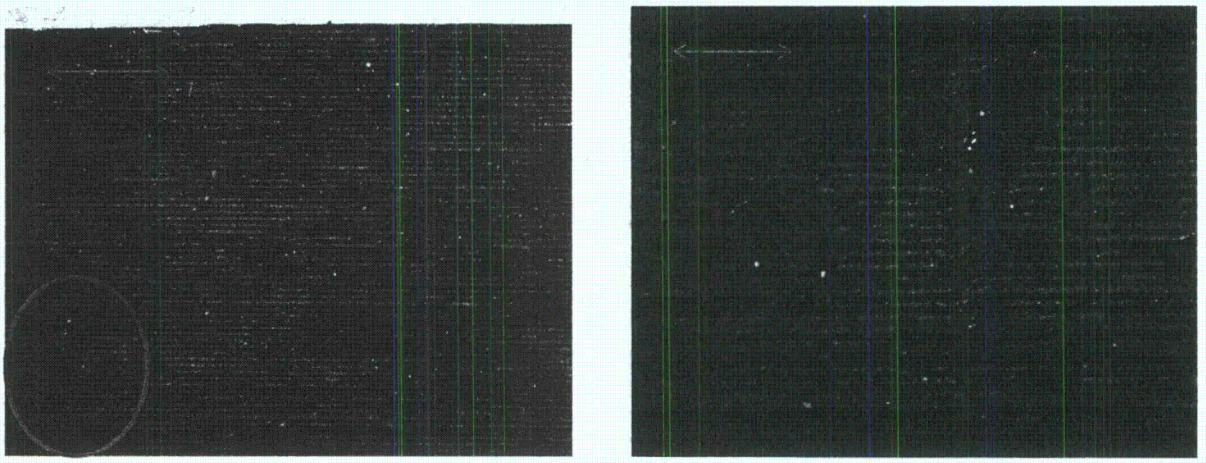

Figure 8.13 Piece 5 from the Interference Fit Region Shows an Indication of a Scrape. In the left image the red line represents 2.0 mm (0.80 in.) in length. The image on the right at twice the magnification of the left shows more detail.

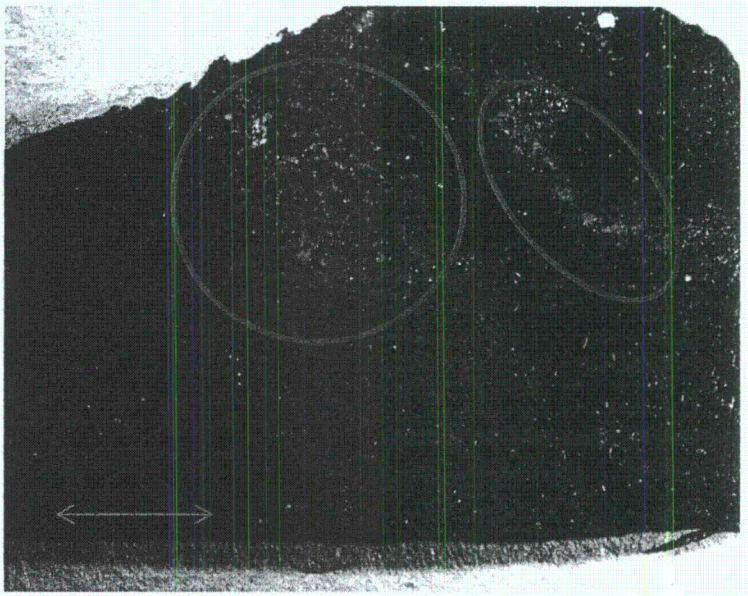

Figure 8.14 Corrosion Areas Observed Above the Interference Fit Region. The red line represents 2.0 mm (0.80 in.) in length.

9 SUMMARY AND CONCLUSIONS

1. The North Anna Unit 2 Nozzle 63 showed evidence of leaking in service and was removed for analysis and testing.
2. Prior to testing the nozzle, a phased-array ultrasonic evaluation on a mockup showed the system capable of identifying corrosion/wastage regions and boric acid deposits in the interference fit region between the nozzle and head. Wastage was distinguished by a high-amplitude ultrasonic response, greater than 60%, indicative of an air gap. Boric acid was distinguished by a low-amplitude ultrasonic response, less than 30%, in the interference fit region, indicating good energy transfer.
3. A phased-array ultrasonic evaluation of the nozzle identified the primary leakage path on the downhill side, as determined by a high-amplitude response, and scattered boric acid deposits throughout the annulus region, identified by low-amplitude response.
4. Destructive examination of the nozzle visually confirmed the presence of the leakage path and boric acid deposits identified in the ultrasonic evaluation.
5. Eddy current measurements of surface-deposit thickness traversing the leak path showed a rapid transition from high thickness just outside the leak path, to low thickness in the leak path (<16 microns [0.63 mils]), and back to high thickness on the other side of the leak path. This corresponded to a rapid change in the ultrasonic response from low amplitude, to high (>60%), and low again. Both the ultrasonic and eddy current responses appear to be characteristic of a well-defined leakage path.
6. Generally, the region of the interference fit gives a lower ultrasonic amplitude response (<50%) compared to regions outside the interference fit suggesting a compact boric acid/corrosion layer that efficiently transfers ultrasonic energy. This surface deposit layer is thinner in the interference fit (15–75 microns [0.59–3.0 mils]) as expected because this region is designed for little or no gap.
7. Surface deposit thickness measurements show thicker deposits (130–190 microns [5.12–7.48 mils]) outside the interference fit as expected due to the wider gap in the annulus region in the presence of a counter bore. UT responses in this area are higher (>50%) suggesting less compact deposits that reflect ultrasonic energy.
8. Surface replication shows that machining marks are still visible in the leakage path, suggesting a low leakage rate that led to minimal wastage of the RPV head.

10 REFERENCES

Bennetch JI, GE Modzelewski, LL Spain and GV Rao. 2002. "Root Cause Evaluation and Repair of Alloy 82/182 J-Groove Weld Cracking of Reactor Vessel Head Penetrations at North Anna Unit 2." In *2002 Proceedings of the ASME Pressure Vessels and Piping Conference (PVP2002), Service Experience and Failure Assessment Applications*, pp. 179-185. August 5-9, 2002, Vancouver, British Columbia, Canada. American Society of Mechanical Engineers, New York.

Clark AF. 1968. "Low Temperature Thermal Expansion of Some Metallic Alloys." *Cryogenics* 8(5):282-289.

Cumblidge SE, SR Doctor, GJ Schuster, RV Harris Jr., SL Crawford, RJ Seffens, MB Toloczko and SM Bruemmer. 2009. *Nondestructive and Destructive Examination Studies on Removed-from-Service Control Rod Drive Mechanism Penetrations*. NUREG/CR-6996, PNNL-18372, U.S. Nuclear Regulatory Commission, Washington, D.C.

Economou J, A Assice, F Cattant, J Salin and M Stindel. 1994. "NDE and Metallurgical Examination of Vessel Head Penetrations." In *3rd International Symposium on Contribution of Materials Investigation to the Resolution of Problems Encountered in Pressurized Water Reactors*. September 12-16, 1994, Fontevraud, France. French Nuclear Energy Society.

EPRI. 2005. *Materials Reliability Program: Destructive Examination of the North Anna 2 Reactor Pressure Vessel Head (MRP-142): Phase 1: Penetration Selection, Removal, Decontamination, Replication, and Nondestructive Examination*. EPRI Report 1007840, Electric Power Research Institute, Palo Alto, California.

EPRI. 2006. *Materials Reliability Program: Destructive Examination of the North Anna 2 Reactor Pressure Vessel Head (MRP-198): Phase 3: A Comparison of Nondestructive and Destructive Examination Findings for CRDM Penetration #54*. EPRI Report 1013414, Electric Power Research Institute, Palo Alto, California.

Gorman J, S Hunt, P Riccardella and GA White. 2009. "Chapter 44, PWR Reactor Vessel Alloy 600 Issues." In *Companion Guide to the ASME Boiler and Pressure Vessel Code, Volume 3, Third Edition*, ed: KR Rao. ASME Press, New York.

Grimmel B. 2005. *U.S. Plant Experience with Alloy 600 Cracking and Boric Acid Corrosion of Light-Water Reactor Pressure Vessel Materials*. NUREG-1823, U.S. Nuclear Regulatory Commission, Washington, D.C.

Hunt S and M Fleming. 2002. *Probability of Detecting Leaks in RPV Upper Head Nozzles by Visual Inspections, Revision 1, June 17, 2002*. Dominion Engineering, Inc., Reston, Virginia. Prepared for MRP PWR Alloy 600 Assessment Committee. U.S. Nuclear Regulatory Commission ADAMS Accession No. ML030860192.

IAEA. 2007. *Assessment and Management of Ageing of Major Nuclear Power Plant Components Important to Safety: PWR Pressure Vessel Internals, 2007 Update*. IAEA-TECDOC-1556, International Atomic Energy Agency (IAEA), Vienna, Austria.

Marquardt ED, JP Le and R Radebaugh. 2002. "Cryogenic Material Properties Database." In *Cryocoolers 11, 11th International Cryocooler Conference*, pp. 681-687. June 20-22, 2000, Keystone, Colorado. DOI 10.1007/0-306-47112-4_84. Springer US.

NRC. 2002. *Recent Experience with Degradation of Reactor Pressure Vessel Head.* Information Notice 2002-11, U.S. Nuclear Regulatory Commission, Washington, D.C. March 12, 2002. U.S. NRC Agencywide Data Access and Management System (ADAMS) Accession Number ML020700556.

APPENDIX A

PRECISION EDM NOTCH INFORMATION

APPENDIX A

PRECISION EDM NOTCH INFORMATION

Precision square-edged electrical discharge machining (EDM) notches were an essential aspect of the CRDM nozzle mockup specimen. As described in the calibration specimen design section, a variety of notches were chosen for the mockup specimen and allowed for a multitude of ultrasonic calibrations to be made. Understanding the phased-array probe resolution and detection characteristics allowed for a more thorough leak-path assessment to occur on North Anna Unit 2 removed-from-service Nozzle 63.

This appendix highlights the exact as-built dimensions and locations for all notches used in the mockup assembly specimen as provided by Western Professional, Inc., the EDM notch subcontractor. Page A-2 lists the as-built dimensions for the 16 EDM notches placed in the carbon steel material representing the RPV head. Page A-3 lists the as-built dimension for the 16 EDM notches place in the outer diameter of the Alloy 600 tube. Page A-4 shows the requested placement and size of the notches on the Alloy 600 tube outer diameter. Page A-5 shows the requested placement and size of notches 9–12. Page A-6 shows the requested placement and size of notches 13–16. Page A-7 shows the requested notch layout and sizing for the carbon steel material inner diameter.

WESTERN PROFESSIONAL, INC.
DBA WESTPRO LAB
3460 BRADY COURT NE
SALEM, OR 97303
(503)585-6263

Electrical Discharge Machining
Reference Standard Manufacturing
Optical Dimensioning System
Non Destructive Evaluation
RT, UT, MT, PT

CUSTOMER:	BATTELLE	**STANDARD:**	BLOCK STANDARD **S/N 5381**
DRAWING #:	CUSTOMER DRAWING	**P.O. #:**	135771
MATERIAL:	CARBON STEEL	**SIZE:**	4.102" Ø HOLE
DATE:	11-11-10	**SPEC(S):**	PER CUSTOMER DRAWING INSTRUCTIONS

BLOCK STANDARD S/N 5381

DEFECT DIMENSIONS (IN INCHES)					
NO.	DEPTH	LENGTH	WIDTH	LOCATION	ORIENTATION
1	.0011"	2.0017"	.0364"	I.D.	LONGITUDINAL
2	.0020"	2.0048"	.0379"	I.D.	LONGITUDINAL
3	.0029"	1.9974"	.0377"	I.D.	LONGITUDINAL
4	.0049"	2.0046"	.0372"	I.D.	LONGITUDINAL
5	.1000"	1.9891"	.0316"	I.D.	LONGITUDINAL
6	.1004"	1.9929"	.0624"	I.D.	LONGITUDINAL
7	.1007"	2.0067"	.1251"	I.D.	LONGITUDINAL
8	.1002"	1.9968"	.2514"	I.D.	LONGITUDINAL
9	.0786"	1.0061"	.0833"	I.D.	TRANSVERSE
10	.0789"	1.0011"	.0826"	I.D.	TRANSVERSE
11	.0768"	1.0015"	.0834"	I.D.	TRANSVERSE
12	.0811"	1.0004"	.0827"	I.D.	TRANSVERSE
13	.0811"	1.0009"	.0807"	I.D.	LONGITUDINAL
14	.0789"	1.0028"	.0821"	I.D.	LONGITUDINAL
15	.0805"	1.0011"	.0828"	I.D.	LONGITUDINAL
16	.0805"	1.0007"	.0810"	I.D.	LONGITUDINAL

SEE ATTACHED DRAWING FOR NOTCH LOCATIONS

NOTE: ALL DEPTH AND WIDTH MEASUREMENTS ARE BASED ON AN AVERAGE OF FOUR OR MORE READINGS.

ALL DIMENSIONS ARE MEASURED WITH DIMENSIONAL EQUIPMENT WHICH IS CERTIFIED AND TRACEABLE TO NIST #(708) #2343033 AND NIST (#783183) #3881145. NUCLEAR REGULATORY COMMISSION RULES AND REGULATIONS 10 CFR PART 21 APPLIES TO THIS ORDER. ALL NOTCHES MANUFACTURED PER WESTPRO PROCEDURE WQC-IV.

CERTIFIED BY: S. CHAMBERLAIN

APPROVED BY: S. Chamberlain

WESTERN PROFESSIONAL, INC.
DBA WESTPRO LAB
3460 BRADY COURT NE
SALEM, OR 97303
(503)585-6263

Electrical Discharge Machining
Reference Standard Manufacturing
Optical Dimensioning System
Non Destructive Evaluation
RT, UT, MT, PT

CUSTOMER:	BATTELLE	**STANDARD:**	PIPE STANDARD **S/N 5382**
DRAWING #:	CUSTOMER DRAWING	**P.O. #:**	135771
MATERIAL:	STAINLESS STEEL, HT# L215S	**SIZE:**	4.112" Ø X .6837" AWT
DATE:	11-11-10	**SPEC(S):**	PER CUSTOMER DRAWING INSTRUCTIONS

PIPE STANDARD S/N 5382

DEFECT DIMENSIONS (IN INCHES)					
NO.	**DEPTH**	**LENGTH**	**WIDTH**	**LOCATION**	**ORIENTATION**
1	.0011"	1.9976"	.0367"	O.D.	LONGITUDINAL
2	.0020"	1.9951"	.0366"	O.D.	LONGITUDINAL
3	.0030"	1.9971"	.0370"	O.D.	LONGITUDINAL
4	.0050"	1.9994"	.0371"	O.D.	LONGITUDINAL
5	.0980"	1.9945"	.0314"	O.D.	LONGITUDINAL
6	.1002"	2.0004"	.0632"	O.D.	LONGITUDINAL
7	.1012"	2.0066"	.1274"	O.D.	LONGITUDINAL
8	.1009"	1.9971"	.2526"	O.D.	LONGITUDINAL
9	.0795"	1.0007"	.0826"	O.D.	TRANSVERSE
10*	.0797"	1.0000"	.0851"	O.D.	TRANSVERSE
11	.0806"	1.0018"	.0807"	O.D.	TRANSVERSE
12	.0806"	1.0007"	.0822"	O.D.	TRANSVERSE
13	.0804"	1.0004"	.0818"	O.D.	LONGITUDINAL
14	.0840"	1.0015"	.0816"	O.D.	LONGITUDINAL
15	.0780"	1.0020"	.0818"	O.D.	LONGITUDINAL
16	.0809"	1.0012"	.0829"	O.D.	LONGITUDINAL

SEE ATTACHED DRAWING FOR NOTCH LOCATIONS

***NOTCH #10 WIDTH IS .001" OVER MAXIMUM TOLERANCE.**

NOTE: ALL DEPTH AND WIDTH MEASUREMENTS ARE BASED ON AN AVERAGE OF FOUR OR MORE READINGS.

ALL DIMENSIONS ARE MEASURED WITH DIMENSIONAL EQUIPMENT WHICH IS CERTIFIED AND TRACEABLE TO NIST #(708) #2343033 AND NIST (#783183) #3881145. NUCLEAR REGULATORY COMMISSION RULES AND REGULATIONS 10 CFR PART 21 APPLIES TO THIS ORDER. ALL NOTCHES MANUFACTURED PER WESTPRO PROCEDURE WQC-IV.

CERTIFIED BY: S. CHAMBERLAIN

APPROVED BY: S. Chamberlain

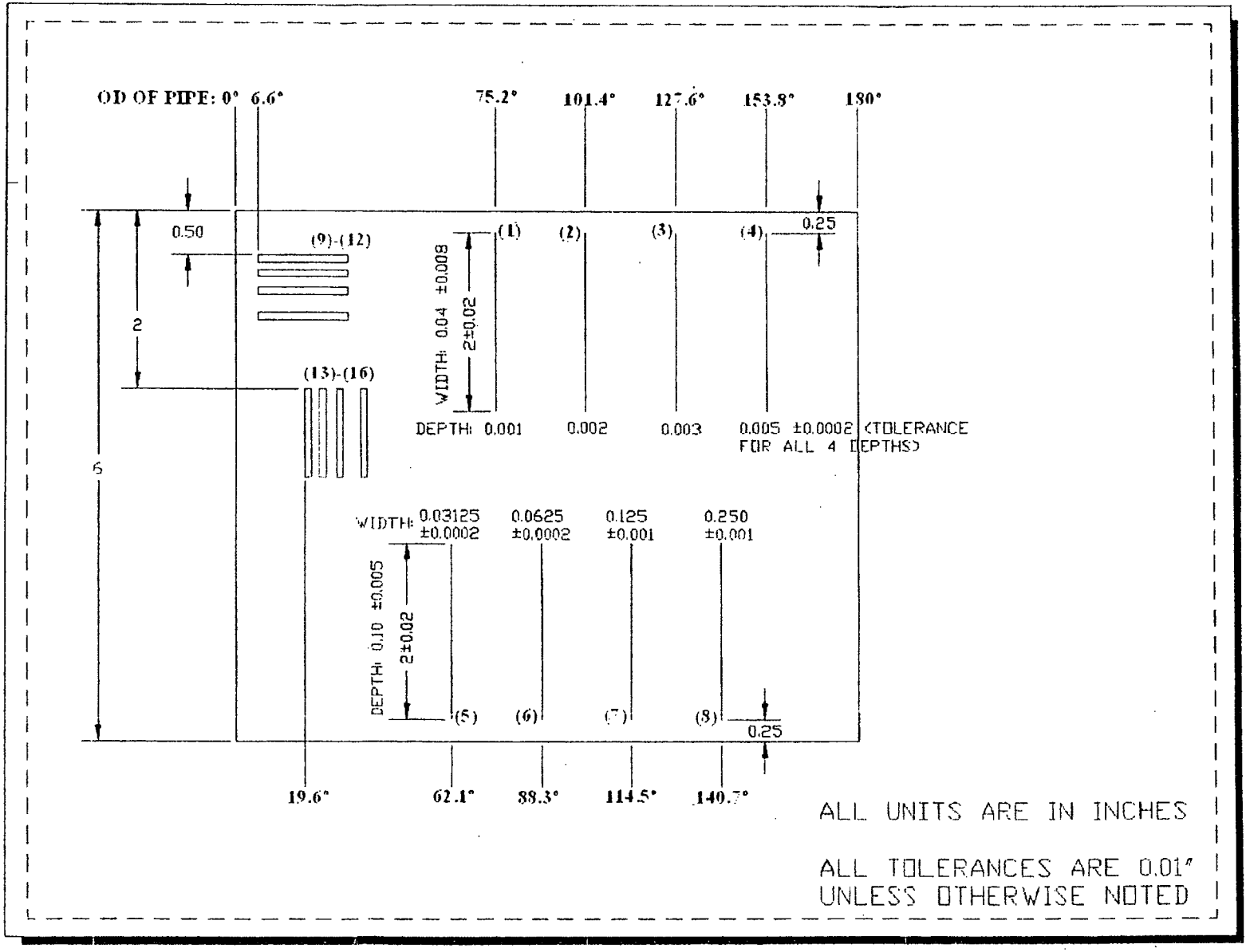
OD OF PIPE: 0°
6.6°
75.2°
101.4°
127.6°
153.8°
180°
0.50
(9)-(12)
2
(13)-(16)
6
(1)
(2)
(3)
(4)
0.25
WIDTH: 0.04 ±0.008
2±0.02
DEPTH: 0.001
0.002
0.003
0.005 ±0.0002 (TOLERANCE FOR ALL 4 DEPTHS)
WIDTH: 0.03125 ±0.0002
0.0625 ±0.0002
0.125 ±0.001
0.250 ±0.001
DEPTH: 0.10 ±0.005
2±0.02
(5)
(6)
(7)
(8)
0.25
19.6°
62.1°
88.3°
114.5°
140.7°
ALL UNITS ARE IN INCHES
ALL TOLERANCES ARE 0.01" UNLESS OTHERWISE NOTED

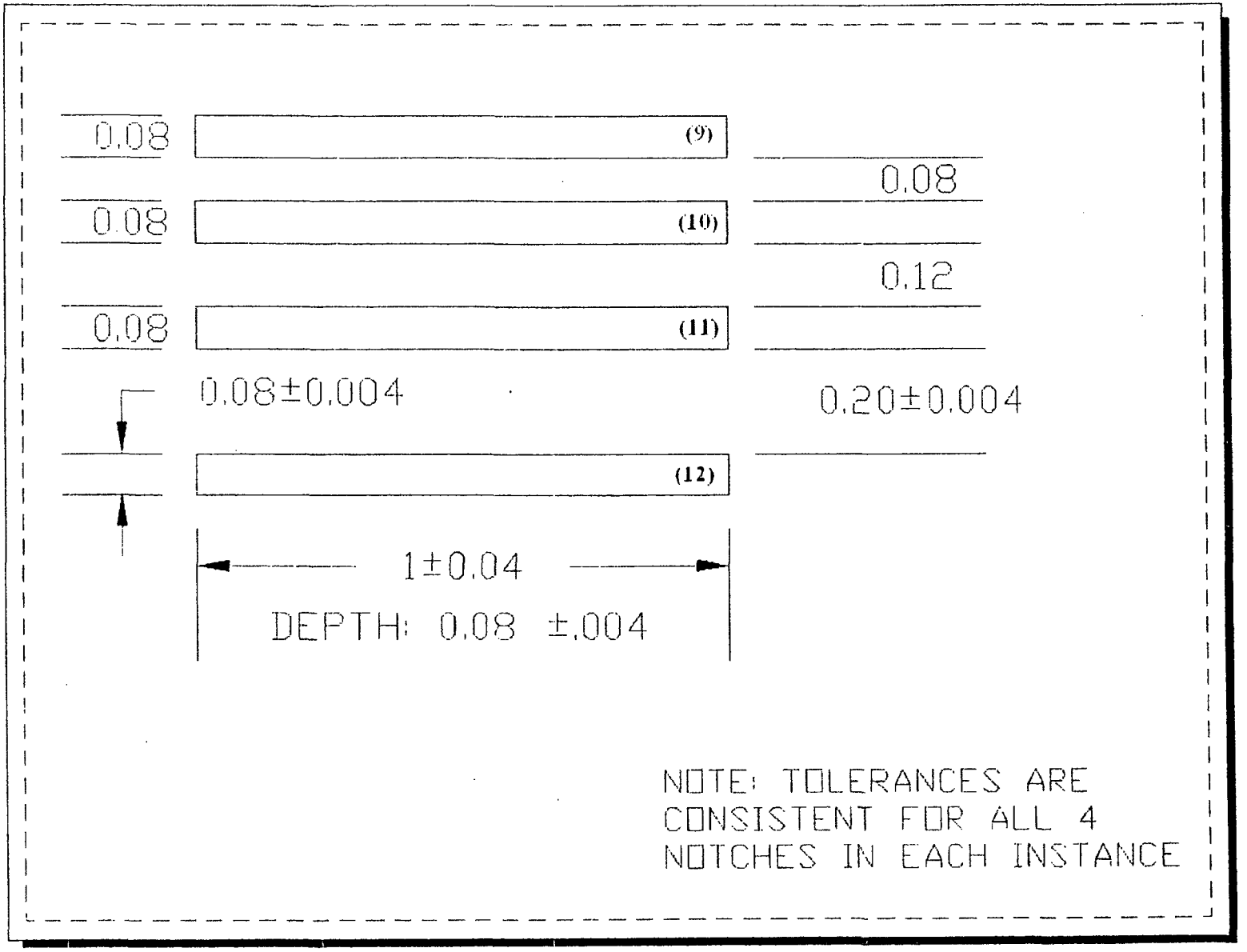
0.08
(9)
0.08
0.08
(10)
0.12
0.08
(11)
0.08±0.004
0.20±0.004
(12)
1±0.04
DEPTH: 0.08 ±.004
NOTE: TOLERANCES ARE CONSISTENT FOR ALL 4 NOTCHES IN EACH INSTANCE

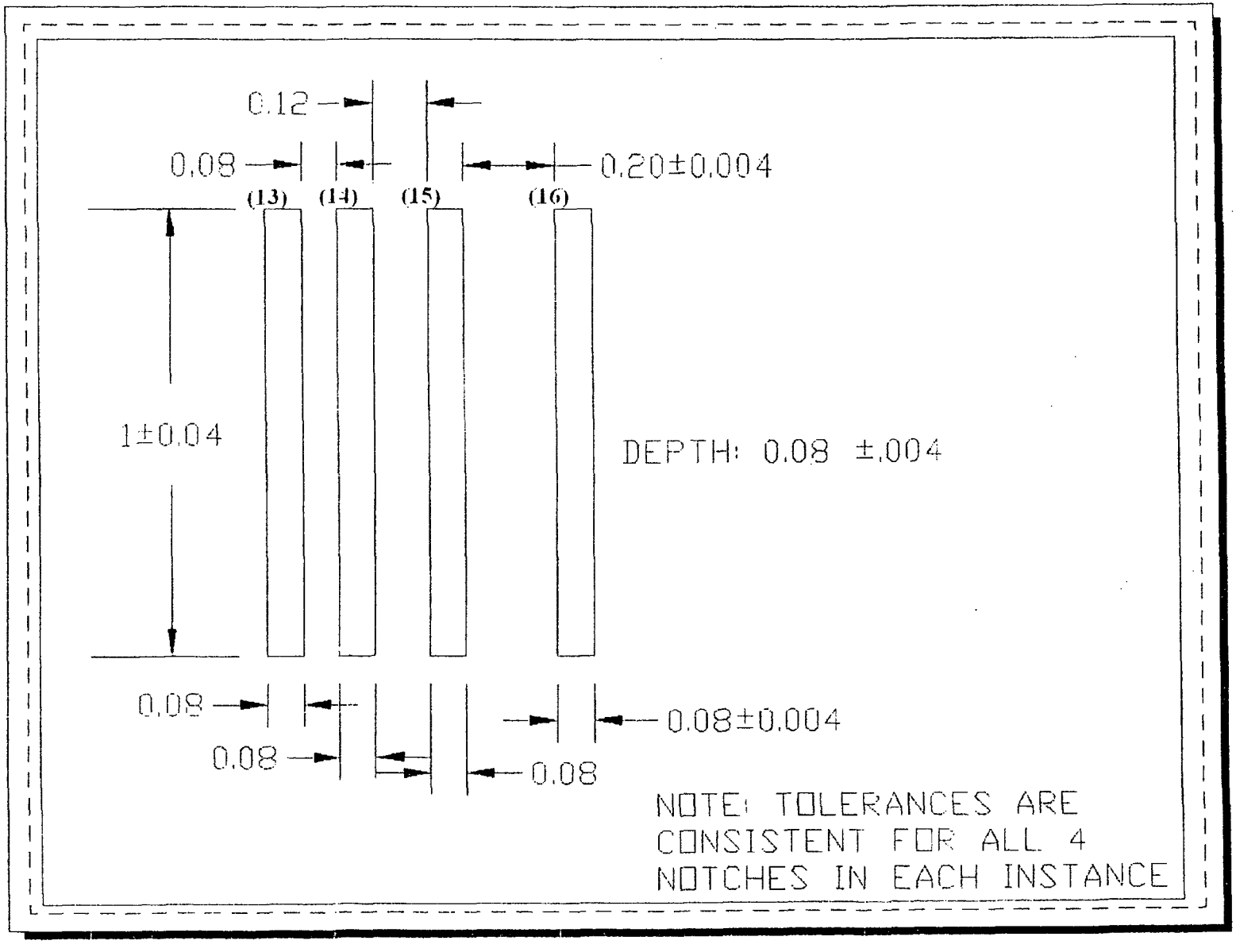
0.12
0.08
0.20±0.004
(13)
(14)
(15)
(16)
1±0.04
DEPTH: 0.08 ±.004
0.08
0.08±0.004
0.08
0.08
NOTE: TOLERANCES ARE CONSISTENT FOR ALL 4 NOTCHES IN EACH INSTANCE

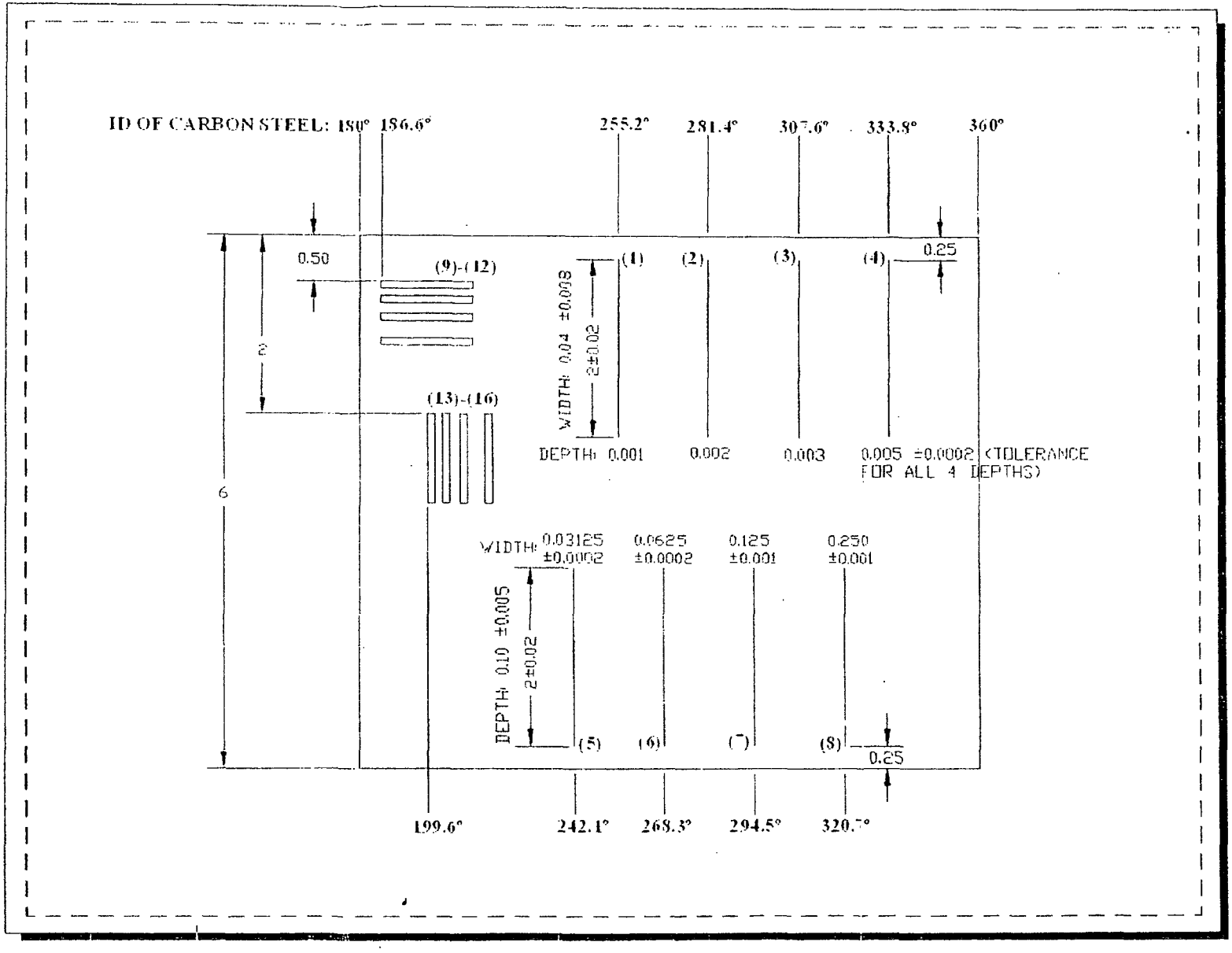
ID OF CARBON STEEL: 180° 186.6°
255.2°
281.4°
307.6°
333.8°
360°
0.50
(9)-(12)
(13)-(16)
(1)
(2)
(3)
(4)
0.25
WIDTH: 0.04 ±0.003
2±0.02
DEPTH: 0.001
0.002
0.003
0.005 ±0.0002 (TOLERANCE FOR ALL 4 DEPTHS)
6
WIDTH: 0.03125 ±0.0002
0.0625 ±0.0002
0.125 ±0.001
0.250 ±0.001
DEPTH: 0.10 ±0.005
2±0.02
(5)
(6)
(7)
(8)
0.25
199.6°
242.1°
268.3°
294.5°
320.7°

Appendix B

THEORETICAL AND PRACTICAL INCONEL TUBE SHRINKAGE

APPENDIX B

THEORETICAL AND PRACTICAL INCONEL TUBE SHRINKAGE

To determine if the interference fit was attainable, the expected thermal shrinkage for the nozzle at liquid nitrogen temperature was calculated. Thermal expansion coefficients are generally given in tabular form for different materials over a particular temperature range. These table values assume a linear relationship over a limited temperature range. Cryogenic material properties were needed for the temperatures used in forming the interference fit. Two reference papers (Clark 1968; Marquardt et al. 2002) discussed material properties of metal alloys at cryogenic temperatures. Inconel 718 was one of the materials studied and represented the nozzle material for the purpose of material shrinkage calculations. To form the interference fit, the nozzle was taken from room temperature, 293°K (19.85°C, 67.73°F), to the temperature of liquid nitrogen, 77.2°K (−195.95°C, −320.71°F). Clark (1968) measured the thermal expansion coefficients from liquid hydrogen temperature to room temperature, 20°K (−253.15°C, −423.67°F) to 293°K (19.85°C, 67.73°F), in 10- or 20-degree steps for different metallic alloys. Results were presented in tabular form for the expansion or shrinkage relative to room temperature. From the table for Inconel 718 at 80°K:

$$223 = \left[\left(L_{293} - L_{80}\right) / L_{293}\right] \times 10^5 \qquad \text{(B.1)}$$

expansion relative to room temperature

where L_n = length at temperature n, in degrees K.

From Eq. (B.1), the shrinkage of the 104.14-mm (4.1-in.) diameter Alloy 600 tube at liquid nitrogen temperature relative to room temperature is calculated as approximately 0.232 mm (0.00914 in.).

Marquardt modeled the material properties over a large temperature range (4 to 300°K [−452.5 to 80.3°F or −269.2 to 26.9°C]) with a polynomial or a logarithmic polynomial equation. An equation for the integrated linear thermal expansion or shrinkage is given as:

$$\left(L_T - L_{293}\right)/L_{293} = \left(a + bT + cT^2 + dT^3 + eT^4\right) \times 10^{-5} \qquad \text{(B.2)}$$

The coefficients for 718 Inconel are listed as:

a = −2.366E+02
b = −2.218E-01
c = 5.601E-03
d = −7.164E-06
e = 0

From Eq. (B.2), the shrinkage of the tube is calculated as approximately 0.233 mm (0.00917 in.) at 77K. This result very closely matches the result from Eq. (B.1) given above.

Prior to assembly of the mockup, experimental verification of the calculated shrinkage was conducted on a section of Alloy 600 tubing cut from a tube similar to that which was used for the mockup. At room temperature, five outside diameter measurements were acquired at 0–180 and five at 90–270 degrees using a calibrated caliper, shown in Figure B.1, at marked locations along the axial length of the specimen. Temperature measurements were obtained using a Raytek ST80XXUS infrared (IR) standoff thermometer. At room temperature the average diameter of the tube was 104.902 mm (4.130 in.). The tube section was then submerged in a liquid nitrogen (LN) bath for approximately 2.5 minutes. The chilled tube section was promptly removed from the LN bath and the diameter of the tube was again measured at the same locations. The temperature of the tube upon removal from the LN bath was unattainable as it surpassed the low end capability of the IR thermometer (−32 to 760 degrees C [−25 to 1400 degrees F]). The theoretical temperature of LN is −195.95 degrees C (−320.71 degrees F). At cold temperatures, the average diameter of the tube was 104.699 mm (4.122 in.). The tube section was allowed to re-equilibrate to room temperature and additional diameter measurements were made. These showed that the average nozzle diameter returned to 104.902 mm (4.130 in.). A full set of diameter data can be viewed in Table B.1, where data were acquired in descending order from position 5 to 1. Figure B.2 shows the tube diameter at the three stages of this experiment as a function of axial position: room temperature initial (RT initial), after LN, and room temperature final (RT final). The results from this test indicated that the Alloy 600 tube material shrank an average of 0.203 mm (8 mils) in diameter when chilled with LN and then was restored to its original size after returning to room temperature. The CRDM calibration specimens were designed and machined for a 0.076-mm (3-mils) diameter interference fit. Tube shrinkage of an additional 0.127 mm (5 mils) provided the necessary room for slipping the machined carbon steel blocks over the tube during mockup assembly. Moreover, it was equally important that the tube return to its original size (at room temperature) in order to create the tight interference fit. This successful preliminary test proved that both necessary requirements could be achieved.

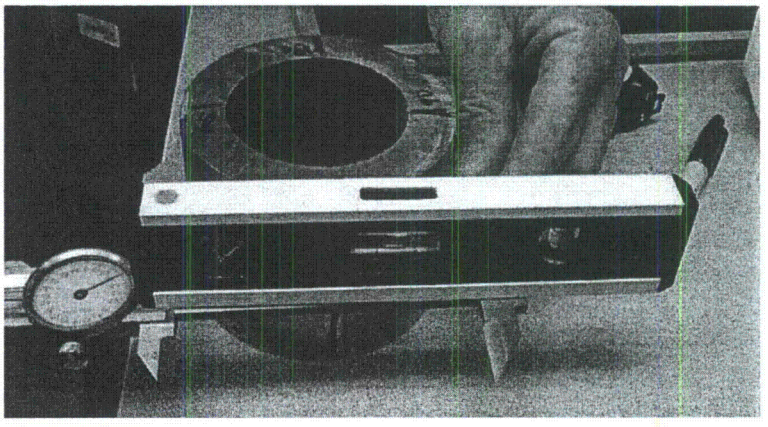

Figure B.1 Diameter Measurements Acquired at Room Temperature Using a Caliper

Table B.1 Alloy 600 Tube Diameter Measurements Verses Temperature

Temp (F)		Room Temp 73.9		Liquid Nitrogen Unknown			Return to Room Temp 73.9	
		0–180	90–270	0–180	90–270		0–180	90–270
Diameter (in.)	1	4.130	4.130	4.122	4.125		4.130	4.130
	2	4.130	4.130	4.122	4.122		4.130	4.130
	3	4.130	4.130	4.124	4.122		4.130	4.130
	4	4.130	4.130	4.120	4.122	/\	4.130	4.129
	5	4.130	4.130	4.120	4.122	t=0	4.130	4.129
Average:		4.130		4.122			4.130	

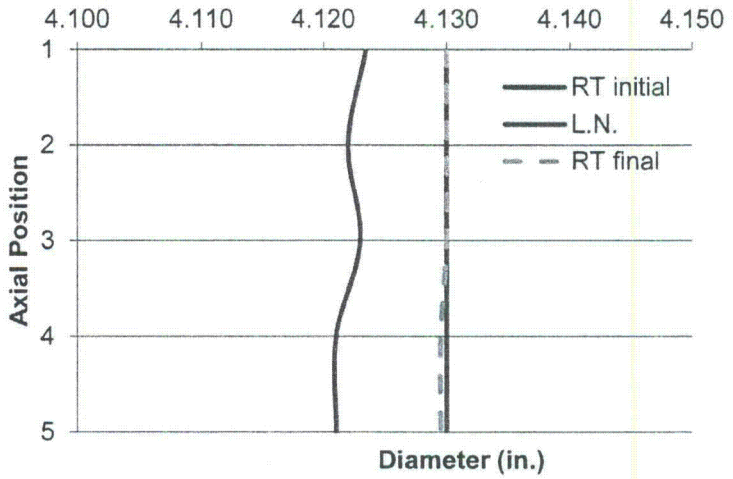

Figure B.2 Tube Shrinkage Measurements

APPENDIX C

SUPPLEMENTAL INFORMATION ON DESTRUCTIVE CUTTING

APPENDIX C

SUPPLEMENTAL INFORMATION ON DESTRUCTIVE CUTTING

B&W used an industrial 19-ft CobraFab Industries, Inc. band saw model VH2532HD with 'Cobra Strike' and an interchangeable blade option for all cutting purposes associated with the destructive activity. This saw was equipped with a ±45° hydraulic miter attachment and was capable of cutting pieces measuring 63.5 cm (25 in.) wide by 81.3 cm (32 in.) high in the vertical position and 63.5 cm (25 in.) wide by 55.9 cm (22 in.) high in the ±45° positions. A total of six 5.8 m (19-ft) blades were acquired from Scarney Industries, Youngstown, Ohio. Two coarse tooth (2-3 teeth per inch) and three fine tooth (4-6 teeth per inch) bimetallic blades with positive rake, variable pitch, and variable tooth were used. Additionally, one carbide grit-abrasive blade was also used. In general, coarse tooth blades were used for thicker section cutting, 20.3 cm (8 in.) and larger, and the fine toothed blades were used for precision cutting material under 20.3 cm (8 in.) in thickness. The carbide grit abrasive blade was used when the bimetallic blades were ineffective. Figure C.1 shows the three blade types used. All cuts in this activity were conducted without lubrication or coolant to minimize disturbance to the interference fit region.

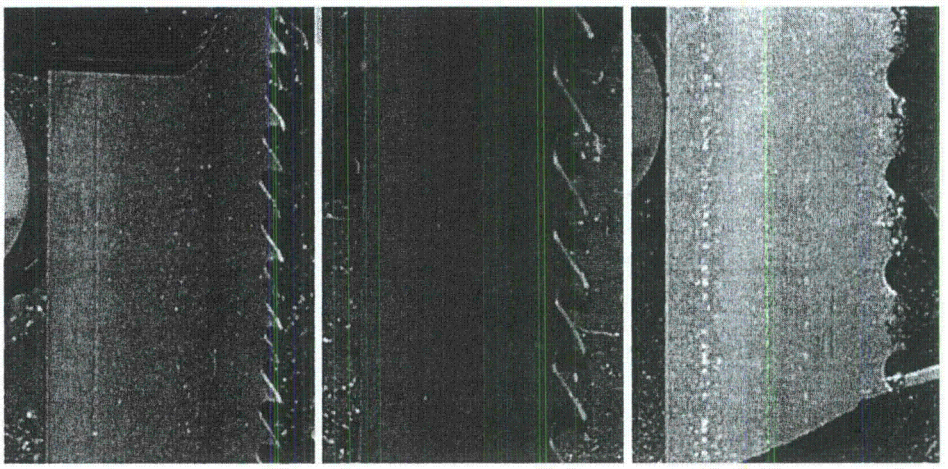

Figure C.1 Three Blade Types were Utilized to Section the RPV Head and CRDM Nozzle. From left: fine tooth blade, coarse tooth blade, and carbide grit blade.

The initial size reduction cuts were performed on the Nozzle 63 specimen using one of the coarse toothed blades prior to the arrival of PNNL staff. Non-essential material was removed to reduce weight and to facilitate proper blade placement on the specimen during critical cuts. Figure C.2 shows images from the size reduction activity. All cuts in this activity were conducted without lubrication or coolant to minimize disturbance to the interference fit region.

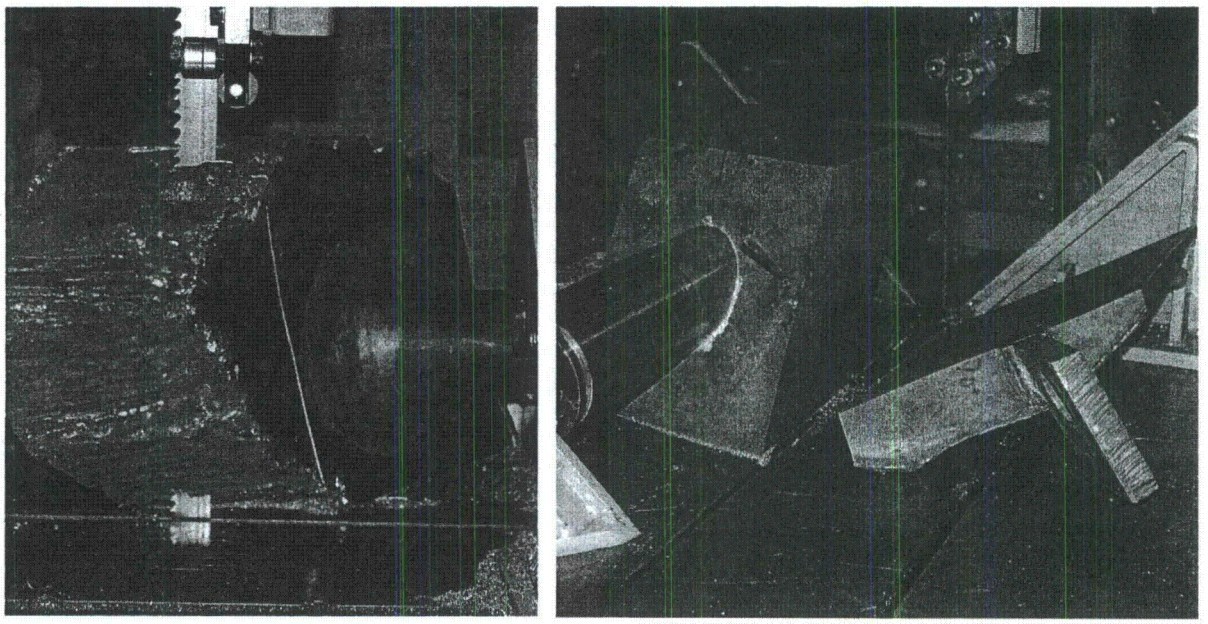

Figure C.2 Size Reduction Cutting Activity

After size reduction, the nozzle assembly was prepared for the dissection cut that separated the high and low sides of the assembly. The cut line was selected to start at approximately the 95-degree mark (Figure C.3), and follow through to the 275-degree mark. The line placement was based on the ultrasonic data and chosen to preserve the primary leak path previously identified in the ultrasonic images.

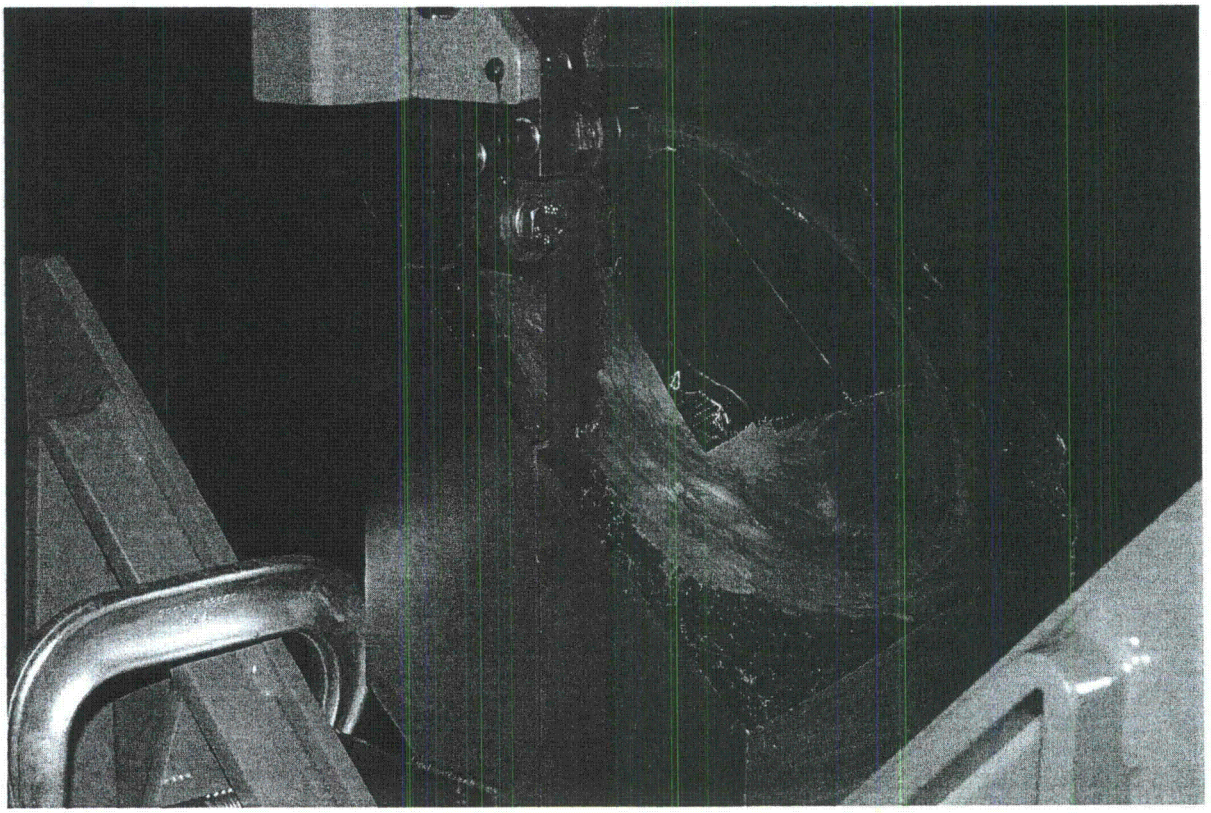

Figure C.3 Start of the Dissection Cut

Dissection cutting began with the coarse-toothed blade. The cut progressed for approximately 20 minutes until an unidentified 'hard spot' was reached at the outer edge of the Alloy 600 nozzle region and stopped the cutting progression. A slower feed rate with a faster blade speed was attempted, but did not traverse the hard spot. The cause of the hard spot was not fully investigated, but a likely cause was from a cold-worked region of material within the heat-affected zone of the J grove weld adjacent to the nozzle outer diameter (OD). The coarse-cut blade was exchanged with a fine-toothed cutting blade and the cut was attempted again without success. Finally, the carbide blade was employed to abrasively grind through the hard spot. This blade required a greatly reduced feed rate, thus lengthened the cutting time. Further, the kerf of the carbide blade was thicker than the cutting blades, requiring the cut to be restarted at the initial cut path. The carbide grit abrasive blade is shown in Figure C.4. The cut through this hard spot required approximately 2 hours to complete.

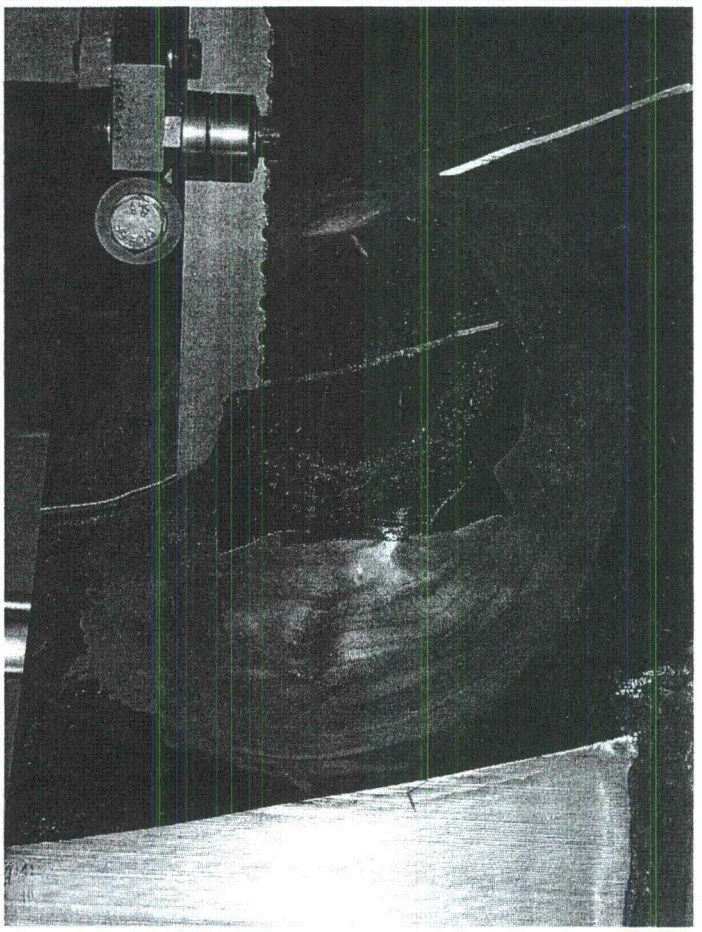

Figure C.4 Abrasive Carbide Blade Progressing Through the Hard Spot

After cutting through the first side of the nozzle, the carbide blade was exchanged with the fine-toothed cutting blade and the dissection cutting continued. Another hard spot was incurred in the J-groove weld region. Again, the carbide blade was used to cut through the hard spot with a slow feed rate. Finally, the fine-toothed blade was re-engaged and the dissection cut completed. From the exposed surfaces, the triple point was identified along with the weld and butter regions as shown in Figure C.5.

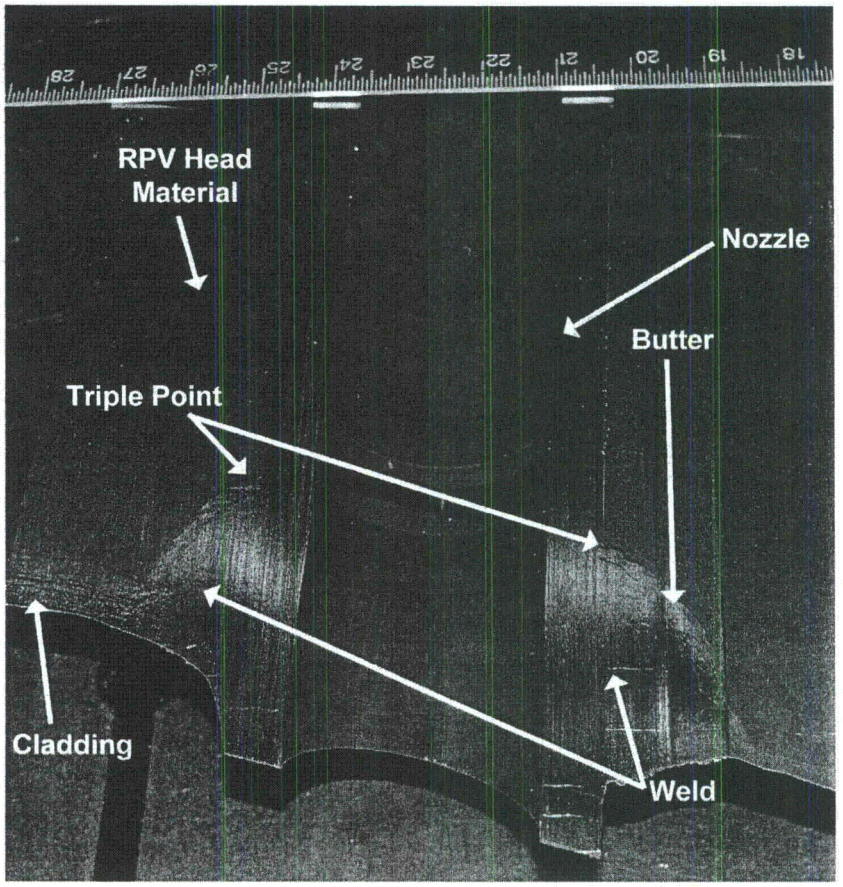

Figure C.5 Nozzle 63 Assembly Cut in Half by Dissection Cut

The cut to remove the J-groove weld was made 6.35 mm (0.25 in.) above the butter/triple point region in the reactor pressure vessel (RPV) head as seen in Figure C.6. The high or uphill side half-portion was selected for the first cutting. As previously stated, the 'high' side has several potential leak paths whereas the 'low' or downhill side had the primary leak path as identified in the ultrasonic data. The specimen was secured and the band saw tilted to an approximate 43-degree angle to match the angle between the nozzle and head as shown in Figure C.7. Cutting at this angle maximized the annulus region that was exposed while keeping the weld and butter regions intact for future evaluation. As the cut was designed to pass only through the low-alloy RVH material, the fine toothed cutting blade was selected for use. During the J-groove weld removal cut, another hard spot was encountered near the outside of the nozzle. Attempts were made to continue cutting with the fine-toothed blade until abrasive wear on one side of the blade resulted in the cut veering away from the desired cut line. Blades were exchanged and the carbide blade was used to cut through the hard spot and also to finish the cut. Before the cut broke through the inside of the tube, a vacuum equipped with a high-efficiency particulate air (HEPA) filter was added to collect and capture any radioactive oxide particles that were discharged from the cut as pictured in Figure C.8.

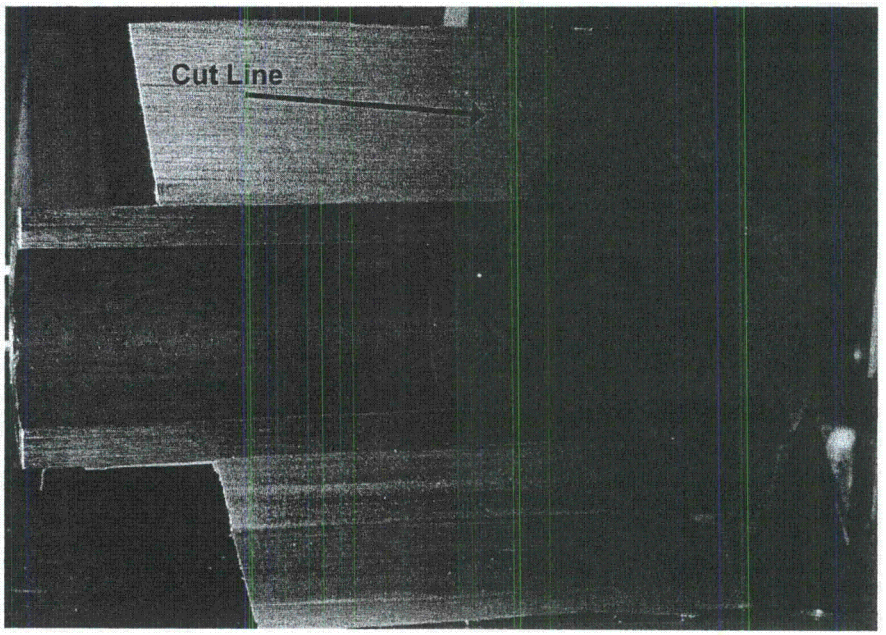

Figure C.6 J-groove Weld Removal Cut Line Placement

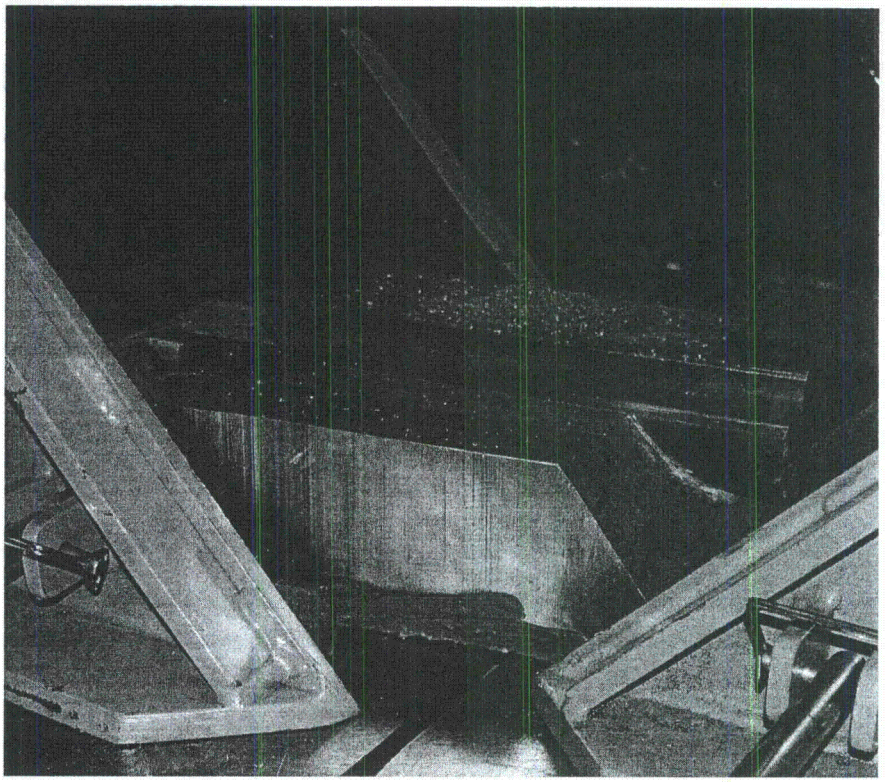

Figure C.7 J-groove Weld Cut on the High Side

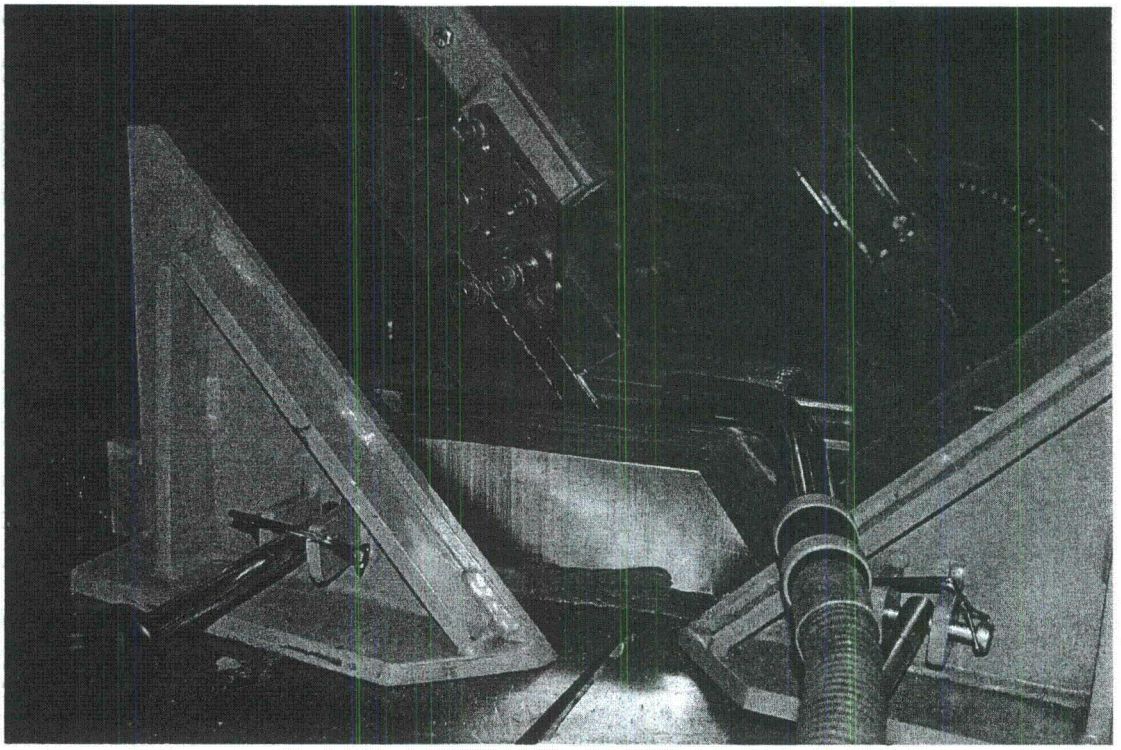

Figure C.8 Abrasive Blade Cutting Through the Nozzle with a HEPA Vacuum Nozzle

The cutting continued until the entire nozzle was separated from the J-groove weld region as pictured in Figure C.9. At this point, the nozzle region above the weld was freely released from the RPV head material. Removal of the nozzle exposed the annulus region of the high-side section as shown in Figure C.10. At this point all available blades were exhausted. Replacement blades were ordered to finish the cut and complete removal of the J-groove weld region. A Nikon D40x camera was used to acquire high-resolution photographic documentation of the annulus region. This activity was provided by B&W. A subsequent cut was conducted on the low-side section to expose its annulus region containing the primary leak path (Figure C.11). The nozzle freely released from this portion as well.

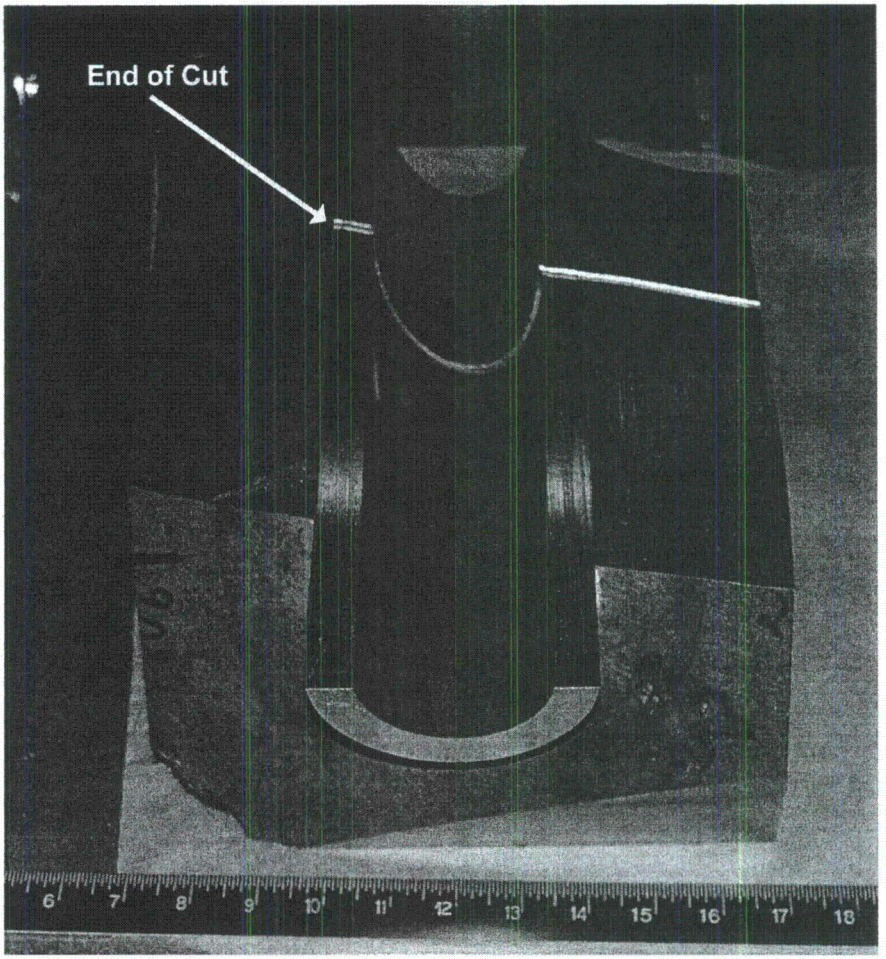

Figure C.9 End of J-groove Weld Removal Cut

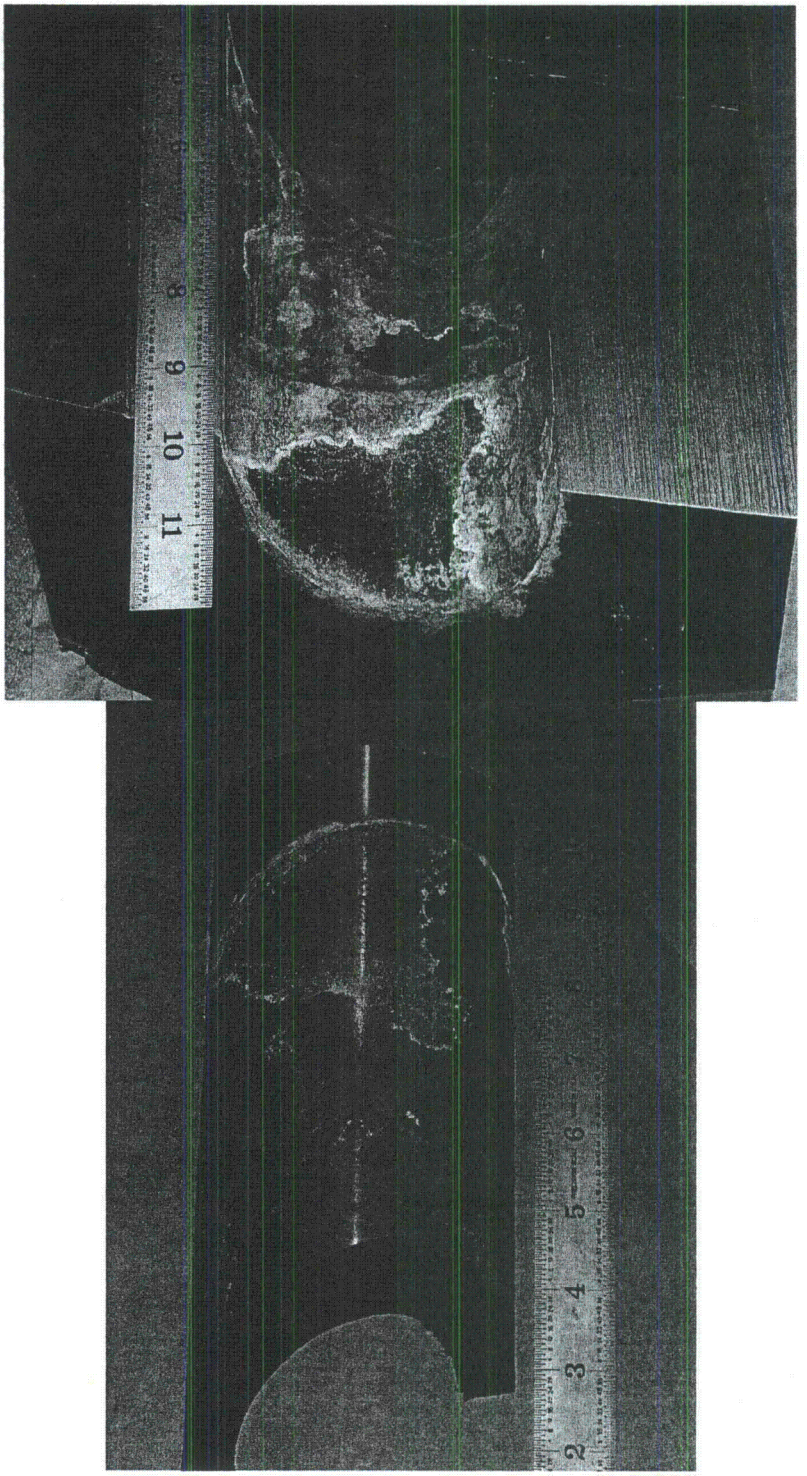

Figure C.10 Exposed RPV Head and Nozzle from High Side Section

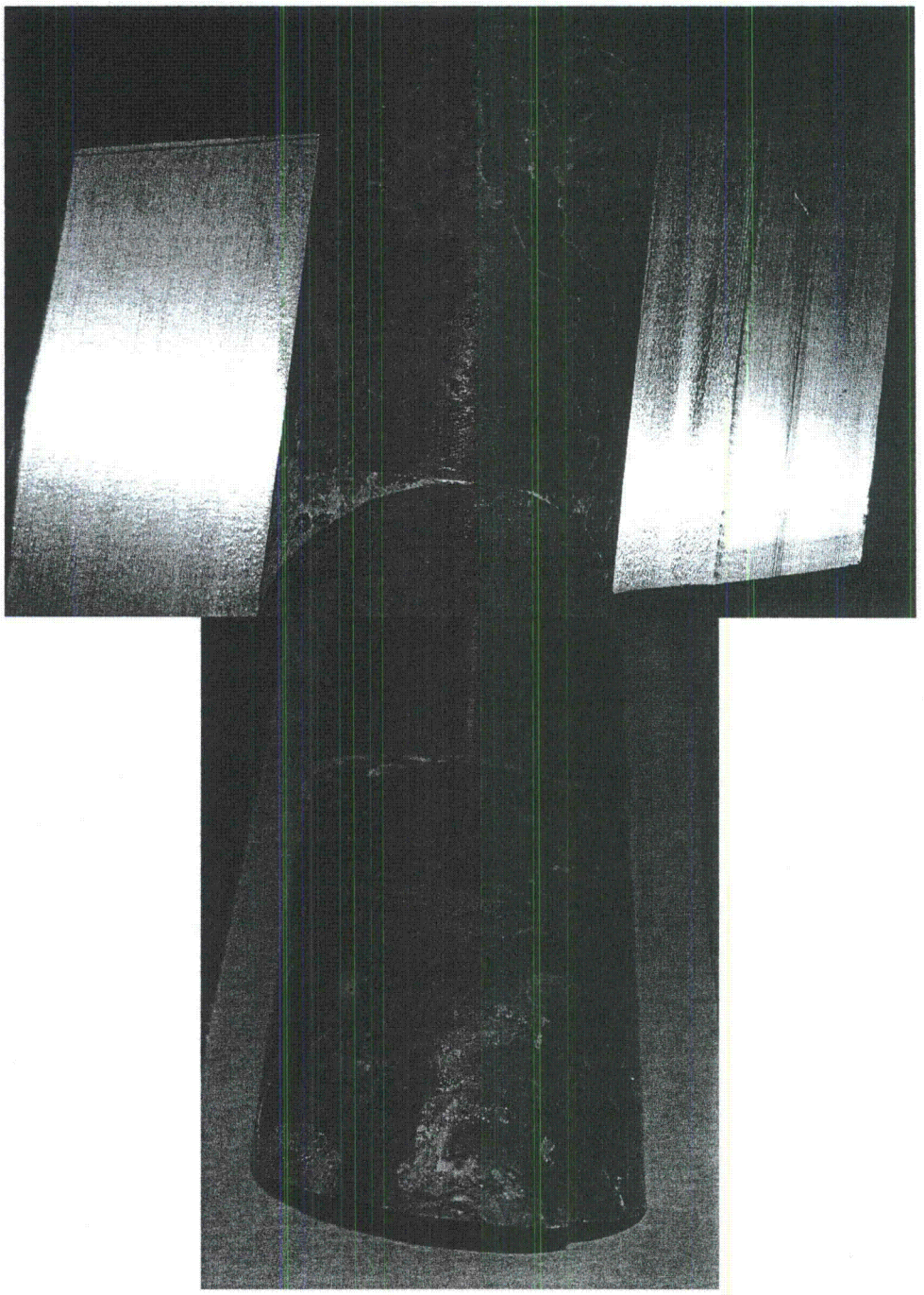

Figure C.11 Exposed RPV Head and Nozzle from Low-Side Section

Chapter 4. Examples Manual

This chapter contains example problems that help users become familiar with set up and usage of the concrete material model. These are single element simulations in tension and compression. These simulations demonstrate two methods of setting up the concrete material property input. The fast and easy method is to use default material properties selected as a function of concrete compressive strength and maximum aggregate size. The more detailed method is to specify all material properties individually. In addition to analyzing plain concrete, the user may wish to analyze reinforced concrete. Modeling steel reinforcement is discussed in appendix B. Numerous other example problems for plain and reinforced concrete are given in the companion concrete model evaluation report.[1]

Concrete material model input is given in Figure 105 for default concrete parameters and in Figure 106 for user-specified properties. A complete input file, with nodes and elements, is given in appendix C. This file is for tensile loading in uniaxial stress of a single element. To convert to compressive loading, change the sign of the ordinate under *DEFINE_CURVE at the bottom of the file.

```
$
*MAT_CSCM_CONCRETE
$
$ Concrete f'c = 30 MPa  Maximum Aggregate Size is 19 mm
$
$      MID        RO      NPLOT      INCRE      IRATE      ERODE      RECOV     IRETRC
       159 2.320E-09          1        0.0          0       1.05        0.0          0
$
$     PreD
       0.0
$
$      f'c       Dagg      UNITS
      30.0       19.0          2
$
```

Figure 105. Computer printout. Example concrete model input for default material property input (option mat_CSCM_concrete).

Single element stress-strain results are shown in Figure 107 for concrete with a compressive strength of 30 MPa (4,351 psi) and a maximum aggregate size of 19 mm (0.75 inches). These results can be achieved using either the default input shown in Figure 105 or the user-specified input shown in Figure 106. Note that the peak strength attained in compression matches the specified strength listed in Figure 105, which is 30 MPa (4,351 psi). Results are plotted with LS-POST as cross-plots of element z-stress versus z-strain. As additional exercises, the user can vary the unconfined compressive strength, aggregate size, and rate effects to examine the variation in concrete behavior with these quantities.

Note that the concrete tensile strength is less than 10 percent of the compressive strength. Because of concrete's low tensile strength, unintended tensile damage may occur in the vicinity of contact surfaces, as discussed in the concrete evaluation report.[1]